

INSTITUTE OF PHYSICS  
FACULTY OF SCIENCE AND TECHNOLOGY  
UNIVERSITY OF SILESIA



Aleksandra Słapik

Ph.D. Thesis

ANOMALOUS TRANSPORT IN NONEQUILIBRIUM SYSTEMS:  
FROM NEGATIVE MOBILITY TO PARTICLE SEPARATION

Supervisor: dr hab. Jakub Spiechowicz, prof. UŚ

Katowice 2021

## Abstract

The presented doctoral dissertation is focused on a very specific transport effect observed in nonequilibrium systems, known as *negative mobility*. This non-intuitive phenomenon manifests in the following way: when a particle traveling in a nonlinear system far from equilibrium is subjected to a biased constant force, the direction of its net movement is observed to be *opposite* to that promoted by the acting force. In this study, by means of numerical methods, the negative mobility features and its origin have been explored. Moreover, it has been demonstrated how this effect can be used for mechanical isolation of one particle species from the others. A number of experiments involving negative mobility have already reported on successful separation of two types of particles with different sizes in microfluidic devices. However, no investigation on how to isolate in a controllable way *desired* particles from a mixture of various species has been conducted. The presented research reveals conditions that offer tailored isolation techniques by means of difference in the particles mobility. The proposed innovative separation mechanisms may prove to be promising for sorting difficult-to-separate mixtures, including those in biological systems.

## Streszczenie

Tematem przewodnim niniejszej rozprawy doktorskiej jest szczególne zjawisko transportu w układach nierównowagowych, zwane *ujemną ruchliwością*. Efekt ten, pozornie sprzeczny z codzienną intuicją, przejawia się w następujący sposób: kiedy cząstka poruszająca się w układzie nieliniowym w warunkach nierównowagowych poddana jest działaniu stałej siły, wypadkowy kierunek jej przemieszczenia okazuje się być *przeciwny* do kierunku działającej siły. W przedstawionej pracy za pomocą metod numerycznych zbadano własności i mechanizmy zjawiska ujemnej ruchliwości, a także pokazano, jak efekt ten może być wykorzystany do mechanicznej separacji różnych typów cząstek. W urządzeniach mikroprzepływowych wykonano szereg eksperymentów, w których za pomocą zjawiska ujemnej ruchliwości udało się rozdzielić cząstki o różnych rozmiarach. Nie przeprowadzono jednak dotychczas badań dotyczących kontrolowanej separacji cząstek o *określonych* własnościach fizycznych spośród ich heterogenicznej mieszaniny. W niniejszej pracy zaprezentowano warunki, które umożliwiają kontrolowaną izolację cząstek na podstawie różnicy w ich ruchliwości. Proponowane innowacyjne metody separacji cząstek mogą okazać się przydatne w przypadku mieszanin, w których rozdzielenie składników jest skomplikowanym zadaniem, co jest szczególnie charakterystyczne dla układów biologicznych.

## Acknowledgements

This dissertation completes a diverse and active stage of my education period and thus, on this occasion, I would like to thank a certain group of people. I would like to thank Marcin Kostur for his patience and inspiring ideas, and after all, for introducing me to computer science. I would like to express my gratitude to Marcin Łobejko for showing me that sometimes it makes sense to question facts even if they are too obvious to discuss. I feel grateful to both Katarzyna Jesionek and Paulina Trybek for their incredibly supporting attitudes during the time of conducting research. Also, all of my university colleagues deserve appreciation for their partnership in the course of our studies, for implementing projects within the Physicists Science Club, and for many endless discussions, which sometimes turned out to be worth much more than many lectures.

I would like to express my special thanks to Jakub Spiechowicz, for his guidance and a great deal of assistance. Without his invaluable support and encouragement this dissertation would never be finished.

In addition, I would like to thank my parents for making me realize from early childhood how logical thinking is important in our everyday life, and in this way directing me towards science. Last but not least, I would like to thank my husband for being ready to help me at any time during the time of this research.

## Articles

The doctoral dissertation is based on the monothematic articles published in the international scientific journals during the period 2018-2020. It constitutes of the *Guidebook*, where the author presents the background and motivation for this work as well as general study of the issues described in the papers, and four attached *scientific articles*. The articles are listed below.

- A1: Ślapiak, Aleksandra, Jerzy Łuczka, and Jakub Spiechowicz. "Negative mobility of a Brownian particle: strong damping regime." *Communications in Nonlinear Science and Numerical Simulation* 55 (2018): 316-325.
- A2: Ślapiak, Aleksandra, Jerzy Łuczka, Peter Hänggi, and Jakub Spiechowicz. "Tunable mass separation via negative mobility." *Physical Review Letters* 122.7 (2019): 070602.
- A3: Ślapiak, Aleksandra, Jerzy Łuczka, and Jakub Spiechowicz. "Temperature-induced tunable particle separation." *Physical Review Applied* 12.5 (2019): 054002.
- A4: Ślapiak, Aleksandra, and Jakub Spiechowicz. "Tunable particle separation via deterministic absolute negative mobility." *Scientific Reports* 10.1 (2020): 16639.

# Guidebook

# Contents

<b>1</b>	<b>Introduction</b>	<b>2</b>
<b>2</b>	<b>The transport model</b>	<b>3</b>
<b>3</b>	<b>Negative mobility</b>	<b>5</b>
3.1	The non-intuitive phenomenon . . . . .	5
3.2	The role of system parameters . . . . .	8
3.3	The origin . . . . .	12
3.4	Strong damping regime . . . . .	15
3.5	Negative mobility in experiments . . . . .	16
<b>4</b>	<b>Computational details</b>	<b>16</b>
<b>5</b>	<b>Separation mechanisms</b>	<b>17</b>
5.1	The mass-based separation mechanism . . . . .	18
5.2	The temperature-induced separation mechanism . . . . .	20
5.3	The size-based separation mechanism . . . . .	23
5.4	Conclusion . . . . .	25
<b>6</b>	<b>Closing discussion</b>	<b>27</b>
<b>7</b>	<b>References</b>	<b>27</b>

# 1 Introduction

The transport phenomena have always played an important role in nature. Transportation is the foundation of all the changes observed in our everyday environment. It entails weather phenomena, geological changes, the water cycle in nature, transmission of nerve impulses, metabolism of living creatures or communication within human global civilization, to name just a few. Transport is ubiquitous in both *micro* and *macro* scale processes. This fact has already been recognized by ancient philosophers – *all entities move and nothing remains still* – has claimed Heraclitus in his treatise *On Nature* [1].

Because of the wide range of applications, transport remains an object of research in many fields of modern science. From applied science and technology (energy and heat transfer [2], hydrological processes [3], electrical circuits [4], gas transportation [5] and many others) to biology and medicine (e.g. cellular transport [6], epidemiology [7], drugs delivery [8]) to human behaviorism and culture (human migration [9] or trade [10]) the need to study transport modeling has tremendously increased in recent years.

The presented doctoral dissertation is focused on a very specific case of transport phenomenon. In this study the anomalous transport effect observed in the *small-scale* systems exposed to nonequilibrium conditions is investigated. By the *small-scale* we understand the systems for which the energy of thermal fluctuations is comparable to energy scales in the system. Therefore, the impact of thermal fluctuations cannot be completely neglected and one is mostly forced to work with probabilistic descriptions of the system. Hence, small-scale transport significantly differs from the macroscopic one which we encounter in our daily life.

The research introduced in this dissertation is based on the classical model of a *Brownian particle*, which has already been thoroughly described in the literature [11, 12]. This model allows including additional factors such as acting forces, thermal fluctuations or geometry of the particles' environment in a straightforward and elegant way. Although the model of Brownian motion appears to be a very basic and commonly used description, under some specific circumstances, in particular for nonequilibrium setting, it exhibits interesting and unique transport behaviour such as noise enhanced transport efficiency [13, 14], anomalous diffusion [15, 16, 17], amplification of normal diffusion [18, 19] or non-monotonic temperature dependence of normal diffusion [20].

Another remarkable transport effect observed for Brownian motion is the *negative mobility*. This non-intuitive phenomenon manifests in a following way: when a particle traveling in a nonlinear system far from equilibrium is subjected to a biased constant force, the direction of its net movement is observed to be *opposite* to that promoted by acting force. In other words, the direction of the particle velocity is opposite to the direction of biased force in the system.

This effect has been known for almost four decades and was observed in multiple experiments [21, 22, 23, 24, 25]. At the beginning, negative mobility was studied in a frame of quantum mechanical effects in semiconductor devices [26, 27], photovoltaic effects in ruby crystals [28, 29], tunnel junctions between superconductors with unequal energy gaps [30, 31] and certain ionized gas mixtures [32, 33]. Then, it was also identified in theoretical studies on interacting Brownian particles, as a collective effect of purely classical features of the nonequilibrium system [34, 35]. Afterwards, relatively recently, it has been proven to exist also in a large variety of classical, single particle models [22, 36, 37, 38, 39].

Negative mobility phenomenon is the leading subject of this dissertation. By means of numerical methods we explore its features and demonstrate how this effect can be used for mechanical isolation of one particle species from the others. Hence, we propose an innovative sorting-like mechanism based on kinetic properties of the particles which may prove to be promising for sorting difficult-to-separate mixtures, including those in biological systems.

The results presented in the following chapters have been published as a monothematic collection of four articles. In the first article (A1) we investigated phenomenon of negative

mobility and its relationship to inertia. We defined three different mechanisms responsible for this effect. We revealed that this phenomenon is also present in the strong damping regime, i.e. when the inertial term is almost negligible compared to the damping impact in the system. Moreover, we discovered interesting parameter regimes, where negative mobility is present only for particles with mass within a narrow interval of investigated mass space.

This led us to the idea of *particle separation*, which is a subject of the second article (A2). In this article we presented an effective particle separation mechanism based on negative mobility. The particles are distinguished by their dimensionless mass and the whole separation process can be tuned by setting a proper value of external time-periodic force frequency. Although our research is limited to strictly theoretical considerations, it can provide a guide for further experimental studies in order to isolate nano- and microparticles, proteins, organelles and cells.

The third article (A3) describes a similar particle separation process, but here the mechanism is triggered by thermal fluctuations. By varying solely the temperature of the system, one can separate particles of various, strictly defined sizes. Because the mechanism is based on negative mobility induced by thermal noise present in the system, it is far less populated in the parameter space. Nonetheless, it may be promising for separating particles that carry no charge or can hardly be manipulated by means of an external field.

Finally, in the fourth article (A4) we supplemented our results by discussing the separation mechanism in the frame of deterministic negative mobility. We demonstrated that when particles are distinguished by their size, the separation can be achieved by adjusting three different parameters that shape the particles' transport. We also proved that this method can be applied to particles of almost all sizes considered in the proposed model.

In this guidebook we lead the reader through the findings published in the articles. We expound reasons and motivations for conducted research as well as its significance and potential future applications. In order to present the most prominent outcomes we use the original illustrations and some of the conclusions from the published articles. When necessary, we refer the reader to the proper section in the articles to see more details and technical information.

## 2 The transport model

Let us consider a one-dimensional collection of non-interacting Brownian particles moving in a spatially periodic landscape. Let the particles be additionally subjected to unbiased time-periodic force  $A \cos(\Omega t)$ , of amplitude  $A$  and frequency  $\Omega$ , and external static force  $F$ . The dynamics of a single particle of mass  $M$  can be described then by the *Langevin equation* [40]

$$M\ddot{x} + \Gamma\dot{x} = -U'(x) + A \cos(\Omega t) + F + \sqrt{2\Gamma k_B T} \xi(t), \quad (1)$$

where the potential  $U(x)$  is assumed to be symmetric with period  $L$  and energy barrier  $2\Delta U$

$$U(x) = \Delta U \sin(2\pi x/L). \quad (2)$$

The energy dissipation is modeled by the Stokesian friction  $\Gamma\dot{x}$ , while the coupling of the particle with thermal bath of temperature  $T$  is modeled by Gaussian white noise of zero mean and unity intensity,

$$\langle \xi(t) \rangle = 0, \quad \langle \xi(t) \xi(s) \rangle = \delta(t - s). \quad (3)$$

The noise intensity factor  $\sqrt{2\Gamma k_B T}$  follows from the fluctuation-dissipation theorem [41], ensuring the equilibrium state for  $A = 0$  and  $F = 0$ . The  $k_B$  stands for the Boltzmann constant. The dot and the prime notation denote differentiation with respect to time and space, respectively.



Since equation (1) is a second-order non-linear stochastic differential equation, the associated Fokker-Planck equation cannot be handled by any analytical method. In order to examine its dynamics and features one needs to perform a comprehensive numerical study. However, before numerical methods can be applied, the equation needs to be transformed into *dimensionless* form. This procedure minimizes the number of parameters in the system and thus reduces the complexity of the system as well as extensive numerical computation. Moreover, it ensures independence of the obtained results on the given system setup. It is crucial for facilitating the choice in realizing the best setup for testing theoretical predictions in experiments. The non-dimensionalization process can be carried out in several ways [42]. In presented articles we used two different parameterization scales. Here we present the provenance of scaling in order to illustrate this procedure.

First, we define dimensionless variables by introducing characteristic units of length and time [43]

$$\hat{x} = \frac{x}{L}, \quad \hat{t} = \frac{t}{\tau_0}, \quad \tau_0 = L\sqrt{\frac{M}{\Delta U}}. \quad (4)$$

The period  $L$  of potential  $U(x)$  is a spatial scaling factor. The  $\tau_0$  is a characteristic time scale for the conservative system (when  $\Gamma = A = 0$ ), related to the period of particle linearized oscillations within one potential well. It comes from a simplified version of Langevin equation (1)

$$M\ddot{x} = -U'(x). \quad (5)$$

This type of parameterization is often found to be useful for investigating the damping influence on the system or for limiting case of small damping when  $\Gamma\dot{x} \rightarrow 0$ .

Next, we insert the dimensionless  $\hat{x}$  and  $\hat{t}$  into equation (1)

$$\frac{L}{\tau_0^2} M\ddot{\hat{x}} + \frac{L}{\tau_0} \Gamma\dot{\hat{x}} = -\frac{1}{L} U'(\hat{x}) + A \cos(\Omega\tau_0\hat{t}) + F + \sqrt{2\Gamma k_B T} \xi(\tau_0\hat{t}), \quad (6)$$

and divide the entire equation by the inertial term coefficient  $LM/\tau_0^2$ . After simplifying the expression, one obtains the following formula

$$\ddot{\hat{x}} + \gamma\dot{\hat{x}} = -\hat{U}'(\hat{x}) + a \cos(\omega\hat{t}) + f + \sqrt{2\gamma D} \hat{\xi}(\hat{t}), \quad (7)$$

which is a *dimensionless form* of Langevin equation (1).

It is important to notice here that parameters in equation (7) have been *rescaled* and they are no longer physical quantities that can be directly measured in the system. It has been explicitly indicated by replacing the uppercase letters  $\{\Gamma, A, \Omega, F\}$  from equation (1) with lowercase letters  $\{\gamma, a, \omega, f\}$ . Therefore, for example, the  $\gamma$  parameter is no longer a physical friction coefficient  $\Gamma$  of the particle, but it is rescaled *dimensionless friction coefficient*, namely

$$\gamma = \tau_0/\tau_1 = \frac{\Gamma L}{\sqrt{M\Delta U}}, \quad \text{where} \quad \tau_1 = \frac{M}{\Gamma}, \quad (8)$$

a combination of physical quantities present in equation (1). This procedure also reduced a number of parameters in the equation: the dimensionless mass is set to unity,  $m = 1$ . The explicit list of rescaled coefficient and their relation to physical quantities are depicted in Table 1. The dimensionless thermal noise  $\hat{\xi}(\hat{t})$  again satisfies the properties

$$\langle \hat{\xi}(\hat{t}) \rangle = 0, \quad \langle \hat{\xi}(\hat{t})\hat{\xi}(\hat{s}) \rangle = \delta(\hat{t} - \hat{s}) \quad (9)$$

and the noise intensity factor is given by  $D = k_B T/\Delta U$ , i.e. by the ratio of thermal fluctuations and potential barrier energies.

Using the scales given in (4) one can investigate the five-dimensional parameter space  $\{\gamma, a, \omega, f, D\}$  of equation (7). This method of scaling is fundamental for two of the presented

Symbol	Dimensionless parameter	Relation
$m$	mass	$m = 1$
$\gamma$	friction coefficient	$\gamma = \tau_0/\tau_1 = \frac{\Gamma L}{\sqrt{M\Delta U}}$
$a$	oscillating force amplitude	$a = A L/\Delta U$
$\omega$	oscillating force frequency	$\omega = \Omega\tau_0$
$f$	constant force	$f = F L/\Delta U$
$D$	noise intensity factor	$D = k_B T/\Delta U$

Table 1: Rescaled parameters and their relationship to physical quantities of the system. Scaling suitable for investigating the damping impact on the system. Dimensionless mass  $m$  is set to unity.

Symbol	Dimensionless parameter	Relation
$m$	mass	$m = \tau_1/\tau_0 = \frac{M\Delta U}{\Gamma^2 L^2}$
$\gamma$	friction coefficient	$\gamma = 1$
$a$	oscillating force amplitude	$a = A L/\Delta U$
$\omega$	oscillating force frequency	$\omega = \Omega\tau_0$
$f$	constant force	$f = F L/\Delta U$
$D$	noise intensity factor	$D = k_B T/\Delta U$

Table 2: Rescaled parameters and their relationship to physical quantities of the system. Scaling suitable for investigating inertia impact on the system. Dimensionless friction coefficient  $\gamma$  is set to unity.

articles (A3, A4). However, because of the condition  $m = 1$ , these units restrict analysis of the mass impact on the system dynamics. In order to enable such opportunity, we need to apply different scaling, suitable for testing the inertia influence on the system and the overdamped limiting case of  $M\ddot{x} \rightarrow 0$  [43], namely

$$\hat{x} = \frac{x}{L}, \quad \hat{t} = \frac{t}{\tau_0}, \quad \tau_0 = \frac{\Gamma L^2}{\Delta U}. \quad (10)$$

Here the characteristic time  $\tau_0$  follows from an overdamped approximation of equation (1), where the mass term is omitted,

$$\Gamma \dot{x} = -U'(x), \quad (11)$$

and it corresponds to the time scale for an overdamped particle to move from the maximum of the potential  $U(x)$  to its minimum. After inserting units (10) into equation (1), the dimensionless Langevin equation transforms into the following form

$$m\ddot{\hat{x}} + \dot{\hat{x}} = -\hat{U}'(\hat{x}) + a \cos(\omega\hat{t}) + f + \sqrt{2D}\hat{\xi}(\hat{t}). \quad (12)$$

This rescaled dimensionless equation was used in the article (A1) and (A2). Table 2 presents the relation between rescaled and physical parameters according to the units (10). From now on, only the dimensionless variables will be used in this study and therefore, in order to simplify the notation, the *hat* symbol will be omitted in all equations.

### 3 Negative mobility

#### 3.1 The non-intuitive phenomenon

Dynamics of the small-scale systems can reveal astounding effects and may often mislead our intuition. However, since the fluctuations play a key role at this scale, unexpected physical

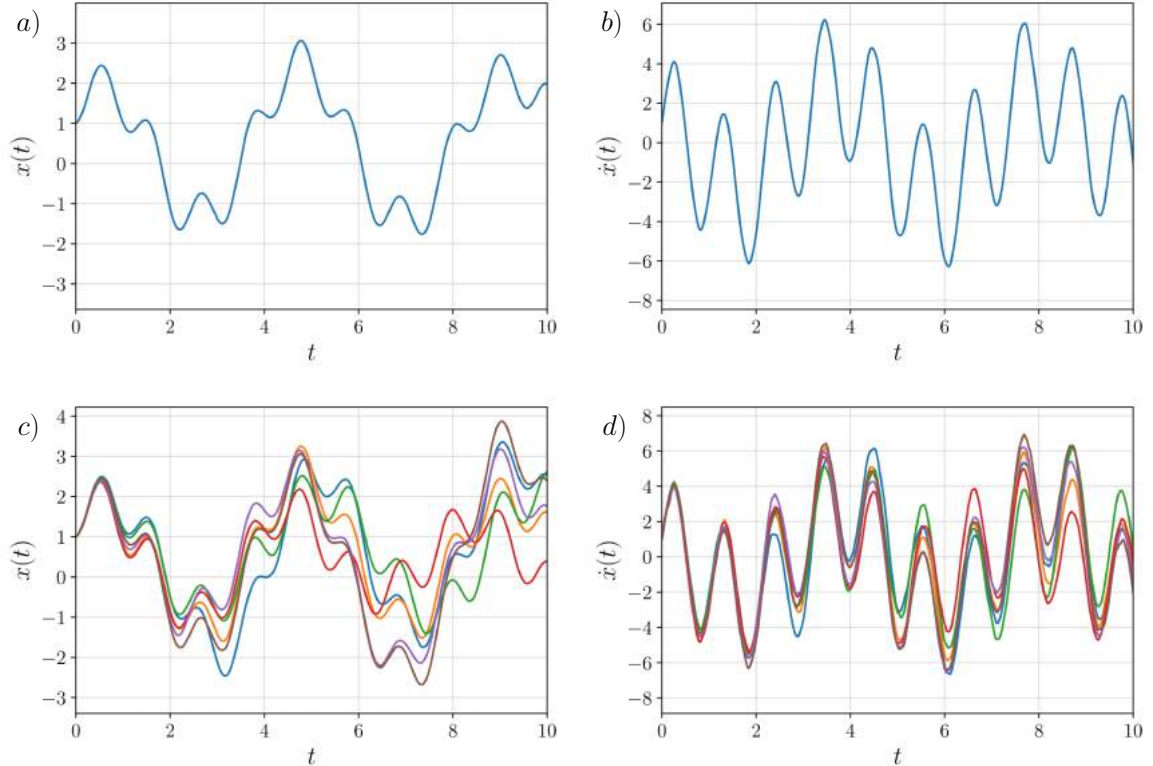


Figure 1: Panel (a) and (b): fragments of exemplary particle trajectory  $x(t)$  and particle velocity  $\dot{x}(t)$ , respectively, resulting from deterministic ( $D = 0$ ) Langevin equation (12). Parameters are set to the following values:  $m = 0.5$ ,  $a = 10$ ,  $\omega = 5.95$ ,  $f = 0.5$ ,  $\gamma = 1$  and initial conditions are given by  $x(0) = 1$ ,  $\dot{x}(0) = 0.5$ . Panel (c): a collection of trajectories  $x(t)$  of 6 particles moving in the system governed by equation (12) with  $D = 0.001$ . All particles are subjected again to the same parameter values, but the trajectories differ by the thermal noise realization. Panel (d): velocity curves  $\dot{x}(t)$  for particles presented in panel (c). The directed velocity calculated based on presented parameters, additionally averaged over different initial conditions ( $x(0) \in [0, 1]$ ,  $\dot{x}(0) \in [-2, 2]$ ) is equal to  $\langle v \rangle = 1.83$ .

phenomena that contradict our everyday experience should not be a surprise. In this section we will discuss the phenomenon of negative mobility, i.e. the particle transport directed *opposite* to the direction indicated by an external static force applied to the system.

The *mobility* describes particle's ability to move through the medium in response to currently operating forces. It can be investigated by tracking the relationship between force acting on the particle and mean particle velocity. Hence, the observable of the foremost interest in this study is *directed velocity* of the particle  $\langle v \rangle$ , which can be expressed by the formula (A1, sec: Model)

$$\langle v \rangle = \lim_{t \rightarrow \infty} \frac{1}{t} \int_0^t ds \langle \dot{x}(s) \rangle, \quad (13)$$

where  $\langle \cdot \rangle$  indicates averaging over all realizations of thermal noise as well as over initial conditions for the particle's position  $x(0)$  and its velocity  $\dot{x}(0)$ . The latter is obligatory for deterministic limit  $D \propto T \rightarrow 0$  when dynamics may be non-ergodic and results can be affected by specific choice of initial conditions [44].

In Fig. 1 we briefly illustrate the procedure of directed velocity  $\langle v \rangle$  determination. First, the collection of particle trajectories according to equation (12) is generated. In panel (a) we present an exemplary fragment of trajectory  $x(t)$  of such a particle for deterministic dynamics ( $D = 0$ ), as well as its velocity curve  $\dot{x}(t)$  in panel (b). Different particle trajectories start

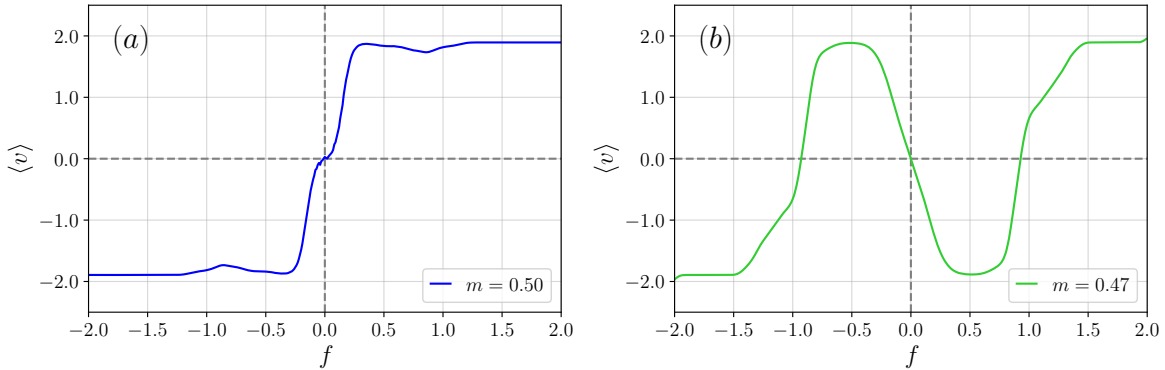


Figure 2: Panel (a): the directed velocity curve  $\langle v \rangle$  as a function of external force  $f$  depicted for parameters presented in Fig. 1:  $m = 0.5$ ,  $a = 10$ ,  $\omega = 5.95$ ,  $D = 0.001$ ,  $f \in [-2, 2]$  and  $\gamma = 1$ . The curve consists of 400 points calculated for different  $f$  value, each based on  $10^4$  sampled particles trajectories. Panel (b): the example of directed velocity curve exhibiting negative mobility phenomenon for the same parameters as in panel (a), but now  $m = 0.47$ . It proves the system high sensitivity to even small changes in parameters values: for  $m = 0.47$  the negative mobility is present, while for slightly increased mass value  $m = 0.5$  the effect vanishes and the regular transport behaviour is observed.

to diverge when we include non-zero thermal noise in the equation (12). In panel (c) all particles are subjected to the same parameter values, but the trajectories differ by thermal noise realization. The given set of trajectories is then additionally multiplied by series of different initial conditions (initial particle position  $x(0)$ , initial particle velocity  $\dot{x}(0)$ ). Each particle trajectory is associated with particle velocity curve  $\dot{x}(t)$  shown in panel (d). From the whole spectrum of particles subjected to the same set of parameters  $\{m, a, \omega, f, D\}$ , the directed velocity  $\langle v \rangle$  is calculated according to equation (13). More details on the computation process is explained in section 4.

Due to the large parameter space and complex dynamics of equation (12) the emerging directed velocity-force curve is typically a nonlinear function of applied bias  $f$ . This relation can be expressed in a form

$$\langle v \rangle(f) = \mu(f) f, \quad (14)$$

where  $\mu(f)$  is a nonlinear particle *mobility*. From the symmetries related to Langevin equation it follows that directed velocity is odd as a function of the external force  $f$ , i.e.  $\langle v \rangle(-f) = -\langle v \rangle(f)$  and in consequence  $\langle v \rangle(f = 0) \equiv 0$  [45]. Since the observable of our interest is anti-symmetric around  $f = 0$ , we limit our further consideration to the positive bias  $f > 0$ . In general,  $\langle v \rangle$  is an increasing function of the static force  $f$  and as one would expect, resultant particle displacement follows the direction of the acting force  $f$ . In Fig. 2 (a) we plot the directed velocity curve versus external static force  $f$  for exemplary set of parameters considered in Fig. 1. For  $f > 0$  we observe  $\langle v \rangle = \mu(f) f > 0$  and thus the particle mobility is positive, i.e.  $\mu(f) > 0$ .

However, in the parameter space there exist also regimes for which the particle moves on average in the direction *opposite* to the applied bias, i.e.  $\langle v \rangle < 0$  for  $f > 0$ , exhibiting anomalous behaviour in the form of *negative mobility* phenomenon [38, 46], namely

$$\text{for } f > 0: \quad \langle v \rangle = \mu(f) f < 0 \implies \mu(f) < 0. \quad (15)$$

This non-intuitive effect is presented in Fig. 2 (b). The velocity curve responds with the sign opposite to the force  $f$  and in consequence  $\langle v \rangle < 0$  for  $f > 0$ : the negative mobility is observed. If the value of  $f$  is high enough, the  $\langle v \rangle$  curve coincides with the force sign again. The plots drawn for a symmetrical range of the  $f$ -axis indeed shows the anti-symmetric shape

of the  $\langle v \rangle(f)$  curve. It is important to notice here that considered system is very sensitive to any changes in parameter values. The curves presented in Fig. 2 are plotted for almost identical set of parameters, they differ only in the mass value. The negative mobility effect visible for  $m = 0.47$  (panel (b)) vanishes completely when  $m = 0.5$  (panel (a)).

At first one might object that this phenomenon is inconsistent with the fundamental laws of physics. According to Newton's second law, when force acting on the particle increases from  $f = 0$  to a finite value, one should always expect a finite acceleration directed in the same course, and thus a change in velocity to a finite value of the same sign. However, this conclusion is not valid for nonlinear dynamics, where we cannot simply use the superposition principle for linear equations and totalize all other forces already present in the system for  $f = 0$  with the effect of the external force  $f$ . In presented model (12) we are dealing with nonlinear dynamics evidenced by the existence of the term  $-U'(x)$ .

Moreover, one might also indicate that directed velocity  $\langle v \rangle$  opposite to a static force  $f$  contradicts thermodynamic stability criteria, the principle of Le Châtelier, and ultimately the second law of thermodynamics. Again, such an argument is no longer conclusive for out of equilibrium systems. This is guaranteed by the periodic driving term  $a \cos(\omega t)$  in equation (12).

Hence, it should be emphasised that the key prerequisite for the occurrence of the negative mobility effect is nonlinear system driven far from thermal equilibrium into a time-dependent nonequilibrium state [38, 40, 46]. To further dispel doubts, it is also worth mentioning that the presence of inertial term in equation (12) is likewise indispensable - in the case of one-dimensional *overdamped* dynamics of Brownian motion the negative mobility was proven not to emerge [46].

### 3.2 The role of system parameters

The exploration of five-dimensional parameter space  $\{m, a, \omega, D, f\}$  of equation (12) is highly challenging. It is difficult to predict any relationship between the presence of negative mobility and the parameters configuration, since equation (12) is nonlinear and highly sensitive to any changes in parameter space. Observed for a fixed set of parameters, it can suddenly vanish when one of the parameters is slightly changed. For another configuration of the parameter space it can last for a very wide parameters range. In this section we look closer at the effect of parameters on negative mobility, and using numerical methods, we investigate more deeply the features of this phenomenon.

In our research we adopted the following strategy. We numerically simulated dimensionless Langevin equation in a form of (7) or (12) for wide range of parameter values, namely for  $a \in [0, 25]$ ,  $\omega \in [0, 20]$ ,  $m \in [0.01, 10]$  or  $\gamma \in [0.01, 10]$  and for several values of  $f \in [0, 2]$  and  $D \in [10^{-5}, 10^{-1}]$ . Then, we explored obtained data in order to isolate the parameter regimes for which negative mobility is observed. Among all those regimes we sought for any correlations that might indicate a parameter influence on negative mobility course. For better clarity we decided to present the data on two-dimensional maps, which enables us to illustrate a connection between the studied phenomenon and two chosen parameters. The examples of such maps are shown in Fig. 3, 4 and 5. The color scale corresponds to directed velocity values and blue areas indicate negative mobility regimes, i.e.  $\langle v \rangle < 0$ . Based on these three figures, we discuss the potential impact of individual parameters on this phenomenon. The data presented here was obtained according to the equation (12).

Let us first analyze the effect of static force  $f$ . In Fig. 3 we introduce four two-dimensional maps of directed velocity  $\langle v \rangle$  for different values of  $f$ : panel (a)  $f = 0.2$ , (b)  $f = 0.4$ , (c)  $f = 0.6$ , (d)  $f = 0.8$ . Each map is plotted for identical ranges of frequency  $\omega$  (Y-axis) and amplitude  $a$  (X-axis). At first glance one can notice that the maps are full of band-like structures, where the stripes of negative velocity are interspersed with the stripes of positive velocity and the difference in its magnitude in the neighbouring regions can be significant.

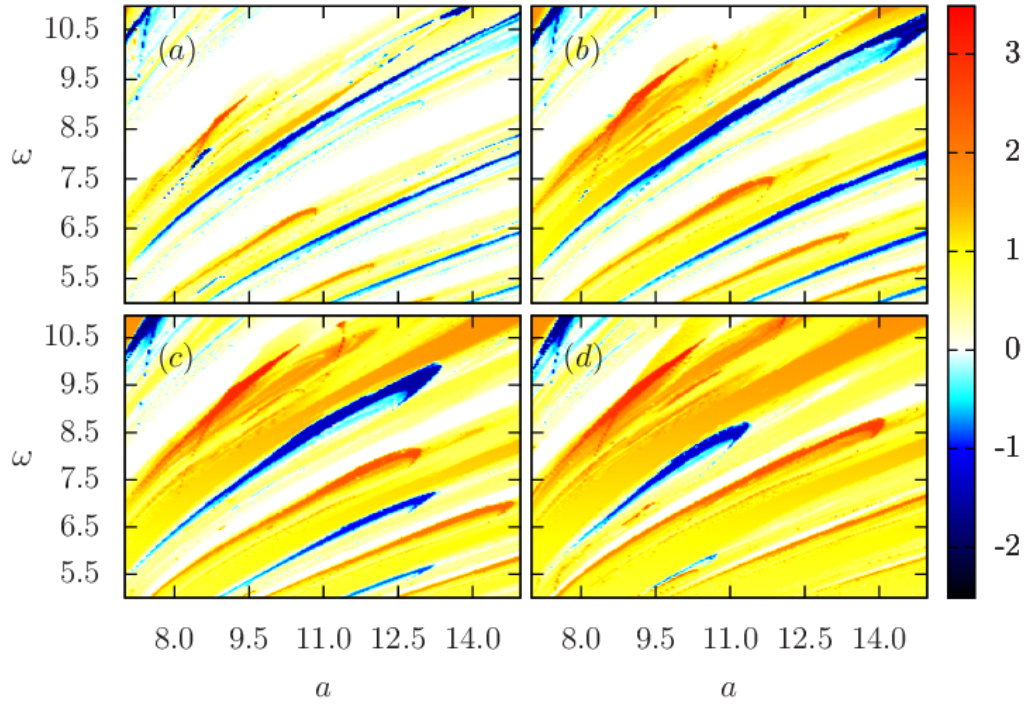


Figure 3: Directed velocity  $\langle v \rangle$  of Brownian particle as a function of the amplitude  $a$  and the frequency  $\omega$  of the external unbiased harmonic driving  $a \cos(\omega t)$  is shown for different values of the bias  $f$  with  $D = 0$  and  $m = 0.1$ . Panel (a)  $f = 0.2$ , (b)  $f = 0.4$ , (c)  $f = 0.6$ , (d)  $f = 0.8$ . The blue areas indicate negative mobility regimes.

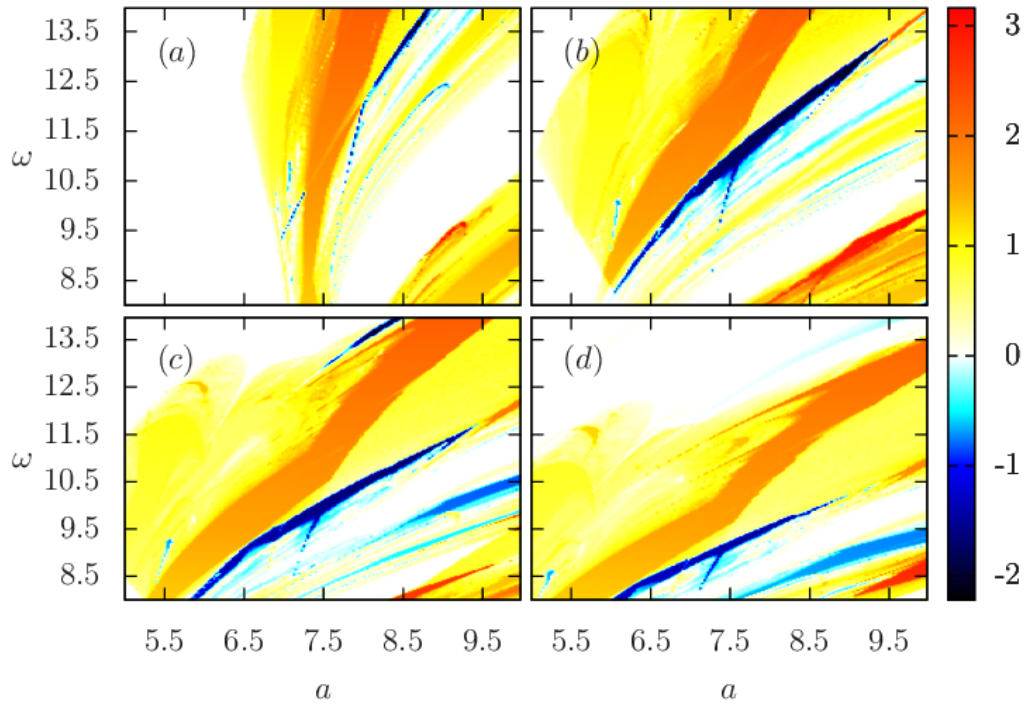


Figure 4: The directed velocity  $\langle v \rangle$  versus the amplitude  $a$  and the frequency  $\omega$  is presented for different values of the particle mass  $m$  with  $D = 0$  and  $f = 0.5$ . Panel (a)  $m = 0.05$ , (b)  $m = 0.1$ , (c)  $m = 0.15$ , and (d)  $m = 0.2$ . The blue areas indicate negative mobility regimes.

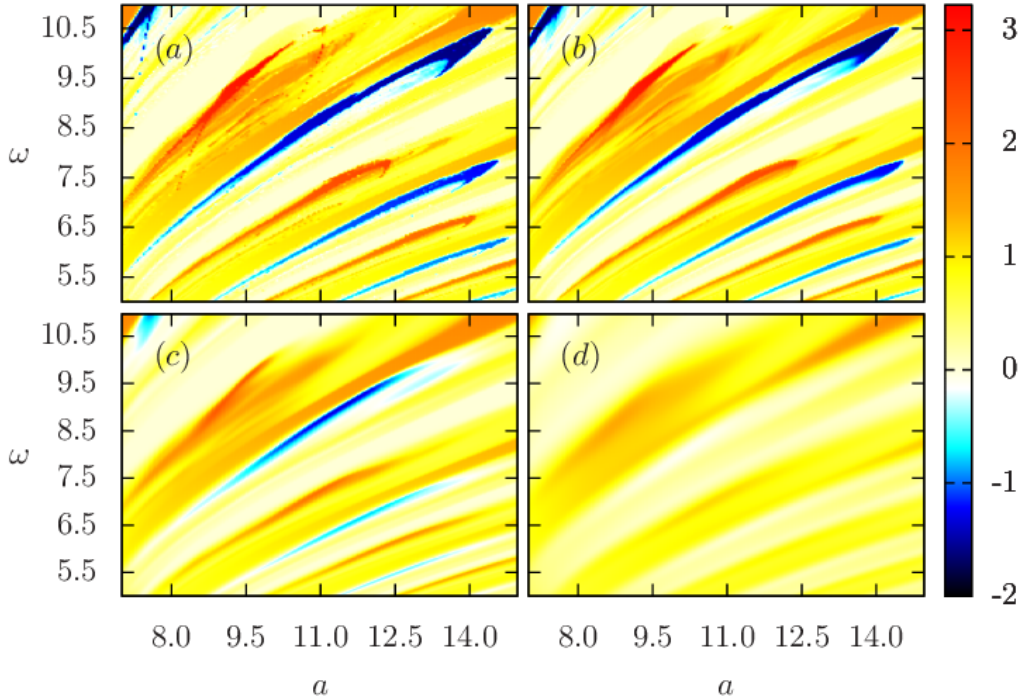


Figure 5: Directed velocity  $\langle v \rangle$  versus the amplitude  $a$  and the frequency  $\omega$  is depicted for different values of thermal noise intensity  $D$  with  $m = 0.1$  and  $f = 0.5$ . Panel (a)  $D = 0$ , (b)  $D = 10^{-5}$ , (c)  $D = 10^{-3}$ , (d)  $D = 10^{-2}$ . The blue areas indicate negative mobility regimes.

This observation applies to all maps presented in Fig. 3 – 5. For small  $f$  negative mobility areas form narrow bands stretched across the entire map. As force value rises higher, these bands become wider, but at the same time they slowly shrink, and finally disappear. This boils down to the conclusion that the greater the force  $f$  value, the less likely it is to encounter the negative mobility regimes. It is also consistent with our intuition – as static force  $f$  become larger and larger it eventually tends to dominate in the transport process.

The role of the particle mass  $m$  in negative mobility phenomenon seems to be non-trivial. Directed velocity  $\langle v \rangle$  maps depicted for different values of the mass  $m$  are shown in Fig. 4: panel (a)  $m = 0.05$ , (b)  $m = 0.1$ , (c)  $m = 0.15$ , and (d)  $m = 0.2$ . Again, the band-like structure slowly transfers as mass value becomes larger – it changes inclination and the pattern becomes more horizontal oriented. However, for higher values of  $m$  some new negative mobility bands appear, while at the same time blue areas tend to disappear in other regions. This effect suggests that there may exist some optimal value of  $m$  for negative mobility to occur. Therefore, in addition to the charts presented in Fig. 4, we simulated two-dimensional maps of directed velocity  $\langle v \rangle$  on  $(a, \omega)$  plane for nearly 110 values of mass  $m \in [0.01, 10]$ . For each  $m$  value we determined the percentage of points with negative velocity in the analyzed parameter space. The result is introduced in Fig. 6. Indeed, we observe a maximum in the negative mobility fraction curve. This calculation has been carried out for several values of external force  $f$  and noise intensity  $D$ . As the force value becomes larger, the fraction of negative mobility for given mass decreases and the curve maximum shifts to the right, i.e. towards higher mass values. The increase of the noise intensity  $D$  does not change the shape of curve, but it rather reduces it. Hence, one can conclude that the thermal fluctuations in the system disturb the negative mobility regimes.

This conclusion is confirmed in Fig. 5, where we present directed velocity maps for different values of the noise intensity  $D$ : panel (a)  $D = 0$ , (b)  $D = 10^{-5}$ , (c)  $D = 10^{-3}$ , (d)  $D = 10^{-2}$ . Along with the increase in the noise value, the structure visible in the maps blurs, areas of

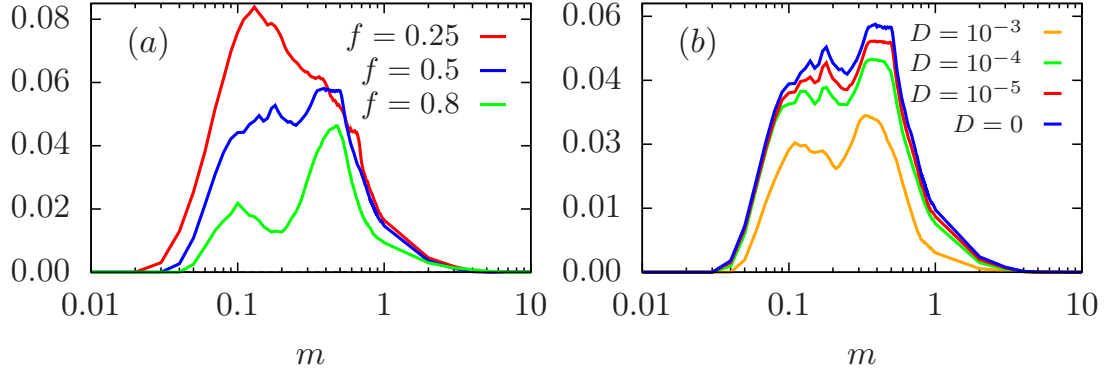


Figure 6: The fraction of negative mobility area as a function of mass  $m$  in the analyzed parameter space:  $a \in [0, 25]$  and  $\omega \in [0, 20]$  is presented in panel (a) for  $D = 0$  and different values of the bias  $f$  and in panel (b) for  $f = 0.5$  and several noise intensity values  $D$ . The blue curves in both charts correspond to the same parameter set.

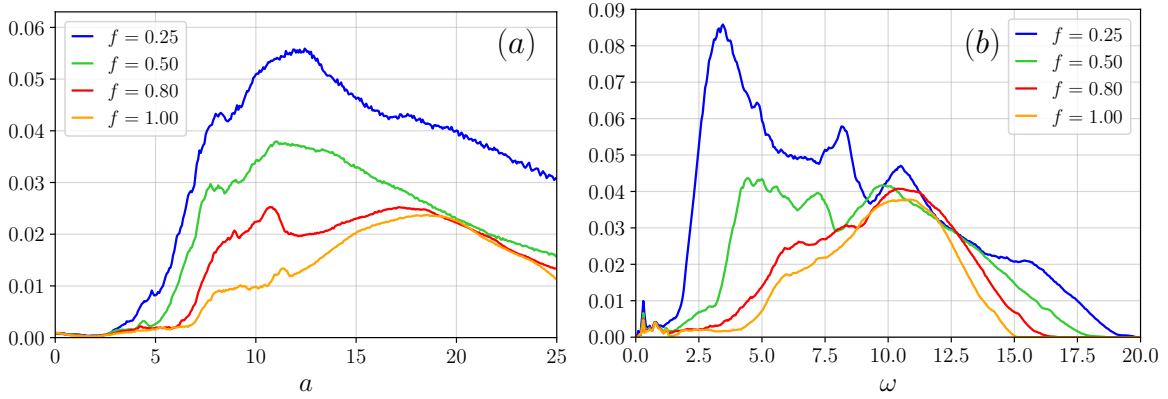


Figure 7: The fraction of negative mobility area in the analyzed parameter space,  $a \in [0, 20]$ ,  $\omega \in [0, 20]$ ,  $m \in [0.1, 10]$  for different values of bias  $f$ . Panel (a): for periodic driving amplitude  $a$  and panel (b): for periodic driving frequency  $\omega$ . The noise intensity value is set to zero, i.e.  $D = 0$ .

negative mobility vanish and finally negative and positive velocity bands disappear almost completely. This is again in line with our intuition: the greater the noise  $D$ , the fewer areas are highlighted and the whole plane of directed velocity tends to a common average state.

Parameters that shape harmonic driving force  $a \cos(\omega t)$  in the system have been chosen to figure as the axes of two-dimensional maps. One cannot definitely say what is the direct trend for negative mobility as  $a$  and  $\omega$  increase or decrease in the system. Similar to the case of mass  $m$ , here we also meet optimal values which are highly dependent on other parameters value, e.g. static force  $f$ . In Fig. 7 we present a fraction of negative mobility dependent on amplitude  $a$  and frequency  $\omega$  for several values of static force  $f$ . In panel (a) all curves are relatively similar and they decrease as the static force  $f$  value becomes higher. At the same time the maximum of the curves is shifted to the right, towards the higher values of amplitude  $a$ . In panel (b) a prominent fraction of negative mobility observed for low frequencies  $\omega$  disappears for  $f > 0.5$ . All curves share a common maximum region, although for curves plotted for  $f < 0.5$  it is only a local extreme. Moreover, we can notice that for  $a < 5$  and  $\omega > 15$  the negative mobility is rather rare to occur.

Although there is no significant correlation between parameter combination and occurrence of negative mobility, the studied system is full of interesting effects accompanying this pheno-



External force $f$	Percentage of negative mobility
$f = 0.05$	4.62%
$f = 0.1$	4.20%
$f = 0.3$	3.29%
$f = 0.5$	2.11%
$f = 0.8$	1.51%
$f = 1.0$	1.21%
$f = 1.5$	0.28%

Table 3: Percentage of negative mobility regimes per  $400 \times 400 \times 400 = 64 \times 10^6$  parameter sets generated for area:  $a \in [0, 25], \omega \in [0, 20], m \in [0.1, 10]$  and  $D = 0$  for several values of  $f$ .

menon. Again, we cannot predict where the directed velocity happens to appear negative in the parameter space, but we can *numerically simulate* the system behaviour and in this way observe its dynamics. There exist many surprising properties of negative mobility regimes, which are too compound to be illustrated by two-dimensional graphs. Therefore in addition to presented figures we also prepared a collection of short animation in the form of the ".gif" files, which can be seen on the website: [https://github.com/aslapik/negative\\_mobility](https://github.com/aslapik/negative_mobility). In these animations one can observe how negative mobility regimes develop according to the parameter changes and how this evolution, although seemingly regular and ordered, forms extremely complicated structures.

### 3.3 The origin

At this point it is important to question the origin of the negative mobility phenomenon. We distinguished three different mechanisms responsible for this effect rooted in: (1) deterministic chaotic dynamics, (2) deterministic non-chaotic dynamics and (3) thermal fluctuations. The second one, to the best of author knowledge, has never been described in the literature before (A1).

The most common reason for existence of negative mobility effect is complex chaotic dynamics of the system. In Fig. 8 in panel (a) directed velocity  $\langle v \rangle$  is plotted versus external force  $f$ . The curve is non-linear and for  $f \approx [0.1, 0.7]$  negative mobility occurs, i.e.  $\langle v \rangle < 0$ . In panel (b), for  $f = 0.66$ , selected from negative interval, we investigate the impact of thermal noise on directed velocity  $\langle v \rangle$ . Indeed one can observe negative mobility existence only for relatively small values of  $D$ . As noise intensity increases, the directed velocity curve rises up and finally it becomes positive. Hence, negative mobility has purely deterministic origin here and thermal fluctuations has destructive impact on this effect. In panel (c) the bifurcation diagram of  $\langle v \rangle$  is shown for the same set of parameters as in panel (a) ( $D = 0$ ). Each blue dot represents an attractor for the asymptotic long time directed velocity  $\langle v \rangle$ . For almost all values of  $f$  in considered range there exist the continuum of directed velocity solutions. This facts suggests that the system is mostly chaotic in this interval. In order to confirm this conclusion in panel (d) we depicted the maximal Lyapunov exponent  $\lambda$  for the parameter set presented in panel (a). The curve is positive in almost entire interval of  $f$  for which negative mobility occurs. Therefore, in the presented parameter regime negative mobility phenomenon is indeed induced by chaotic deterministic ( $D = 0$ ) dynamics of the system described by equation (12).

Appearance of the noise term in equation (12) has usually a devastating consequence, i.e. the regimes of negative mobility present in deterministic parameter space wane, and as the noise intensity increases, they completely vanish. However, for a certain combination of parameters negative mobility can be *induced* by a proper value of the noise intensity  $D$  [38, 47]. This effect is illustrated in Fig. 9. In panel (a) the directed velocity  $\langle v \rangle$  is presented

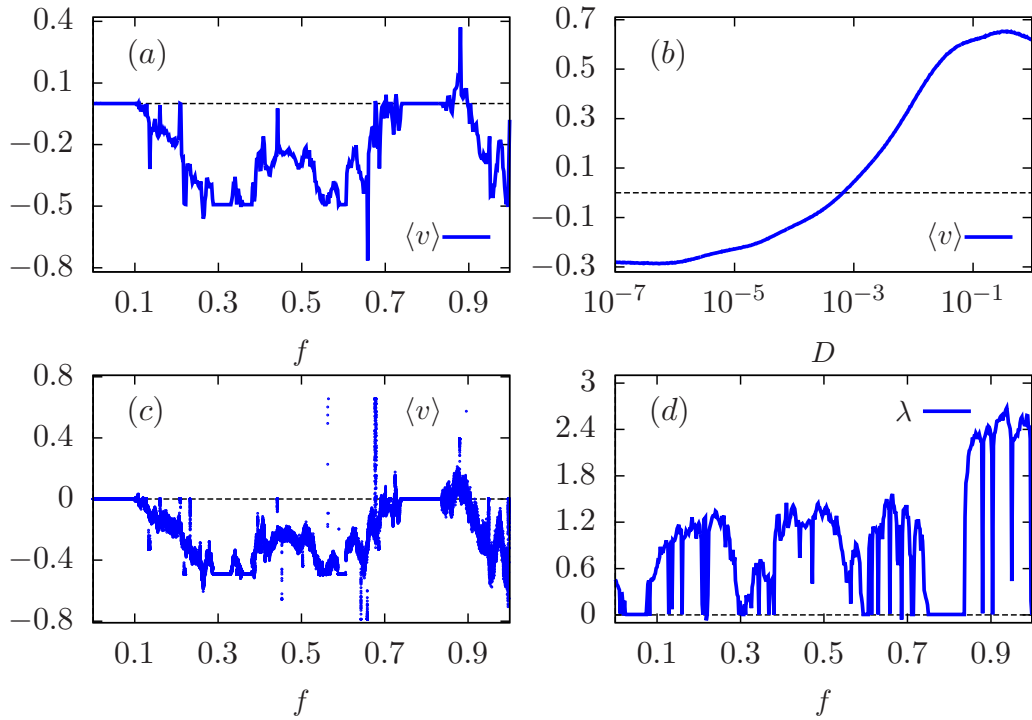


Figure 8: The negative mobility of Brownian particle induced by the deterministic chaotic dynamics. Panel (a) the directed velocity  $\langle v \rangle$ , (c) bifurcation diagram of the directed velocity  $\langle v \rangle$ , (d) the maximal Lyapunov exponent  $\lambda$  as the function of the external static bias  $f$  with  $D = 0$ . Panel (b) the directed velocity  $\langle v \rangle$  versus thermal noise intensity  $D$  for  $f = 0.66$ . Parameter values:  $m = 0.0555$ ,  $a = 8.55$ ,  $\omega = 12.38$ .

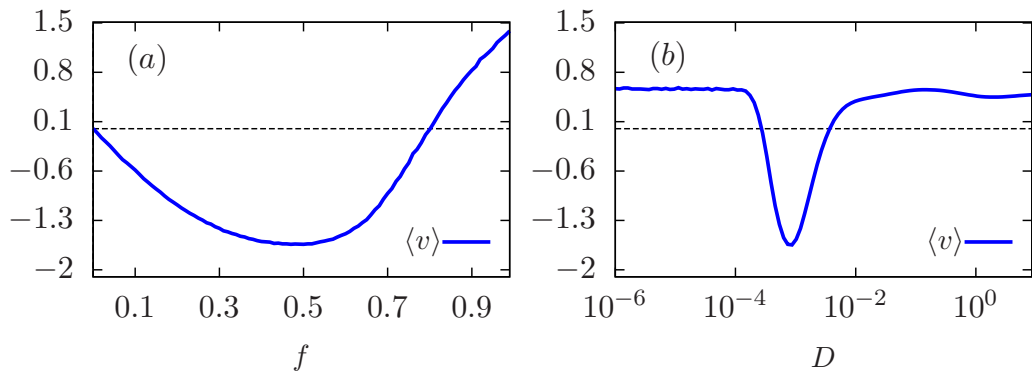


Figure 9: The negative mobility of the Brownian particle induced by thermal fluctuations. The directed velocity  $\langle v \rangle$  is presented versus external static bias  $f$  in panel (a) and versus thermal noise intensity  $D$  in panel (b). Parameter values:  $a = 8.55$ ,  $\omega = 12.38$ ,  $m = 0.1047$ ,  $f = 0.5$  and  $D = 0.0009$ .

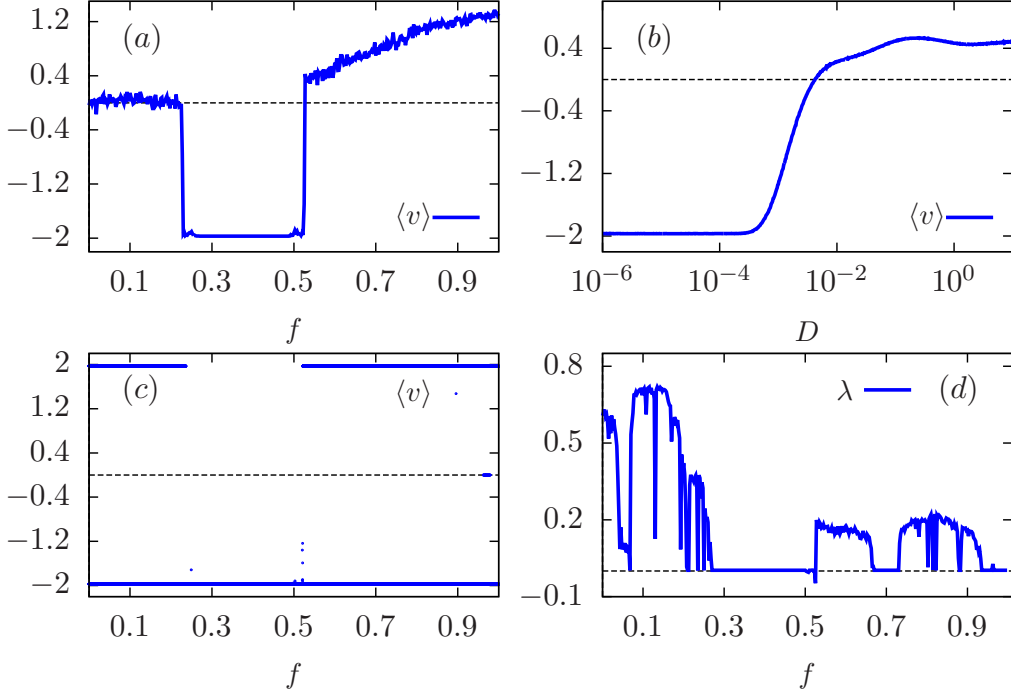


Figure 10: The negative mobility of the strongly damped Brownian particle  $m \ll 1$  induced by the deterministic non-chaotic dynamics. Panel (a) the directed velocity  $\langle v \rangle$ , (c) bifurcation diagram of the directed velocity  $\langle v \rangle$ , (d) the maximal Lyapunov exponent  $\lambda$  as the function of the external static bias  $f$  with  $D = 0$ . Panel (b) the directed velocity  $\langle v \rangle$  versus thermal noise intensity  $D$  for  $f = 0.5$ . Other parameters values:  $m = 0.1$ ,  $a = 8.55$ ,  $\omega = 12.38$ .

again as a function of external force  $f$  for non-zero noise intensity  $D = 0.0009$ . Negative mobility emerges in the wide interval for  $f \in [0, 0.8]$ . In panel (b) directed velocity is plotted against the noise intensity  $D$  for  $f = 0.5$ , i.e for static force value correlated with the strongest negative mobility effect. Unlike the previous case, here the effect is only visible for a narrow interval of the noise intensity  $D$ . Both low and high noise values eliminate this effect. Only a very well defined noise value around  $D = 10^{-3}$  can induce negative mobility effect in given regime of parameters.

The third mechanism of negative mobility formation is rooted in the non-chaotic dynamics of the system (12). The example of such parameters regime is presented in Fig. 10. In panel (a) directed velocity curve depicted for external force  $f$  exhibits negative mobility in the interval  $f \approx [0.25, 0.5]$ . The same quantity, depicted for  $f = 0.5$  versus thermal noise intensity  $D$  demonstrates destructive impact of noise on negative mobility effect. It proves that deterministic dynamics stands behind negative directed velocity  $\langle v \rangle$  value in presented parameters regime. The bifurcation diagram in panel (c) shows a surprising simple structure of attractors for directed velocity  $\langle v \rangle$  in deterministic case. There are two asymptotically stable solutions corresponding to  $\langle v \rangle = \pm 2$ . What is interesting, in the negative mobility window  $f \approx [0.25, 0.5]$  only one attractor  $\langle v \rangle = -2$  survives. This suggests that in the considered parameter regime deterministic dynamics is non-chaotic, but still negative mobility manifests itself. The diagram of maximal Lyapunov exponent  $\lambda$  in panel (d) confirms this fact: the  $\lambda$  is positive when two attractors coexists (chaotic dynamics) and  $\lambda = 0$  for single-attractor-window related to negative mobility interval, pointing to *non-chaotic* dynamics. Again, to the best of author knowledge, this kind of mechanism has never been reported before.

In general, the negative mobility is low populated in the parameter space of equation (12) and due to the lack of correlation with particular parameter values it is not easy to

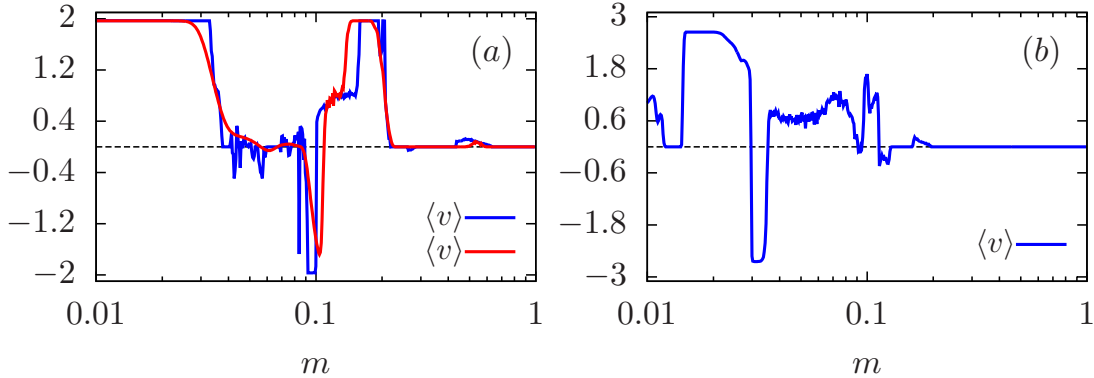


Figure 11: The directed velocity  $\langle v \rangle$  of the driven Brownian particle versus its inertia  $m$ . Panel (a):  $a = 8.55$ ,  $\omega = 12.38$  and  $f = 0.5$ . The blue curve is for the deterministic case  $D = 0$  and the red curve is for the noisy system with  $D = 0.0009$ . Panel (b):  $a = 9.845$ ,  $\omega = 16.64$ ,  $f = 0.25$  and  $D = 10^{-5}$ . Negative mobility effect is present for relatively small values of mass  $m \ll \gamma = 1$ .

detect. For example, for a single run of simulation with given parameter set  $a \in [0, 25]$ ,  $\omega \in [0, 20]$ ,  $m \in [0.1, 10]$ ,  $f = 0.5$  and  $D = 0$  we generate  $400 \times 400 \times 400 = 64 \times 10^6$  values of directed velocity, from which only 2.11% exhibit negative mobility. Numerical analysis shows that this percentage decreases as external force  $f$  value becomes higher. The percentage of the negative mobility occurrence in presented regime for several values of  $f$  is shown in Table 3. More details on the mechanisms of this effect formation can be found in (A1).

### 3.4 Strong damping regime

The impact of inertia on the negative mobility phenomenon was a main topic of the first article (A1). Since the inertial term is often neglected when dissipation outweighs dynamics in equation (1), in so called *overdamped* cases, we wanted to investigate the negative mobility effect without using this approximation, i.e. for a *strong damping regime* for which  $m \ll \gamma = 1$ . We attempted to answer the question whether it is still possible to observe this phenomenon in such a case.

Omitting the inertial term in (1) enormously simplifies the modeling and in many cases it allows for analytical solution of the corresponding Fokker-Planck equation. However, properties and features which occur in the system with inertia term can completely disappear when the mass term is neglected. This is the case for negative mobility. As it turned out from our research, negative mobility indeed manifests itself even for relatively small masses, for strongly damped dynamics, i. e.  $m \ll \gamma$ . However, the inertial term is a key element for negative mobility formation and this effect cannot be observed for a one-dimensional dynamics in overdamped approximation, when  $m = 0$  [46].

An example of such parameter regime is shown in Fig. 11. In panel (a) we depict directed velocity  $\langle v \rangle$  of the Brownian particle versus its mass  $m$  for deterministic dynamics ( $D = 0$ ) and for noisy system ( $D = 0.0009$ ) for parameter set already used in Fig. 8-10. The minimum of directed velocity falls near  $m = 0.1$ . The curve smooths and the negative mobility interval shrinks as the thermal fluctuation appears. In panel (b) we observe directed velocity curve for different set of parameters – the negative  $\langle v \rangle$  occurs for significant smaller value of mass  $m$ , which undoubtedly indicates strong damping regime, since  $m \approx 0.03 \ll 1 = \gamma$ .

Moreover, one can also notice that the maximum of the curve for  $f = 0.25$  presented in Fig. 6 corresponds to  $m \approx 0.1$ . It means that for weak external force  $f$  we expect the maximum number of negative mobility regimes to arise for mass  $m$  an order of magnitude

smaller than friction coefficient  $\gamma = 1$ , that is for strong damping regime. Therefore, when adapting overdamped approximation one may lose significant information about the dynamics of the system – even for tiny value of mass  $m$  the dynamics of model (12) can be rich and may exhibit anomalous transport effects.

### 3.5 Negative mobility in experiments

The negative mobility effect for a one-dimensional dynamics was described theoretically in 2007 for a system very similar to one described in this study [38, 48]. A year later it was confirmed experimentally in the measurements involving determination of current-voltage characteristics of the microwaved-driven Josephson junction [49]. Since then this phenomenon has been a subject of many studies concerning electrokinetic effects, stochastic dynamics, laminar flow and transport in biological-based systems. Further examples of this effect has been described theoretically in companionship of coloured noise [50], white Poissonian noise [14, 47], dichotomous process [51] and for Brownian motion with presence of time-delayed feedback [52, 53], non-uniform space-dependent damping [54] and potential phase modulation [55]. Other illustrations include a vibrational motor [56], two coupled resistively shunted Josephson junctions [57, 58], active Janus particles in a corrugated channel [59], entropic electrokinetics [60] as well as nonlinear response of inertial tracers in steady laminar flows [61].

However, this phenomenon has also been examined in experimental research. In 2010 negative mobility has been observed for a system consisting of *colloidal particles* [24]. In this study the authors managed to observe the migration of colloidal beads in a structured microfluidic channel in the opposite direction to the static force, realized by a static dc-voltage potential. The experiment setup and microfluid device structure was based on the previous theoretical research [22]. In addition, it was noticed that negative mobility response is very sensitive to particles properties. It was found that not every species of particles subjected to the same conditions exhibits negative mobility. This opened the possibility of steering different particle species in opposite directions under identical experimental conditions. The proof-of-principle of such a separation scheme has been demonstrated in [62]. Focusing on two different species of colloidal beads, it has been possible to identified a suitable amplitude and frequency of ac-driving, such that one particle species exhibits negative mobility, whereas the other species responds in a classical transport, according to the direction of the bias.

Finally, in 2016 the scientists from Arizona University performed similar experiment involving intracellular organelles [25]. Therefore, negative mobility opened up new, fascinating perspectives for the separation of micrometre-sized colloidal particles or even biological compounds of comparable size, like cells or cell organelles. The prominent results of these experiments, together with previously mentioned discovery of special directed velocity regimes, led us to the idea of *separation mechanisms* based on negative mobility phenomenon, which are to be introduced in the next sections of this guidebook.

## 4 Computational details

In order to investigate the transport behaviour of the considered model we performed a large number of numerical simulations for equation (7) and (12). Before introducing the idea of separation mechanisms, we would like to briefly discuss the computational details of performed simulations.

The computation is based on the software created by one of the authors of the published articles (JS). It is an optimized program coded in C++ language that performs numerical integration grounded on the predictor-corrector algorithm [63, 64]. The fundamental advantage of this software is the use of *parallel computation* based on graphical processing units technology

(GPU). Since the particle trajectories are mutually independent and no data sharing needs to take place between them, the simultaneous calculation of paths for different realizations of noise and initial conditions enables a significant speed up of the computation time. Depending on the algorithm implementation, it allows to accelerate the calculations of the order of  $10^3$  times compared to classical computing based on processors (CPU) performance. This method of coding is becoming more and more popular in computational physics. More information about GPU computing and its efficiency can be found in [65] and [66].

Each simulation process produces a directed velocity  $\langle v \rangle$  data set consisting of  $400 \times 400 \times 400 = 64 \times 10^6$  values corresponding to different regimes of model parameters. The value of directed velocity  $\langle v \rangle$  for every parameter combination is calculated by averaging over 4096 particle trajectories generated independently for a range of initial conditions distributed uniformly over the intervals  $x_0 \in [0, L = 1]$  and  $v_0 \in [-2, 2]$ . Each trajectory is spanned over 1000 periods  $2\pi/\omega$  of the external time-periodic force with 400 – 800 numerical integration steps per period. Therefore, producing one trajectory of the system requires minimum  $4 \times 10^5$  integration steps. For deterministic dynamics, when the thermal noise is absent ( $D = 0$ ), it took on average 4 full days to simulate the whole data set. For non-zero fluctuations, even up to 8 days were needed. All simulation have been performed using GeForce GTX TITAN graphics cards manufactured by Nvidia.

The generated data sets have been thoroughly analyzed for the presence of negative mobility phenomenon. The examination has been performed by the use of Python scripts specially prepared for this purpose. A careful investigation of the obtained data sets was a difficult and time-consuming procedure. However, at this stage of our research we were able to observe the effects and mechanisms presented in this guidebook and in the accompanying articles. It turned out that analyzed data contains a whole range of interesting regimes related to negative mobility. In the published results we decided to exemplify the most prominent outcomes.

## 5 Separation mechanisms

Separation and fractionation of micrometer-sized and submicrometer-sized particles has growing importance in both research and industrial applications, including chemical and biological research as well as medical diagnostics. Although there exist many methods of isolating particles based on both passive and active techniques – from classical filtration and dielectrophoresis to optical, magnetic and acoustic sorting, to name just a few – more efficient and innovative methods are constantly being sought [67, 68]. For example, in the latest report on particle separation in passive microfluidic devices [68] the authors described a whole range of different methods for particle separation. They highlighted the significant improvement in design productivity and fabrication of microseparators since 2014. However, they also pointed out the high need of simple portable solutions to separate and detect the particles. The achievement of a low-cost and simple setup is still required for practical applications such as medical and clinical ones. Moreover, clogging and throughput remain still a challenge for researchers.

The separation mechanism we propose in this dissertation is based on described phenomenon of *negative mobility*. In terms of Brownian motion we consider the following problem: is it possible to use negative mobility in order to mechanically separate a mixture of various particles in a controlled manner? A number of experiments involving negative mobility already reported on successful separation of two types of particles with different sizes in a microfluidic devices [24, 25]. However, no investigation on how to isolate *desired* particles among others has been conducted. Here we reveal conditions that guarantee controlled particles isolation by the means of difference in their mobility. Since in the data sets considered at the beginning of our research we encountered unusual parameter regimes for which negative mobility is

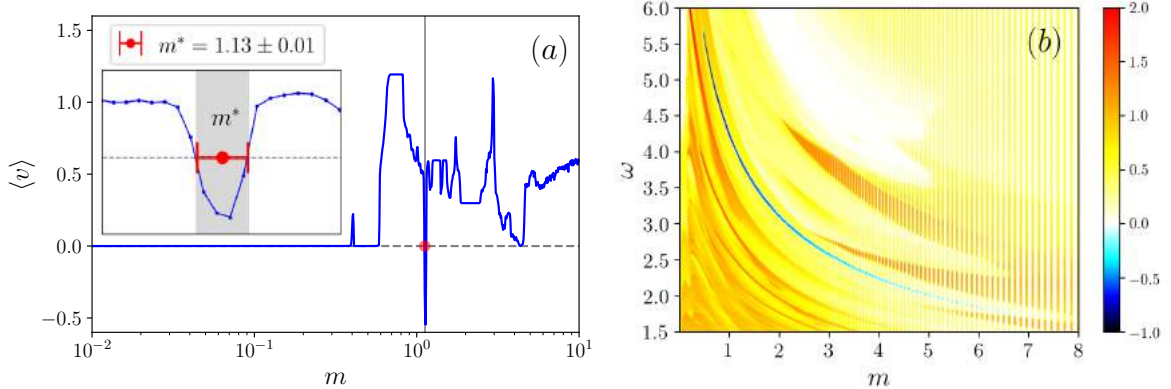


Figure 12: Panel (a): the directed velocity  $\langle v \rangle$  as a function of particle mass  $m$ . The negative mobility is observed only for a very narrow interval of mass  $m$ . In the inset we present the enlarged area showing the negative mobility interval (grey area in the plot). Parameter values:  $a = 5.125$ ,  $\omega = 3.75$ ,  $f = 1$ ,  $D = 0.0001$ . Panel (b): two-dimensional map of directed velocity  $\langle v \rangle$  of the Brownian particle as a function of external periodic driving frequency  $\omega$  and particle mass  $m$ . The magnitude of velocity  $\langle v \rangle$  is illustrated by the colour scale where the shades of blue indicate negative mobility. Parameter values:  $a = 5.9375$ ,  $f = 1$ ,  $D = 0.0001$ .

observed only for a specific mass value among the whole mass interval, we came up with an idea of *mass-based particle separation*.

## 5.1 The mass-based separation mechanism

The first separation strategy is based on the data sets obtained from the simulations of the Langevin equation rescaled according to the units given in (10). This scaling enables to investigate the five-dimensional parameter space:  $\{m, a, \omega, f, D\}$ .

As already mentioned, the idea of particle separation arose after the discovery of certain parameter regimes, for which negative mobility was observed only for a very narrow interval of mass  $m$ . In Fig. 12 in panel (a) we depict an example of such a data set. Among many particles with masses from a wide interval  $m \in [0.01, 10]$  only those with mass  $m^* \approx 1.13$  will move in the opposite direction to the acting bias  $f = 1$ , because here  $\langle v \rangle < 0$ . All other particles with positive velocity  $\langle v \rangle > 0$  will follow the direction of the bias  $f$ . As a consequence, after a finite time, the particles with mass close to  $m^* \approx 1.13$  will be separated from the others. The  $m^*$  value stands here for a mass point situated in the middle of the negative directed velocity interval.

This interesting transport property can be very promising for particle separation as long as we can somehow control and adjust the mass value  $m^*$  of the particle. Hence, we attempted to explore the parameter space of the Langevin equation (12) in order to find regimes that would enable us to control the occurrence of the negative mobility by tuning just one parameter value. After comprehensive numerical analysis we identified all regimes for which negative directed velocity appears only for a small interval of mass  $[m^* - \delta m, m^* + \delta m]$ . Among selected parameter regimes we focused on those which reveal a specific functional dependence between the isolated mass  $m^*$  and one of the parameter  $\{a, \omega, f, D\}$ .

In Fig. 12 in panel (b) we present an example of directed velocity map as a function of external driving frequency  $\omega$  and dimensionless mass  $m$ . The value of directed velocity  $\langle v \rangle$  is depicted by a colour scale. Blue area on the plot indicates negative velocity, i.e. occurrence of negative mobility. Here, for a given value of  $\omega$  negative mobility is present only for a very narrow interval of mass  $m$ . Therefore, by applying parameters presented in Fig. 12 (b), namely setting  $f = 1.0$ ,  $a = 5.9375$ ,  $D = 0.0001$ , one is able to tune up negative mobility to

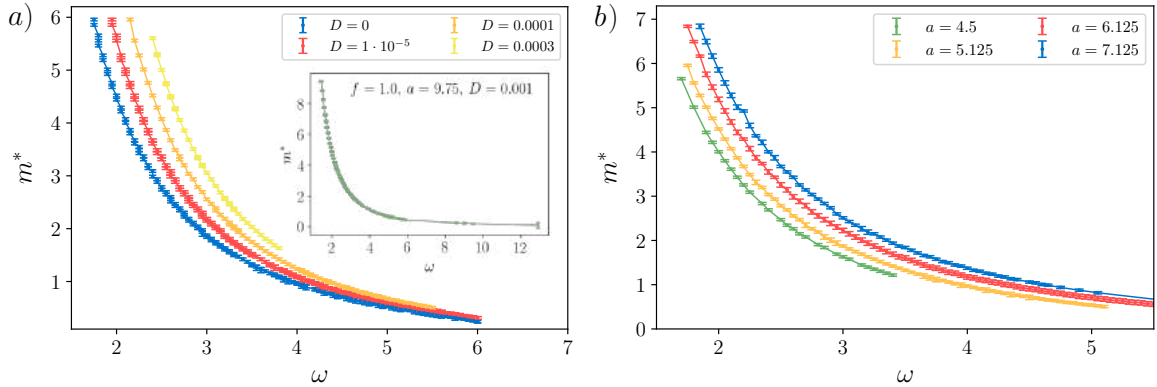


Figure 13: Panel (a): dependence of mass  $m^*$  tailored for separation as a function of the external driving frequency  $\omega$  for different temperatures  $D \propto T$  with fixed values of  $a = 5.125$  and  $f = 1$ . Originally the curves overlap at the deterministic line  $D = 0$ , but have been manually separated to improve readability. Panel (b): the same characteristics shown for various values of the external driving amplitude  $a$  with  $D = 0.0001$  and  $f = 1$ . In the inset of panel (a) we present additional parameter regime with very wide mass  $m^*$  interval.

given mass value  $m \in [0.5, 7]$  by changing only the value of frequency  $\omega$ , and as a consequence, isolate particles with chosen mass  $m$  from the others.

In order to examine our results more carefully we isolated negative velocity area from two-dimensional map into a functional graph. On the horizontal axis we depicted  $\omega$  values. On the vertical axis the  $m^*$  for given  $\omega$  value is marked by a point, while the interval of width  $2\delta m$  is indicated as an error bar. As depicted in Fig. 12 (a), the  $m^*$  is the mass value situated in the middle of the mass interval for which negative mobility appears. The directed velocity is classified to be negative if  $\langle v \rangle \leq -0.01$ .

In Fig. 13 in panel (a) negative mobility is plotted against frequency  $\omega$  and mass  $m$  for several values of noise intensity  $D$ . Since originally the curves overlap, i.e. all data sets coincide the deterministic dynamic case with  $D = 0$ , the subsequent plots have been shifted to the right in order to improve readability of the chart. The data sets prove that the thermal fluctuations does not affect location of the negative mobility area, but rather cause them to shrink. For  $D = 0.0003$  only few points remain. In the subplot of Fig. 13 (a) another regime of parameters is presented for  $f = 1.0$ ,  $a = 9.75$  and relatively high noise value  $D = 0.001$ . In this case the points of negative mobility emerge over nearly entire area of investigated mass interval, i.e for  $m \approx [0.01, 10]$ . In Fig. 13 in panel (b) analogues graph is shown for different values of amplitude  $a$ . The negative mobility in this parameters regime is present for a wide range of amplitude values, from  $a \approx 4$  to  $a \approx 8$ .

The dependence presented in Fig. 13 can be also identified for negative mobility regimes in the domains of  $m^*(a)$  and  $m^*(f)$ , however, in these cases it covers only small subintervals of mass axis. It is also worth mentioning, that here we focused on the parameter regimes which enable us to use negative mobility mechanism in order to select particles of given mass among the whole considered interval  $m \in [0.01, 10]$  unambiguously. There exist a wide range of other parameter regimes that enable to use this mechanism locally, i.e. regimes for which negative velocity is observed for  $m \approx m_1$  and  $m \approx m_2$  ( $m_1 \ll m_2$ ), which can still be useful in many situations while particle mass is limited to  $m \ll m_2$ .

At this point it may be interesting to verify how many points from the considered mass interval  $m \in [0.01, 10]$  can be triggered by the mechanism described in this section. For several values of static force  $f$ , we investigated deterministic data sets ( $D = 0$ ) and selected all such pairs of amplitude and frequency ( $a, \omega$ ) for which negative mobility was found only for one interval  $[m^* - \delta m, m^* + \delta m]$ . The results are shown on the graphs presented in Fig. 14. The



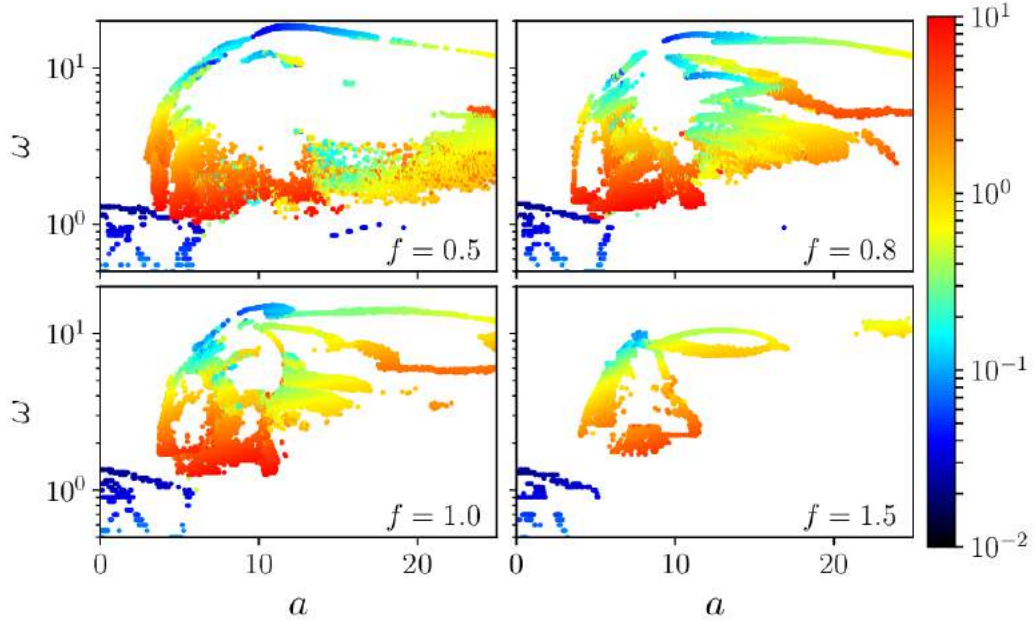


Figure 14: The mass  $m^*$  targeted for separation (color coded scale) by the negative mobility effect as a function of the external driving amplitude  $a$  and frequency  $\omega$  for different values of the bias  $f$ . Thermal noise intensity is set to zero  $D = 0$ .

color scale refers to the mass value which is shown on the logarithmic scale.

It turned out that the number of triggered mass  $m^*$  points depends on applied static bias  $f$ . For  $f = 0.1$  the percentage of triggered points was found to be the highest (88% of all mass values considered in the model). A careful study of the maps in Fig. 14 can reveal more interesting conclusions. The color distribution, and so the mass  $m^*$  distribution as well, seems to be very similar within all plots. Moreover, the shape formed by the coloured points is somehow *rescaled* as the value of static force  $f$  increases. Namely, the structure visible for  $f = 1.5$  seems to be *stretched out* for smaller values of  $f$ . This may give us a generalized image of connection of negative mobility distribution on the  $(a, \omega)$  plane and a magnitude of mass  $m$ . Small masses can be rather isolated by negative mobility mechanism with low values of frequency  $\omega$  and amplitude  $a$  (dark blue dots). For moderate values of  $\omega$  and  $a$  island of red and yellow-green points can be observed, i.e. masses close to  $m \approx 10$  and  $m \approx 1$  respectively. Then, for high frequencies and moderate amplitude value again blue areas can be found, which corresponds to  $m \approx 0.1$ .

The idea of particle separation introduced in this section has been presented in article (A2). We demonstrated that under an additional action of applied constant bias only particles of the specific mass value migrate in the direction opposite to this net force whereas the others move concurrently towards it. The biggest advantage of proposed mechanism is fact, that unlike many popular particle sieving-based isolation methods, here the particles are distinguished due to their masses, not sizes. Therefore, this mechanism would enable to detect a difference in masses even in a mixture of identical size particles.

## 5.2 The temperature-induced separation mechanism

Encouraged by the successful definition of separation mechanism tuned by the proper value of external driving force frequency  $\omega$ , in the next step, we attempted to find an evidence whether this effect can be also controlled by the temperature of the system  $T \propto D$ . In article (A3) we investigated a role of the thermal noise in the negative mobility phenomenon and we sought for such parameter regimes that would enable to trigger and thus *control* separation

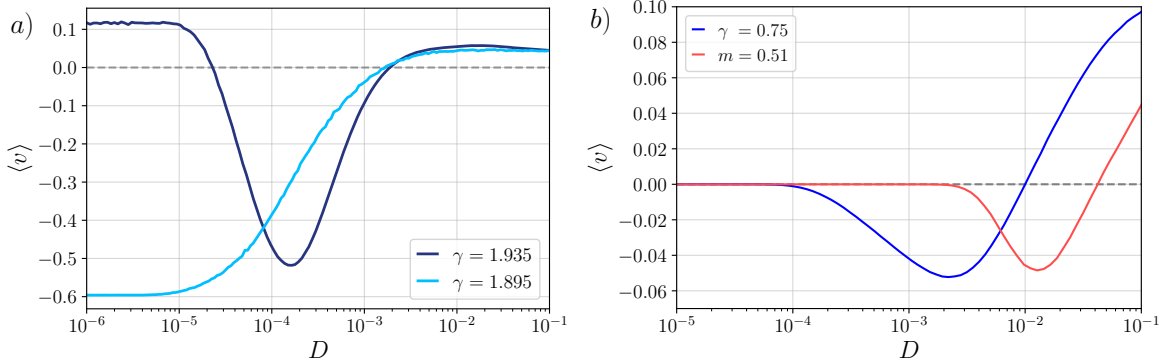


Figure 15: Panel (a): the directed velocity versus the thermal noise intensity  $D \propto T$  for two values of  $\gamma$ . For  $\gamma = 1.895$  the increase in noise intensity reduces the negative mobility effect. For  $\gamma = 1.935$  the curve forms a peak and thus the noise induced negative mobility is observed. Parameter values:  $a = 5.75$ ,  $\omega = 3.75$ ,  $f = 0.1$ . Panel (b): the noise induced negative mobility regimes observed for relatively high temperatures. The blue curve is obtained according to equation (7) with parameter values  $a = 5.75$ ,  $\omega = 1.6$ ,  $f = 0.1$ , while the red curve comes from equation (12) with parameter set  $a = 8.25$ ,  $\omega = 5.15$ ,  $f = 0.1$ .

mechanism by the magnitude of noise intensity  $D$ .

In the following discussion the Langevin equation is rescaled according to the units given in (4). Because the mass parameter value is set to unity, i.e.  $m = 1$ , we distinguish the particles due to their friction coefficient  $\gamma$ , which is closely related to the particle linear size by the Stokes formula

$$\Gamma = 6\pi\eta R \quad \text{and} \quad \gamma = \frac{\Gamma L}{\sqrt{M\Delta U}}, \quad (16)$$

where  $\eta$  is a viscosity of the surrounding medium and  $R$  is the radius of the spherical particle.

We have already demonstrated that thermal fluctuations have a destructive impact on the negative mobility phenomenon. However, as mentioned before, in the parameter space one may also encounter the *noise induced negative mobility* regimes, i.e. the negative mobility effect present only for a specific range of non-zero noise intensity values. Moreover, for such regimes, by adjusting the noise intensity one can amplify the negative velocity effect. Let us re-introduce this phenomenon in Fig. 15 in panel (a). For  $\gamma = 1.895$  the negative value of directed velocity  $\langle v \rangle$  observed for deterministic dynamics ( $D = 0$ ) is fading away as noise intensity increases, until eventually it becomes positive. This is a classical – deterministic – negative mobility effect. However, for  $\gamma = 1.935$ , different behaviour is observed – the positive value of  $\langle v \rangle$ , present for the deterministic regime ( $D = 0$ ), turns negative for a non-zero noise intensity, only within a certain  $D$  interval, and the strongest effect is visible for  $D \approx 2 \times 10^{-4}$ . This is where the noise induced effect comes in.

The noise induced negative mobility can be observed for the nearly whole spectrum of the thermal fluctuations intensity  $D \in [10^{-6}, 10^{-1}]$ . However, it is rarely to be found in the parameter space of considered model. Despite the destructive impact of rising temperature, negative mobility can be induced even by relatively high value of noise intensity. In Fig. 15 in panel (b) we present a regime of this effect induced by thermal fluctuations with noise intensity  $D > 10^{-3}$  (blue curve). Furthermore, it should be emphasized that analogous regimes can be also identified for the alternatively rescaled Langevin equation (12), i.e. when  $\gamma = 1$ . The example of such regime is also shown in panel (b) (red curve).

In order to construct a temperature-tuned separation mechanism we first isolated all negative mobility regimes induced by thermal fluctuations. In the next step the obtained data was numerically explored to search for any pattern or correlations between the presence of negative mobility and magnitude of the noise intensity  $D$ . Among many negative mobility

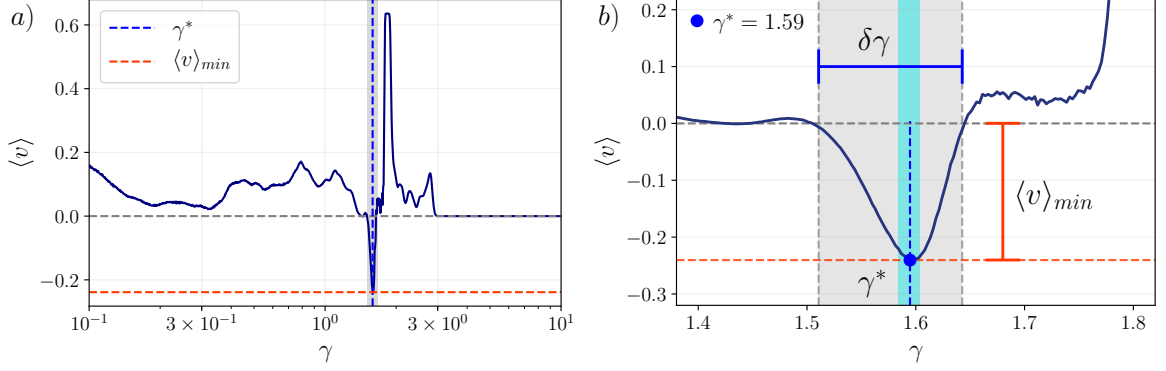


Figure 16: Panel (a): directed velocity as a function of friction coefficient  $\gamma$  depicted for a specific parameters regime for which the negative mobility occurs only for a one indivisible interval of  $\gamma$ . The  $\gamma$  value for which directed velocity reaches its minimum (red dashed line) is marked with vertical blue dashed line and is defined as  $\gamma^*$ . Panel (b): enlarged region of negative mobility (grey field in panel (a)) with  $\gamma^*$  point and width of negative mobility window  $\delta\gamma$  marked on the friction coefficient  $\gamma$  axis. The cyan field stands for all  $\gamma$  points that correspond to 5% vicinity of directed velocity minimum  $\langle v \rangle_{min}$ .

regimes we isolated those for which this effect is present only for *indivisible* intervals of friction coefficient  $\gamma$ . This procedure is briefly sketched in Fig. 16. For a given set of parameters in panel (a) directed velocity  $\langle v \rangle$  is negative only for  $\gamma$  values included in the interval marked with grey. Therefore, the information about negative mobility regime can be restricted to just pointing out the  $\gamma^*$  value for which minimal directed velocity is observed and the width of negative velocity interval, denoted here by  $\delta\gamma$ . In this way the isolated data can be redraw into a  $\gamma^*(D)$  plane in such a manner, that for given value of noise intensity  $D$  (x-axis) the marked point surrounded by a vertical error bar will represent the  $\gamma$  interval (y-axis) for which the negative mobility occurs. In this way a  $\gamma^*(D)$  plots were constructed in Fig. 17. The  $\gamma^*(D)$  curves, presented in Fig. 17 (a) – (c) for different values of the external driving amplitude  $a$  and frequency  $\omega$ , actually show the dependence between the particle size  $R$  and the noise intensity  $D$ . These parameter regimes enable to tune the negative mobility to all particles of the size  $R$  by manipulating with the system temperature  $T \propto D$ . The blue dots represent the  $\gamma^* \propto R^*$  value at fixed thermal fluctuations intensity and grey error bars show the width of negative velocity interval  $\delta\gamma$ .

Since the grey error bars in the  $\gamma^*(D)$  plots seem significant, in panel (d) we additionally depict the minimal velocity  $\langle v \rangle_{min}$  (left axis) as well as the resolution capacity  $\delta\gamma$  (right axis) versus temperature  $D$  for the parameter regime corresponding to panel (c). In order to better understand the dependence between the negative mobility interval  $\delta\gamma$  and directed velocity  $\langle v \rangle$  one should take a look at this chart. The thermal noise initially increases both the negative velocity interval  $\delta\gamma$  as well as the absolute value of minimal velocity  $\langle v \rangle_{min}$ . Also, there exists a noise intensity  $D$  for which  $\delta\gamma$  is maximal and  $\langle v \rangle_{min}$  is minimal. When thermal noise increases, the negative mobility peaks for  $\langle v \rangle(\gamma)$  dependence become wider and more pronounced. This fact guarantees that the particle size  $R^* \propto \gamma^*$  for which the negative mobility is tailored will be well distinguished from the others. In order to illustrate this fact, in panels (a)-(c) we additionally depicted the cyan regions that indicate the range of the particle size  $\gamma^* \propto R^*$  corresponding to the vicinity of minimum, i.e.  $[\langle v \rangle_{min} - 0.05\langle v \rangle_{min}, \langle v \rangle_{min} + 0.05\langle v \rangle_{min}]$ . In this range  $\delta\gamma$  is usually equal to several percent of the value  $\gamma^*$ , which seems to be reasonable for separation purposes. A more detailed discussion on this topic can be found in article (A3) in section "Discussion".

After a careful analysis of the investigated parameter space we conclude that there is

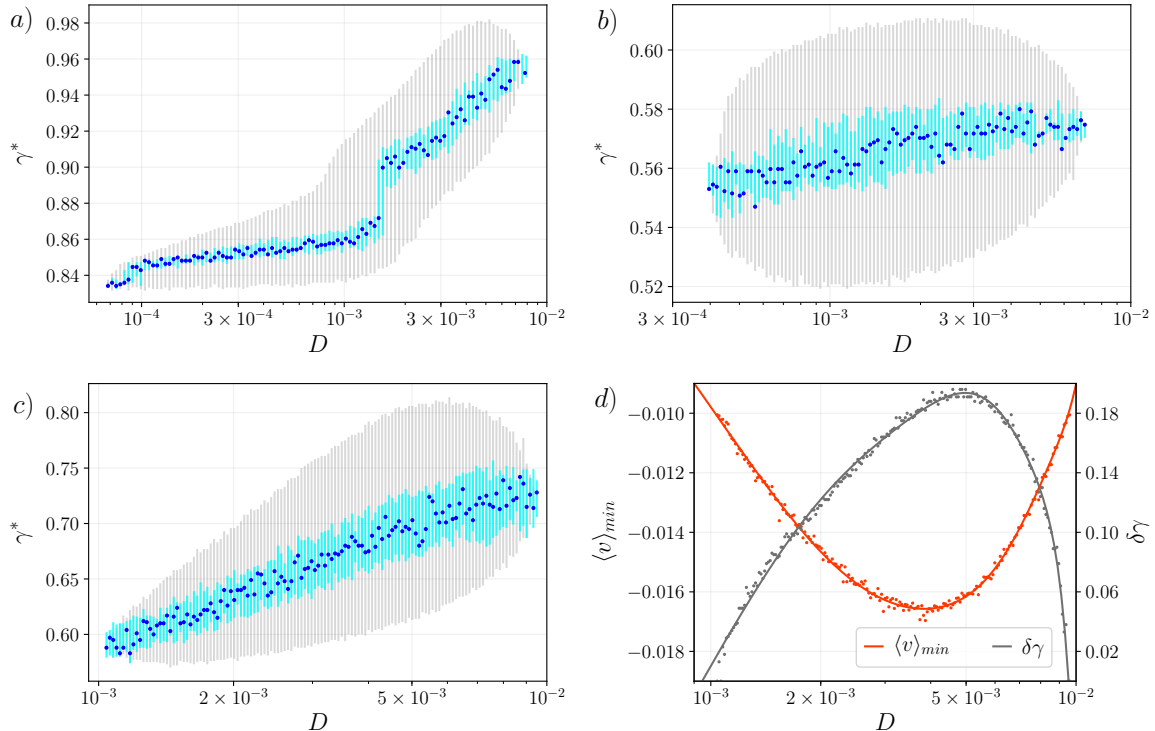


Figure 17: Panel (a)-(c): The friction coefficient, proportional to the particle size  $\gamma^* \propto R$ , for which the Brownian particle velocity attains its global minimum  $\langle v \rangle_{min} \equiv \langle v \rangle(\gamma^*)$  as a function of temperature  $D \propto T$ . The grey bars represent the friction coefficient interval  $\delta\gamma$  in which the ANM effect takes place (see Fig. 16). The cyan region marks the range of the particle size  $\gamma \propto R$  corresponding to the vicinity of minimum, i.e.  $[\langle v \rangle_{min} - 0.05\langle v \rangle_{min}, \langle v \rangle_{min} + 0.05\langle v \rangle_{min}]$ . Parameter values: (a)  $a = 5.55$ ,  $\omega = 1.5$ ; (b)  $a = 5.55$ ,  $\omega = 1.65$ ; (c)  $a = 5.75$ ,  $\omega = 5.65$ . In all panels the bias value is set to  $f = 0.1$ . Plot (d) depicts the minimal velocity  $\langle v \rangle_{min}$  (left axis) as well as the resolution capacity  $\delta\gamma$  (right axis) versus temperature  $D$  for the parameter regime illustrated in panel (c).

no single parameter regime covering a wide range of the particle size  $R^* \propto \gamma^*$  targeted for temperature tuned separation. However, parameters  $a$ ,  $\omega$  and  $f$  give enough freedom to cover by parts a physically significant interval of moderate to large friction that is characteristic for small particles at low Reynolds numbers (A3). The exemplary sets of data presented in Fig. 17 provide the separation mechanism for particles characterized by  $\gamma \in [0.5, 1]$ .

### 5.3 The size-based separation mechanism

Finally, we broadened the scope of our research and took a closer look at the separation mechanism that distinguishes particles due to their size  $R \propto \gamma$ . Since for the temperature induced mechanism there was found no single parameter regime that includes a wide range of friction coefficient  $\gamma$ , it seemed reasonable to investigate other model parameters for triggering negative mobility to given particle size  $R \propto \gamma$  and thus entailing a separation process. Using similar procedures to those presented in previous section, we investigated the parameter space in order to extract separation regimes controlled by the external static force  $f$ , external harmonic driving frequency  $\omega$  or amplitude  $a$ . The step-by-step description of the data analysis can be found in article (A4).

In Fig. 18 we present four data regimes for which negative mobility occurs in relation to  $\gamma^*$  and three selected parameters  $\{f, \omega, a\}$ . Negative mobility effect is most prominent for deterministic system, i.e. when  $D = 0$ . However, one may speculate that  $D = 0$  case cannot

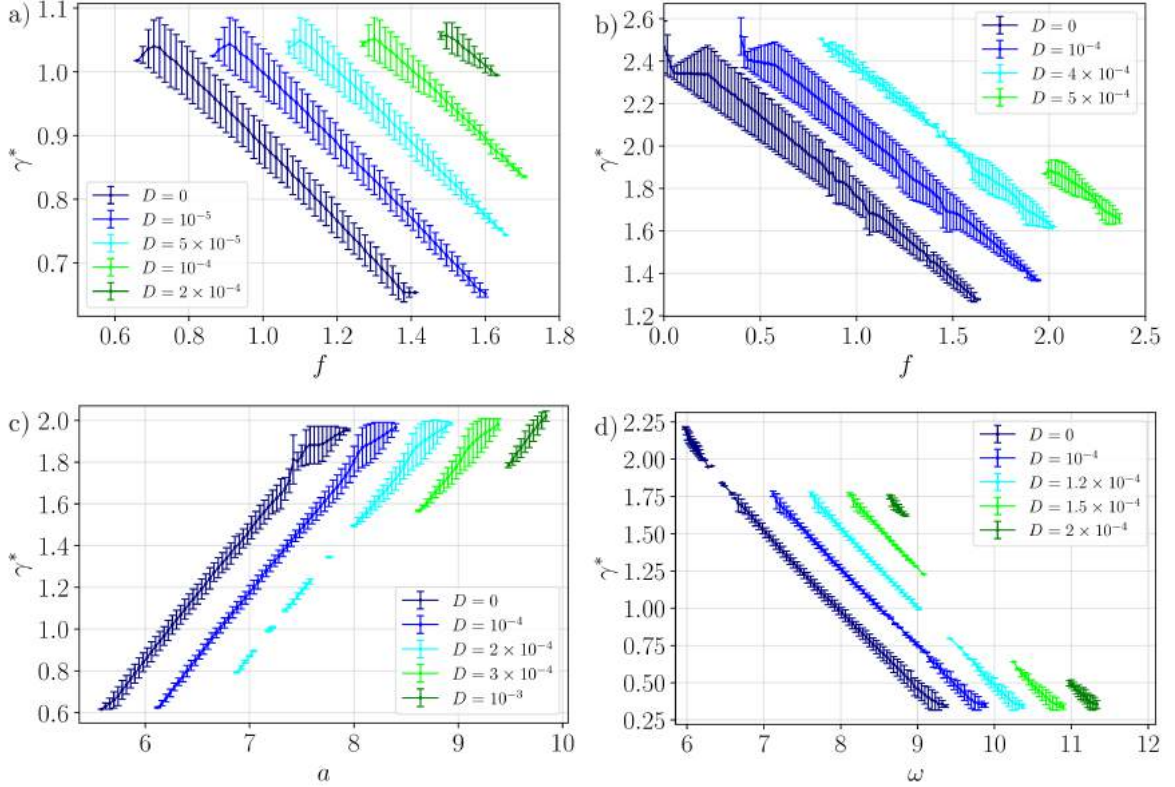


Figure 18: The size targeted for separation  $\gamma^*$  is depicted as a function of the parameters of external forces applied to the system. Panel (a)–(b): regimes selected for static force  $f$  dependence,  $a = 4.5, \omega = 3.75$  and  $a = 11.25, \omega = 6.8$ , respectively. Panel (c): regimes selected for time-periodic driving amplitude  $a$  dependence,  $f = 1.5, \omega = 4.2$ . Panel (d): regimes selected for time-periodic driving frequency  $\omega$  dependence,  $f = 0.8, a = 9.375$ . The data is depicted for different temperature  $D \propto T$  of the system. It should be emphasized here, that in order to avoid overlapping data for subsequent  $D$  values, the curves in each panel were visually separated by manually shifting slightly to the right.

be properly applied to real-based problems, where the thermal fluctuations affect the system. Therefore, in addition we also depicted several curves for non-zero noise intensity  $D$ . Even for  $D$  of magnitude near to  $10^{-3}$  the negative mobility curve is observed for some parameter regimes. It is important to notice here that when the noise intensity  $D$  increases, the negative mobility areas do not change their position, but they tend to shrink and vanish. For this reason, the subsequent data sets in every panel of Fig. 18 have been slightly shifted to the right side of the plot.

By the detailed examination of curve for  $D = 0$  in panel (a) let us remind how the data presented in Fig. 18 can be used in the process of separating one particle species from the others. The negative mobility curve, i.e. the points with directed velocity  $\langle v \rangle < 0$ , is depicted in  $\gamma^*(f)$  plane. For selected  $f$  value on the horizontal axis there exists only one  $\gamma^*$  value for which negative mobility occurs – for the others  $\gamma^*$  values the positive directed velocity  $\langle v \rangle$  is observed. Since friction coefficient  $\gamma^*$  is closely related to the particle size  $R$  (see equation 16), by choosing a proper value of bias  $f$  we can trigger negative mobility effect to the particle species of this particular size, represented by  $\gamma^*$ , and therefore force those particles to move in the opposite direction to applied bias. In this way, after a finite time, they will separate from the rest of particles by moving in the reversed direction to the general trend, which is along the bias  $f$  direction.

According to parameter regimes shown in Fig. 18, the method of particle separation can

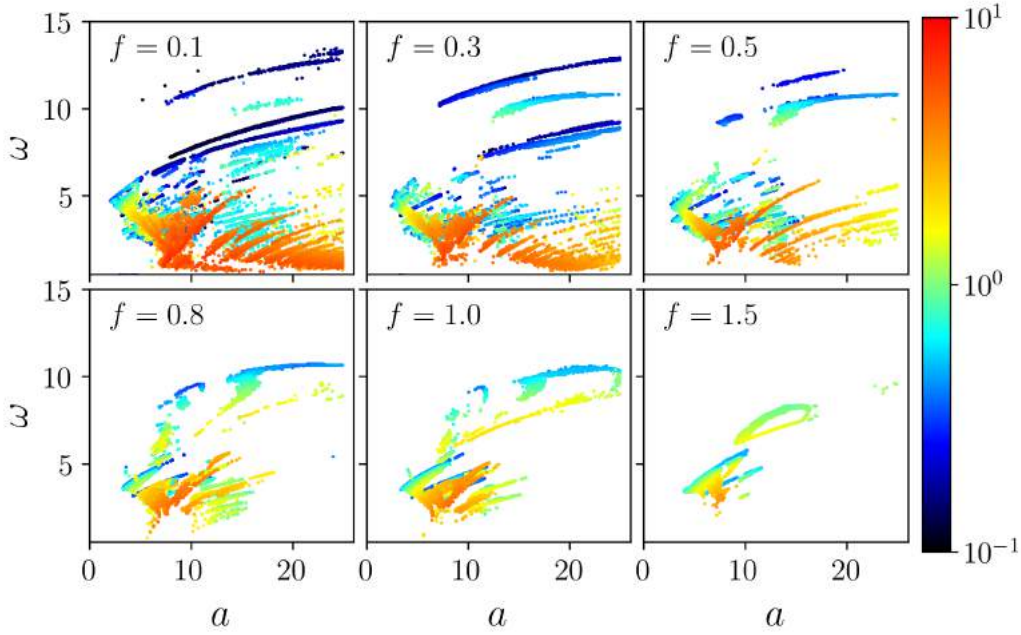


Figure 19: The  $\gamma^*$  value targeted for separation by the negative mobility effect as a function of amplitude  $a$  and frequency  $\omega$  for different values of the bias  $f$ . The color scale indicates  $\gamma^*$  value. Thermal noise intensity  $D$  is set to zero,  $D = 0$ .

be based on three different characteristics: external static force  $f$  – panel (a) and (b), external periodic driving amplitude  $a$  – panel (c) and external periodic driving frequency  $\omega$  – panel (d). In  $\gamma^*(a)$  chart, the  $\gamma^*$  value is proportional to amplitude  $a$ , while for the rest of charts proportionality is inverted. The proposed data sets allows to select a wide range of particle sizes  $R \propto \gamma^* \in [0.25, 2.5]$ . For example, providing the mixture of particles with the conditions specified by data presented in panel (d), by manipulating just with frequency  $\omega$  value one can select, and thus isolate, a range of particles with  $\gamma^* \in [0.25, 2.25]$ . It is important to notice here, that presented data is only a sample data and there exist many parameter regimes that can be used to establish the separation mechanism.

Finally, we also verified how many  $\gamma^*$  values can be triggered out using introduced separation mechanism. In Fig. 19 we present a collection of two-dimensional maps, which illustrate the  $\gamma^*$  values targeted for separation as a function of amplitude  $a$  and frequency  $\omega$  for different values of bias  $f$ . The color scale symbolizes the  $\gamma^*$  value. Similar to the case of mass-based separation mechanism, color points depicted for given values of  $a$  and  $\omega$  form an interesting pattern, which shape seems to evolve according to increasing values of  $f$ . Small  $\gamma^*$  values are mostly targeted by small values of  $f$  and moderate to high values of frequency  $\omega$  and amplitude  $a$ . Higher values of  $\gamma^*$  are related with small values of  $\omega$ . As value of bias  $f$  increases in the subsequent plots, the amount of  $\gamma^*$  values slowly disappears.

At the end of this analysis let us recall the fact, that dimensionless parameters from equation (7) are not directly equal to corresponding physical quantities that define the system. Therefore, a given parameter value of  $\{f, \omega, a\}$  that trigger a particular particle type isolation can be obtained in experimental setup ambiguously – there exist several combinations of physical quantity values that come down to desired value of dimensionless triggering parameter.

## 5.4 Conclusion

The separation mechanisms discussed in this section allow to isolate a given type of particles from the others. Supposed that one could expose a mixture of particles to the specific

conditions given by the Langevin equation (7) or (12) along with appropriate parameter values chosen on the base of the regimes presented in the figures, one would be able to efficiently isolate one species of particles from the whole mixture. Moreover, by changing a single parameter value (e.g. external driving frequency  $\omega$ ) one could further fluently trigger the different types of particles and in this way isolate subsequent particle species from the mixture.

This separation process based on the Brownian mechanics appears to be quite unique for several reasons. First of all, it has a significant advantage over the well-known sieving methods. It allows to distinguish particles due to their sizes, as well as due to their masses. The mass distinction may prove useful when particles sizes are very similar but the masses vary significantly and thus the particles are difficult to sieve out. This problem is commonly encountered when dealing with diseased cells in the living organisms [69].

Secondly, the main advantage of the proposed scheme is that it combines the benefits of both active and passive separation techniques. The method uses an external driving force as well as a constant bias, so the particle-sorting efficiency and throughput are expected to be higher than for alternative passive and some active (e.g., ratchet) techniques. Moreover, this scheme allows one not only to deflect different particle species along different transport angles but also to steer them in opposite directions, and therefore it is ideal for separation and fractionation purposes.

Thirdly, it should be emphasized once again that in the proposed model we operate on dimensionless variables. Therefore, the presented model is independent of physical units and can be easily adapted to given experimental setup. Each of the dimensionless parameters from equations (7) and (12) is a combination of more than one physical quantity of the considered system, and thus, the desired dimensionless value can be accomplished in several ways.

Finally, the presented mechanisms of the particles isolation can be used in biological systems where the thermal fluctuations are an inherent feature of the system. We not only incorporated thermal noise into presented model, but as one could already see, we also demonstrated how to use it in order to trigger and amplify the separation of demanded particles species. Furthermore, presented mechanisms allow for separation processes in which particle isolation is possible even when the noise intensity value remains relatively high (Fig. 18). In addition, because the negative mobility can be induced by thermal fluctuations and further, the whole separation process may be controlled by the intensity of thermal noise, proposed mechanism can be successfully applied to electrically neutral particles and molecules.

In the end, let us refer to the issue mentioned at the beginning of the chapter, regarding the search for low-cost separation methods and simple experimental setup required for practical applications. The separation mechanisms presented in this chapter have not been involved in any experimental research yet. Such action highly exceeds the scope of our study so far. This dissertation has been typically focused on computational investigation on proposed mechanisms. However, in recent years, at least several lab-on-chip experiments, in which for the same condition negative mobility has been observed for one species of the particles and not for the other, have been performed [23, 24, 25]. This fact fulfills the basic assumption of proposed separation mechanisms. The lab-on-chip technology, known for low fabrication costs and high-effective parallelization, is gaining more and more attention. Although the technology is not easy to manufacture, a lot of bottleneck problems can be currently overcome by the recent technology advancement on low-cost 3D printing and laser engraving [70, 71]. The progress made in this field of technology is astonishing, especially in the last two years of global pandemic [72, 73, 74]. We believe that mechanisms presented in this dissertation may inspire some further research that would put into practice negative mobility based concept of particle separation and thus, based on the flexibility of introduced models, an innovative low-costs and simple implementation particle separation method would be formulated.

## 6 Closing discussion

In this guidebook we introduced the reader to the concept of negative mobility and we described three variations of the particles isolation techniques established by this phenomenon: (1) mass-based separation mechanism, (2) temperature-induced separation mechanism and (3) size-based separation mechanism. We considered systems governed by Brownian dynamics and we obtained our results by performing the complex numerical simulations. We demonstrated that under an additional action of applied constant bias only particles of a given mass or size migrate in the direction opposite to this net force, whereas the others move concurrently towards it. The outcomes of our research have been published in four articles which are listed at the beginning of this dissertation (A1, A2, A3, A4). The full text of the articles is provided below. The negative mobility mechanisms described in this guidebook enable novel particle isolation methods. We recalled some experiments that had already implemented the basic concepts of the considered separation strategies and we commented extensively on the advantages of introduced schemes.

However, we are also aware of some disadvantages of proposed ideas. In particular, our consideration was limited only to one-dimensional Brownian dynamics which is a simplification of the real-world situation and lab-on-chip devices geometry. Therefore, the application of presented solutions may require further study to account for an extended dimensionality of given experimental setup. However, we considered the minimal model for the negative mobility effect to occur and thus we expect that in two or three dimensional models the proposed separation strategies will be even more feasible. Furthermore, we formulated our predictions in terms of the dimensionless variables which give opportunity to adapt given experimental parameters to those appearing in the considered model.

Moreover, we did not include in our model any hydrodynamic corrections that may play a crucial role in experimental reality. We adopted the simplest hydrodynamic effect expressed by the friction term in Langevin equation (1) and ignored the number of phenomena that may prove experimentally important. Therefore we are aware that our theoretical predictions should be used as a guide towards physical reality indicating the direction for the future experimental and theoretical research rather than taken as granted without approximation.

Future microfluidic applications would require development of suitable separation and sorting devices that would need simple and low-cost fabrication techniques, provide ease of operation and handling and offer high throughput and separation efficiency with lower energy input [67]. Sorting based on mechanical properties may be a good candidate to respond to these needs. It can provide a new avenue for sample preparation, detection and diagnosis for a number of emerging biological and medical analyzes.

Being aware of both the advantages and disadvantages of the solutions we propose, we remain optimistic and envision that the separation strategy introduced in this dissertation provides selectivity required in present and future isolation of nano- and micro-particles, proteins, organelles and cells, and thus it will constitute a base for a flexible and low-cost modern isolation techniques.

## 7 References

- [1] Thomas Wekerle and Rainer Oberbauer. All entities move and nothing remains still-heraclitus, 2015.
- [2] Saeed Mohammad Bagheri, Mohammad Vajdi, Farhad Sadegh Moghanlou, Milad Sakkaki, Mohsen Mohammadi, Mohammadreza Shokouhimehr, and Mehdi Shahedi Asl. Numerical modeling of heat transfer during spark plasma sintering of titanium carbide. *Ceramics International*, 46(6):7615–7624, 2020.



- [3] Josep Fortesa, Giovanni Francesco Ricci, Julián García-Comendador, Francesco Gentile, Joan Estrany, Eric Sauquet, Thibault Datry, and Anna Maria De Girolamo. Analysing hydrological and sediment transport regime in two mediterranean intermittent rivers. *Catena*, 196:104865, 2020.
- [4] Ben L Werkhoven and René van Roij. Coupled water, charge and salt transport in heterogeneous nano-fluidic systems. *Soft Matter*, 16(6):1527–1537, 2020.
- [5] Pasquale Francesco Zito, Adele Brunetti, and Giuseppe Barbieri. Selective mass transport of co2 containing mixtures through zeolite membranes. *Journal of Membrane Science and Research*, 2020.
- [6] Paul C Bressloff. Modeling active cellular transport as a directed search process with stochastic resetting and delays. *Journal of Physics A: Mathematical and Theoretical*, 53(35):355001, 2020.
- [7] Hamada S Badr, Hongru Du, Maximilian Marshall, Ensheng Dong, Marietta M Squire, and Lauren M Gardner. Association between mobility patterns and covid-19 transmission in the usa: a mathematical modelling study. *The Lancet Infectious Diseases*, 2020.
- [8] Florina-Daniela Cojocaru, Doru Botezat, Ioannis Gardikiotis, Cristina-Mariana Uritu, Gianina Dodi, Laura Trandafir, Ciprian Rezus, Elena Rezus, Bogdan-Ionel Tamba, and Cosmin-Teodor Mihai. Nanomaterials designed for antiviral drug delivery transport across biological barriers. *Pharmaceutics*, 12(2):171, 2020.
- [9] Anna Nagurney and Patrizia Daniele. International human migration networks under regulations. *European Journal of Operational Research*, 2020.
- [10] Jose Asturias. Endogenous transportation costs. *European Economic Review*, 123:103366, 2020.
- [11] Albert Einstein. On the theory of the brownian movement. *Ann. Phys*, 19(4):371–381, 1906.
- [12] Hannes Risken. Fokker-planck equation. In *The Fokker-Planck Equation*, pages 63–95. Springer, 1996.
- [13] CA Condat and GJ Sibona. Noise-enhanced mechanical efficiency in microorganism transport. *Physica A: Statistical Mechanics and its Applications*, 316(1-4):203–212, 2002.
- [14] Jakub Spiechowicz, Peter Hänggi, and Jerzy Łuczka. Brownian motors in the microscale domain: Enhancement of efficiency by noise. *Physical Review E*, 90(3):032104, 2014.
- [15] Hiroshi Orihara and Yoshinori Takikawa. Brownian motion in shear flow: Direct observation of anomalous diffusion. *Physical Review E*, 84(6):061120, 2011.
- [16] Jakub Spiechowicz and Jerzy Łuczka. Subdiffusion via dynamical localization induced by thermal equilibrium fluctuations. *Scientific Reports*, 7(1):1–7, 2017.
- [17] Ralf Metzler. Brownian motion and beyond: first-passage, power spectrum, non-gaussianity, and anomalous diffusion. *Journal of Statistical Mechanics: Theory and Experiment*, 2019(11):114003, 2019.
- [18] Peter Reimann, Christian Van den Broeck, H Linke, Peter Hänggi, JM Rubi, and Agustín Pérez-Madrid. Giant acceleration of free diffusion by use of tilted periodic potentials. *Physical review letters*, 87(1):010602, 2001.

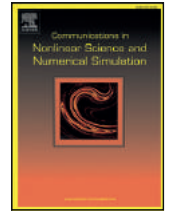
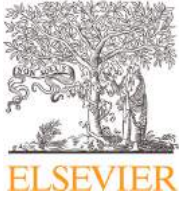
- [19] Benjamin Lindner and Igor M Sokolov. Giant diffusion of underdamped particles in a biased periodic potential. *Physical Review E*, 93(4):042106, 2016.
- [20] J Spiechowicz and J Łuczka. Diffusion in a biased washboard potential revisited. *Physical Review E*, 101(3):032123, 2020.
- [21] John M Warman, Ulrich Sowada, and Matthijs P De Haas. Transient negative mobility of hot electrons in gaseous xenon. *Physical Review A*, 31(3):1974, 1985.
- [22] Ralf Eichhorn, Peter Reimann, and Peter Hänggi. Paradoxical motion of a single brownian particle: Absolute negative mobility. *Physical Review E*, 66(6):066132, 2002.
- [23] Alexandra Ros, Ralf Eichhorn, Jan Regtmeier, Thanh Tu Duong, Peter Reimann, and Dario Anselmetti. Absolute negative particle mobility. *Nature*, 436(7053):928–928, 2005.
- [24] Ralf Eichhorn, Jan Regtmeier, Dario Anselmetti, and Peter Reimann. Negative mobility and sorting of colloidal particles. *Soft Matter*, 6(9):1858–1862, 2010.
- [25] Jinghui Luo, Katherine A Muratore, Edgar A Arriaga, and Alexandra Ros. Deterministic absolute negative mobility for micro-and submicrometer particles induced in a microfluidic device. *Analytical chemistry*, 88(11):5920–5927, 2016.
- [26] JURAS POZHELA. Plasma and current instabilities in semiconductors. 1981.
- [27] Federico Capasso. Physics of quantum electron devices, 1990.
- [28] Herbert Krömer. Proposed negative-mass microwave amplifier. *Physical Review*, 109(5):1856, 1958.
- [29] Boris I Sturman and Vladimir M Fridkin. *Photovoltaic and Photo-refractive Effects in Noncentrosymmetric Materials*, volume 8. CRC Press, 1992.
- [30] AG Aronov and BZ Spivak. Photoeffect in a josephson junction. Technical report, Nuclear Physics Institute, USSR Academy of Sciences, 1975.
- [31] ME Gershenzon and MI Falei. Absolute negative resistance of a tunnel contact between superconductors with a nonequilibrium quasiparticle distribution function. *ZhETF Pisma Redaktsiiu*, 44:529–532, 1986.
- [32] NA Dyatko, Igor’Valerianovich Kochetov, and Anatolii Petrovich Napartovich. Absolute negative conductivity of low-temperature plasma. *Pisma v Zhurnal Tekhnicheskoi Fiziki*, 13(23):1457–1461, 1987.
- [33] Z Rozenberg, M Lando, and M Rokni. On the possibility of steady state negative mobility in externally ionised gas mixtures. *Journal of Physics D: Applied Physics*, 21(11):1593, 1988.
- [34] Peter Reimann, R Kawai, Christian Van den Broeck, and Peter Hänggi. Coupled brownian motors: Anomalous hysteresis and zero-bias negative conductance. *EPL (Europhysics Letters)*, 45(5):545, 1999.
- [35] J Buceta, JM Parrondo, C Van den Broeck, and FJ de La Rubia. Negative resistance and anomalous hysteresis in a collective molecular motor. *Physical Review E*, 61(6):6287, 2000.
- [36] Ralf Eichhorn, Peter Reimann, and Peter Hänggi. Brownian motion exhibiting absolute negative mobility. *Physical review letters*, 88(19):190601, 2002.

- [37] Ralf Eichhorn, Peter Reimann, and Peter Hänggi. Absolute negative mobility and current reversals of a meandering brownian particle. *Physica A: Statistical Mechanics and its Applications*, 325(1-2):101–109, 2003.
- [38] Lukasz Machura, Marcin Kostur, Peter Talkner, Jerzy Łuczka, and Peter Hänggi. Absolute negative mobility induced by thermal equilibrium fluctuations. *Physical review letters*, 98(4):040601, 2007.
- [39] Ralf Eichhorn, Peter Reimann, B Cleuren, and C Van den Broeck. Moving backward noisily. *Chaos: An Interdisciplinary Journal of Nonlinear Science*, 15(2):026113, 2005.
- [40] Peter Hänggi and Fabio Marchesoni. Artificial brownian motors: Controlling transport on the nanoscale. *Reviews of Modern Physics*, 81(1):387, 2009.
- [41] Umberto Marini Bettolo Marconi, Andrea Puglisi, Lamberto Rondoni, and Angelo Vulpiani. Fluctuation–dissipation: response theory in statistical physics. *Physics reports*, 461(4-6):111–195, 2008.
- [42] P HÄNGGI, J ŁUCZKA, and J SPIECHOWICZ. Many faces of non-equilibrium: Anomalous transport phenomena in driven periodic systems. *Acta Physica Polonica B*, 51(5), 2020.
- [43] Łukasz Machura, Marcin Kostur, and Jerzy Łuczka. Transport characteristics of molecular motors. *Biosystems*, 94(3):253–257, 2008.
- [44] Jakub Spiechowicz, Jerzy Łuczka, and Peter Hänggi. Transient anomalous diffusion in periodic systems: ergodicity, symmetry breaking and velocity relaxation. *Scientific reports*, 6:30948, 2016.
- [45] Sergey Denisov, Sergej Flach, and Peter Hänggi. Tunable transport with broken space–time symmetries. *Physics Reports*, 538(3):77–120, 2014.
- [46] David Speer, Ralf Eichhorn, and Peter Reimann. Transient chaos induces anomalous transport properties of an underdamped brownian particle. *Physical Review E*, 76(5):051110, 2007.
- [47] Jakub Spiechowicz, Jerzy Łuczka, and Peter Hänggi. Absolute negative mobility induced by white poissonian noise. *Journal of Statistical Mechanics: Theory and Experiment*, 2013(02):P02044, 2013.
- [48] Jakub Spiechowicz, Peter Hänggi, and Jerzy Łuczka. Coexistence of absolute negative mobility and anomalous diffusion. *New Journal of Physics*, 21(8):083029, 2019.
- [49] J Nagel, David Speer, T Gaber, A Sterck, R Eichhorn, Peter Reimann, K Ilin, M Siegel, D Koelle, and R Kleiner. Observation of negative absolute resistance in a josephson junction. *Physical review letters*, 100(21):217001, 2008.
- [50] Marcin Kostur, Jerzy Łuczka, and Peter Hänggi. Negative mobility induced by colored thermal fluctuations. *Physical Review E*, 80(5):051121, 2009.
- [51] J Spiechowicz, J Łuczka, and L Machura. Efficiency of transport in periodic potentials: dichotomous noise contra deterministic force. *Journal of Statistical Mechanics: Theory and Experiment*, 2016(5):054038, 2016.
- [52] Dirk Hennig. Current control in a tilted washboard potential via time-delayed feedback. *Physical Review E*, 79(4):041114, 2009.

- [53] Lu-Chun Du and Dong-Cheng Mei. Time delay control of absolute negative mobility and multiple current reversals in an inertial brownian motor. *Journal of Statistical Mechanics: Theory and Experiment*, 2011(11):P11016, 2011.
- [54] Colm Mulhern. Persistence of uphill anomalous transport in inhomogeneous media. *Physical Review E*, 88(2):022906, 2013.
- [55] Bruno S Dandogbessi and Anatole Kenfack. Absolute negative mobility induced by potential phase modulation. *Physical Review E*, 92(6):062903, 2015.
- [56] Luchun Du and Dongcheng Mei. Absolute negative mobility in a vibrational motor. *Physical Review E*, 85(1):011148, 2012.
- [57] M Januszewski and J Łuczka. Indirect control of transport and interaction-induced negative mobility in an overdamped system of two coupled particles. *Physical Review E*, 83(5):051117, 2011.
- [58] L Machura, J Spiechowicz, M Kostur, and J Łuczka. Two coupled josephson junctions: dc voltage controlled by biharmonic current. *Journal of Physics: Condensed Matter*, 24(8):085702, 2012.
- [59] Pulak K Ghosh, Peter Hänggi, Fabio Marchesoni, and Franco Nori. Giant negative mobility of janus particles in a corrugated channel. *Physical Review E*, 89(6):062115, 2014.
- [60] Paolo Magaretti, Ignacio Pagonabarraga, and J Miguel Rubi. Entropic electrokinetics: recirculation, particle separation, and negative mobility. *Physical review letters*, 113(12):128301, 2014.
- [61] A Sarracino, F Cecconi, A Puglisi, and A Vulpiani. Nonlinear response of inertial tracers in steady laminar flows: Differential and absolute negative mobility. *Physical review letters*, 117(17):174501, 2016.
- [62] Jan Regtmeier, Ralf Eichhorn, TT Duong, Peter Reimann, Dario Anselmetti, and Alexandra Ros. Pulsed-field separation of particles in a microfluidic device. *The European Physical Journal E*, 22(4):335–340, 2007.
- [63] Richard Wesley Hamming. Stable predictor-corrector methods for ordinary differential equations. *Journal of the ACM (JACM)*, 6(1):37–47, 1959.
- [64] William B Gragg and Hans J Stetter. Generalized multistep predictor-corrector methods. *Journal of the ACM (JACM)*, 11(2):188–209, 1964.
- [65] Jakub Spiechowicz, Marcin Kostur, and Lukasz Machura. Gpu accelerated monte carlo simulation of brownian motors dynamics with cuda. *Computer Physics Communications*, 191:140–149, 2015.
- [66] Michal Januszewski and Marcin Kostur. Accelerating numerical solution of stochastic differential equations with cuda. *Computer Physics Communications*, 181(1):183–188, 2010.
- [67] P Sajeesh and Ashis Kumar Sen. Particle separation and sorting in microfluidic devices: a review. *Microfluidics and nanofluidics*, 17(1):1–52, 2014.
- [68] Morteza Bayareh. An updated review on particle separation in passive microfluidic devices. *Chemical Engineering and Processing-Process Intensification*, page 107984, 2020.

- [69] Subra Suresh. Biomechanics and biophysics of cancer cells. *Acta biomaterialia*, 3(4):413–438, 2007.
- [70] Feng Li, Niall P Macdonald, Rosanne M Guijt, and Michael C Breadmore. Increasing the functionalities of 3d printed microchemical devices by single material, multimaterial, and print-pause-print 3d printing. *Lab on a Chip*, 19(1):35–49, 2019.
- [71] Amr AM Elrouby, Ahmed SM Ali, Ahmed AR Abdel-Aty, Abdelhamid M Abu-Elnaga, and Ahmed SG Khalil. Low-cost production of 3d printed lab-on chip (loc) device for oil-in-water emulsion separation. In *2020 27th IEEE International Conference on Electronics, Circuits and Systems (ICECS)*, pages 1–4. IEEE, 2020.
- [72] Hanliang Zhu, Zdenka Fohlerová, Jan Pekárek, Evgenia Basova, and Pavel Neužil. Recent advances in lab-on-a-chip technologies for viral diagnosis. *Biosensors and Bioelectronics*, 153:112041, 2020.
- [73] Vigneswaran Narayanamurthy, ZE Jeroish, KS Bhuvaneshwari, Pouriya Bayat, R Premkumar, Fahmi Samsuri, and Mashitah M Yusoff. Advances in passively driven microfluidics and lab-on-chip devices: a comprehensive literature review and patent analysis. *RSC Advances*, 10(20):11652–11680, 2020.
- [74] Carly Tymm, Junhu Zhou, Amogha Tadimety, Alison Burklund, and John XJ Zhang. Scalable covid-19 detection enabled by lab-on-chip biosensors. *Cellular and Molecular Bioengineering*, 13(4):313–329, 2020.

Scientific articles



# Negative mobility of a Brownian particle: Strong damping regime



A. Słapik, J. Łuczka\*, J. Spiechowicz

<sup>a</sup> Institute of Physics, University of Silesia, 40-007 Katowice, Poland

<sup>b</sup> Silesian Center for Education and Interdisciplinary Research, University of Silesia, 41-500 Chorzów, Poland

## ARTICLE INFO

### Article history:

Received 9 May 2017

Revised 18 July 2017

Accepted 20 July 2017

Available online 24 July 2017

### Keywords:

Brownian motion

Periodic symmetric systems

Negative mobility

Strong damping regime

## ABSTRACT

We study impact of inertia on directed transport of a Brownian particle under non-equilibrium conditions: the particle moves in a one-dimensional periodic and *symmetric* potential, is driven by both an unbiased time-periodic force and a constant force, and is coupled to a thermostat of temperature  $T$ . Within selected parameter regimes this system exhibits negative mobility, which means that the particle moves in the direction opposite to the direction of the constant force. It is known that in such a setup the inertial term is *essential* for the emergence of negative mobility and it cannot be detected in the limiting case of overdamped dynamics. We analyse inertial effects and show that negative mobility can be observed even in the strong damping regime. We determine the *optimal* dimensionless mass for the presence of negative mobility and reveal three mechanisms standing behind this anomaly: deterministic chaotic, thermal noise induced and deterministic non-chaotic. The last origin has never been reported. It may provide guidance to the possibility of observation of negative mobility for strongly damped dynamics which is of fundamental importance from the point of view of biological systems, all of which *in situ* operate in fluctuating environments.

© 2017 Elsevier B.V. All rights reserved.

## 1. Introduction

If a system is at thermal equilibrium, its reaction to a weak external static force is so that the response is in the same direction of this applied force, towards a new equilibrium. E.g., when a constant force acts on a particle, it moves in the same direction of the force. If it is an electronic (electrical) device, the current-voltage dependence exhibits the similar properties, i.e. if the voltage increases the current increases. The ohmic characteristics is an example of it. It is what we call the normal transport. This restriction is no longer valid under nonequilibrium conditions when already an unperturbed system may exhibit a current due to the ratchet effect [1]. Another example is the seemingly paradoxical situation of the negative mobility phenomenon when the system response is opposite to the applied constant force [2]. Such anomalous transport behaviour was predicted theoretically in 2007 in a system consisting of an *inertial* Brownian particle moving in a one-dimensional periodic symmetric potential [3]. Within a year of this discovery, negative mobility was confirmed experimentally in the experiment involving determination of current-voltage characteristics of the microwaved-driven Josephson junction [4]. Yet further examples of this phenomenon have been described theoretically in companionship of coloured noise [5], white Poissonian noise [6], dichotomous process [7] and for Brownian motion with presence of time-delayed feedback

\* Corresponding author.

E-mail address: [jerzy.luczka@us.edu.pl](mailto:jerzy.luczka@us.edu.pl) (J. Łuczka).

[8,9], non-uniform space-dependent damping [10] and potential phase modulation [11]. Other illustrations include a vibrational motor [12], two coupled resistively shunted Josephson junctions [13,14], active Janus particles in a corrugated channel [15], entropic electrokinetics [16] as well as nonlinear response of inertial tracers in steady laminar flows [17].

Modelling systems and understanding their generic properties discloses which components of the setup are crucial and which elements may be sub-relevant. For instance, transport in the micro-world is strongly influenced by fluctuations and random perturbations. In some systems, like biological cells [18], they can even play a dominant role and a typical situation is that motion of particles is strongly damped. This fact justifies the use of an overdamped dynamics for which the particle inertial term  $M\ddot{x}$  can be formally neglected in comparison to the dissipation term  $\Gamma\dot{x}$  ( $M$  is the particle mass,  $\Gamma$  is the friction coefficient and dot denotes a differentiation with respect to time  $t$ ). Omission of the inertial term enormously simplifies the modelling and in many cases allows for an analytical solutions of the corresponding Fokker–Planck equation. However, properties and features which are allowed to occur in systems with inertia can completely disappear when the inertial term is put to zero. Certainly a more correct approach in such a situation is to include the inertial term and use a technique of mathematical sequences of smaller and smaller dimensionless mass. Our main objective is to investigate impact of inertia on negative mobility of a Brownian particle moving in one-dimensional periodic systems. It is known that in such setups the inertial term is one of the key ingredients for the occurrence of this form of anomalous transport [19] and negative mobility is absent for the overdamped dynamics when  $M\ddot{x} = 0$ . We address the question whether it is still possible to observe the negative mobility phenomenon in strongly dissipative systems. In doing so, we first formulate the model and introduce the quantities of interest. Then we investigate the general transport behaviour as a function of model parameters and detect the optimal dimensionless mass for the presence of negative mobility. In the next part we demonstrate three mechanisms responsible for the emergence of this anomalous transport phenomenon: deterministic chaotic, thermal noise induced and deterministic non-chaotic. Finally, we discuss impact of inertia on the directed long time particle velocity and provide some conclusions.

## 2. Model

The model of a Brownian particle moving in a one-dimensional periodic landscape has been already well established in the literature [20]. It has been used to explore a wide range of phenomena including ratchet effects [21–23], noise induced transport [24], the negative mobility [3], the enhancement of transport [25], diffusion phenomena [26,27] and Gaussian white noise as a resource for work extraction [28]. Here, we consider exactly the same model as in [3]: a classical inertial Brownian particle of mass  $M$ , which moves in a spatially periodic potential  $U(x) = U(x + L)$  of period  $L$  and is subjected to both an unbiased time-periodic force  $A\cos(\omega t)$  of amplitude  $A$  and angular frequency  $\Omega$  and an external static force  $F$ . Dynamics of such a particle is described by the following Langevin equation [3]

$$M\ddot{x} + \Gamma\dot{x} = -U'(x) + A\cos(\Omega t) + F + \sqrt{2\Gamma k_B T}\xi(t), \quad (1)$$

where prime denotes a differentiation with respect to the particle coordinate  $x$ . Thermal fluctuations due to the coupling of the particle with the thermal bath of temperature  $T$  are modelled by Gaussian white noise of zero mean and unity intensity, namely

$$\langle \xi(t) \rangle = 0, \quad \langle \xi(t)\xi(s) \rangle = \delta(t - s). \quad (2)$$

The noise intensity factor  $2\Gamma k_B T$  (where  $k_B$  is the Boltzmann constant) follows from the fluctuation-dissipation theorem [29] and ensures the canonical equilibrium Gibbs state when  $A = 0$  and  $F = 0$ . The potential  $U(x)$  is assumed to be in a *symmetric* form with the period  $L$  and the barrier height  $2\Delta U$ , namely,

$$U(x) = \Delta U \sin\left(\frac{2\pi}{L}x\right). \quad (3)$$

There exists a wealth of physical systems that can be described by the Langevin equation (1). Important cases that come to mind are the semiclassical dynamics of a phase difference across a resistively and capacitively shunted Josephson junction [30] and a cold atom moving in an optical lattice [1,31]. Other examples include superionic conductors [32], dipoles rotating in external field [33], charge density waves [34] and adatoms on a periodic surface [35].

### 2.1. Scaling and dimensionless Langevin equation

Since only relations between scales of length, time and energy are relevant for the observed phenomena, not their absolute values, we next formulate the above presented equation of motion in its dimensionless form. This can be achieved in several ways [36]. Because investigation of impact of the particle inertia on the system dynamics is our main goal, in the present consideration we propose the use of the following scales as the characteristic units of length and time [36]

$$\hat{x} = \frac{x}{L}, \quad \hat{t} = \frac{t}{\tau_0}, \quad \tau_0 = \frac{\Gamma L^2}{\Delta U}. \quad (4)$$

Under such a procedure the Langevin equation (1) takes the dimensionless form

$$m\ddot{\hat{x}} + \dot{\hat{x}} = -\hat{U}'(\hat{x}) + a\cos(\omega\hat{t}) + f + \sqrt{2D}\hat{\xi}(\hat{t}). \quad (5)$$



In this scaling, the dimensionless mass is

$$m = \frac{\tau_1}{\tau_0} = \frac{M\Delta U}{\Gamma^2 L^2}, \quad (6)$$

where the second characteristic time is  $\tau_1 = M/\Gamma$  and the dimensionless friction coefficient is  $\gamma = 1$ . Other parameters are:  $a = (L/\Delta U)A$ ,  $\omega = \tau_0\Omega$ ,  $f = (L/\Delta U)F$ . The rescaled thermal noise reads  $\hat{\xi}(\hat{t}) = (L/\Delta U)\xi(\tau_0\hat{t})$  and assumes the same statistical properties as  $\xi(t)$ , namely  $\langle \hat{\xi}(\hat{t}) \rangle = 0$  and  $\langle \hat{\xi}(\hat{t})\hat{\xi}(\hat{s}) \rangle = \delta(\hat{t} - \hat{s})$ . The dimensionless noise intensity  $D = k_B T/\Delta U$  is the ratio of thermal energy and half of the activation energy the particle needs to overcome the nonrescaled potential barrier. The dimensionless potential  $\hat{U}(\hat{x}) = \sin(2\pi\hat{x})$  possesses the period  $\hat{L} = 1$  and the barrier height  $\Delta\hat{U} = 2$ . From now on, we will use only the dimensionless variables and therefore, in order to simplify the notation, we will omit the *hat* notation in the above equation.

## 2.2. Quantities of interest

In the present study we are particularly interested in the impact of inertia on properties of directed transport of particles in the stationary state. In the dimensionless formulation (5) it can be realized by changing the dimensionless mass (6). The case  $m = 0$  corresponds to overdamped dynamics and the setting  $m \ll 1$  represents the strong damping regime, which means that  $\tau_1 \ll \tau_0$ . The characteristic time  $\tau_1$  is obtained from a particular form of Eq. (1), i.e.  $M\dot{v} + \Gamma v = 0$  and has the interpretation of the relaxation time of the velocity of the free Brownian particle. The parameter  $\tau_0$  is extracted from the equation  $\Gamma\dot{x} = -U'(x)$  which can be viewed as the characteristic time to travel a distance from a maximum of the potential  $U(x)$  to its minimum in the overdamped case (it is not exactly this time which is infinite in the considered case but  $\tau_0$  scales it). It is remarkable that parameters of the potential  $U(x)$  such as its barrier height  $\Delta U$  and period  $L$  are crucial for controlling the regimes of weak or strong damping. For instance, if  $M$  and  $\Gamma$  are fixed and the system is in a weak damping regime  $m \gg 1$ , the transition to the strong damping case  $m \ll 1$  can be achieved by lowering the barrier height and lengthening the period of  $U(x)$ . We have checked that for values  $m \sim 0.1$  and smaller the system (5) can be considered to be in the strong damping regime.

Due to the presence of the external time-periodic driving  $a\cos(\omega t)$ , as well as the friction term  $\dot{x}$ , the particle velocity  $\dot{x}(t)$  approaches a unique non-equilibrium asymptotic long time state, in which it is characterized by a temporally periodic probability density. This latter function has the same period as the driving  $T = 2\pi/\omega$  [37]. Therefore, the first statistical moment of the instantaneous particle velocity  $\langle \dot{x}(t) \rangle$  assumes for an asymptotic long time regime the form of a Fourier series over all possible harmonics [37]

$$\lim_{t \rightarrow \infty} \langle \dot{x}(t) \rangle = \langle v \rangle + v_\omega(t) + v_{2\omega}(t) + \dots \quad (7)$$

where  $\langle v \rangle$  is the directed (time independent) velocity, while  $v_{n\omega}(t)$  denote time periodic higher harmonics of vanishing time-average over the fundamental period  $T = 2\pi/\omega$ . The observable of foremost interest in this study is the directed transport component  $\langle v \rangle$ , which due to the mentioned particular decomposition can be obtained in the following way

$$\langle v \rangle = \lim_{t \rightarrow \infty} \frac{\omega}{2\pi} \int_t^{t+2\pi/\omega} ds \langle \dot{x}(s) \rangle, \quad (8)$$

where  $\langle \cdot \rangle$  indicates averaging over all realizations of thermal noise as well as over initial conditions for the position  $x(0)$  and the velocity  $\dot{x}(0)$ . The latter is obligatory for the deterministic limit  $D \propto T \rightarrow 0$  when dynamics may be non-ergodic and results can be affected by specific choice of initial conditions [26].

Due to the multidimensionality of the parameter space of the considered model, as well as its nonlinearity, the force-velocity curve  $\langle v \rangle = \langle v \rangle(f)$  is typically a nonlinear function of the applied bias  $f$ . From the symmetries of the underlying Langevin equation (5) it follows that this observable is odd as a function of the external static force  $f$ , i.e.  $\langle v \rangle(-f) = -\langle v \rangle(f)$  and in consequence  $\langle v \rangle(f = 0) \equiv 0$  [1]. This is in clear contrast to the case of a ratchet mechanism, which exhibits the finite directed transport  $\langle v \rangle \neq 0$  even at the vanishing static bias when  $f = 0$  [2]. Since the observable of our interest is symmetric around  $f = 0$ , we limit our consideration to the positive bias  $f > 0$ . Then, for sufficiently small values of the external force  $f$  the directed transport velocity  $\langle v \rangle$  is usually its increasing function. Such regimes correspond to the normal, expected transport behaviour. However, in the parameter space there are also regimes for which the particle moves on average in the direction opposite to the applied bias, i.e.  $\langle v \rangle < 0$  for  $f > 0$ , exhibiting anomalous transport behaviour in the form of the negative mobility phenomenon [3,19]. It has been already shown that there are two fundamentally various mechanisms responsible for negative mobility in this setup, (i) generated by chaotic dynamics and (ii) induced by thermal equilibrium fluctuations [3]. The latter situation is nevertheless rooted in the sophisticated evolution of the corresponding deterministic system described by Eq. (5) with  $D = 0$ . Its three-dimensional phase space  $\{x, \dot{x}, \omega t\}$  is minimal for chaotic evolution, which is important for negative mobility to occur.

For the considered deterministic system with  $D = 0$  there are three Lyapunov exponents  $\lambda_1$ ,  $\lambda_2$  and  $\lambda_3$ . It can be easily checked that the system is dissipative, i.e. the phase space volume is contracting during the time evolution. Therefore the sum of all Lyapunov exponents must be negative [40]

$$\lambda_1 + \lambda_2 + \lambda_3 < 0. \quad (9)$$

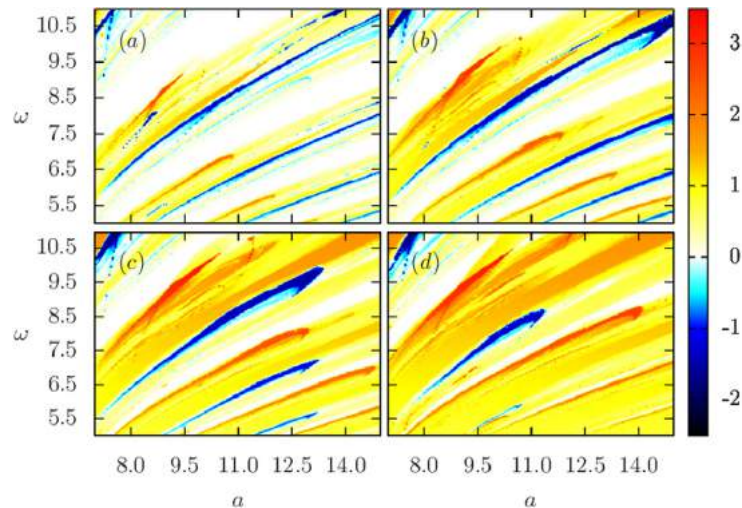


**Fig. 1.** The Brownian particle asymptotic long time directed velocity  $\langle v \rangle$  as a function of the amplitude  $a$  and the angular frequency  $\omega$  of the external unbiased harmonic driving  $a\cos(\omega t)$  is shown for different values of the bias  $f$  with  $D = 0$  and  $m = 0.1$ . Panel (a)  $f = 0.2$ , (b)  $f = 0.4$ , (c)  $f = 0.6$ , (d)  $f = 0.8$ .

One of the exponents, say  $\lambda_3 = 0$  and the other, say  $\lambda_2 < 0$ . If the system is chaotic  $\lambda_1$  must be positive indicating divergence of the trajectories. Therefore to detect chaotic behaviour of the system it is sufficient to calculate the maximal Lyapunov exponent  $\lambda = \lambda_1$  and check whether it is larger than zero [41].

### 3. Numerical simulation

Unluckily, the Fokker–Planck equation corresponding to the Langevin equation (5) cannot be handled by any known analytical methods. For this reason, in order to analyse transport properties of the system, we carried out comprehensive numerical simulations. We integrated the Langevin equation (5) by employing a weak version of the stochastic second order predictor corrector algorithm with a time step typically set to about  $10^{-2} \times 2\pi/\omega$ . We chose the initial coordinates  $x(0)$  and velocities  $\dot{x}(0)$  equally distributed over the intervals  $[0, 1]$  and  $[-2, 2]$ , respectively. The quantities of interest were ensemble averaged over  $10^3 - 10^4$  different trajectories, which evolved over  $10^3 - 10^4$  periods of the external harmonic driving. All numerical calculations were performed by the use of CUDA environment implemented on a modern desktop GPU. This gave us possibility to speed up the computations up to a factor of the order  $10^3$  times as compared to a common present day CPU method. Details on this promising scheme can be found in Ref. [42]. Dynamics described by Eq. (5) is characterized by a 5-dimensional parameter space  $\{m, a, \omega, f, D\}$ , the detailed exploration of which is a very challenging task even for our innovative computational method. However, we focus on the impact of the particle inertia on the anomalous transport processes occurring in this setup. This task is very tractable numerically with the currently available hardware. In order to find an anomalous transport regime, we start our analysis by looking at the deterministic system  $D = 0$ . We set the bias to a low value, e.g.  $f = 0.5$ , and check how the directed velocity  $\langle v \rangle$  depends on the remaining parameters. In doing so we performed scans of the following area  $m \times a \times \omega \in [0.01, 10] \times [0, 20] \times [0, 20]$  at a resolution of 200 points per dimension to determine the general behaviour of the system and obtain reasonable bounds on the system parameters. Our results reveal that negative mobility is not present for  $\omega > 18$  and  $\omega < 2$ . This is in agreement with the approximate solutions of Eq. (5). In the limit of the low frequency  $\omega \ll 1$  an adiabatic approximation is valid [43]. In such a situation the Brownian particle velocity  $\dot{x}$  adiabatically follows the total external force  $f(t) = f + a\cos(\omega t)$ . For high frequencies a solution can be formulated in terms of Bessel functions [38]. To derive the Bessel function form one assumes that the Brownian particle velocity is sinusoidal and satisfy the deterministic variant of Eq. (5), see page 947 of Ref. [38]. Shapiro et al. [39] originally suggested that in order to determine necessary coefficients of the assumed sinusoidal form of solution it is useful to expand the conservative force  $-U'(x)$  appearing in the model in a harmonic series given by the Bessel function. Finally, from our initial scans of the parameter space we infer that there is no net transport for  $a < 4$ .

## 4. Results

### 4.1. General behaviour of the system

The study of various aspects of transport in the system (5) has been presented elsewhere [3,19]. Here, we focus our analysis primarily on the relationship between inertia and negative mobility. In Fig. 1 we present the asymptotic long time directed velocity  $\langle v \rangle$  depicted as a function of the amplitude  $a$  and angular frequency  $\omega$  of the external harmonic driving  $a\cos(\omega t)$ , for the strongly damped Brownian particle with the dimensionless mass  $m = 0.1$  and different values of the external bias  $f$ . Surprisingly, despite the fact that the inertia is one order smaller than the dimensionless friction coefficient  $\gamma = 1$ ,

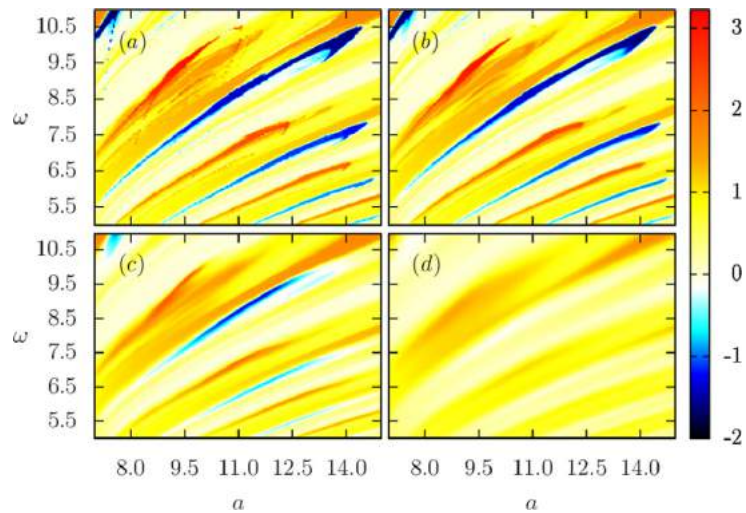


**Fig. 2.** The directed velocity  $\langle v \rangle$  versus the amplitude  $a$  and the angular frequency  $\omega$  is depicted for different values of thermal noise intensity  $D$  with  $m = 0.1$  and  $f = 0.5$ . Panel (a)  $D = 0$ , (b)  $D = 10^{-5}$ , (c)  $D = 10^{-3}$ , (d)  $D = 10^{-2}$ .

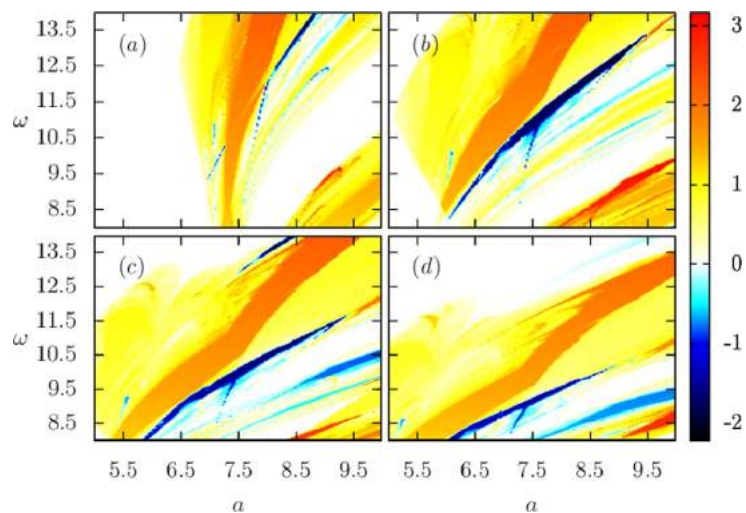


**Fig. 3.** The directed velocity  $\langle v \rangle$  versus the amplitude  $a$  and the angular frequency  $\omega$  is presented for different values of the particle mass  $m$  with  $D = 0$  and  $f = 0.5$ . Panel (a)  $m = 0.05$ , (b)  $m = 0.1$ , (c)  $m = 0.15$ , and (d)  $m = 0.2$ .

there are regions in the parameter space of the system where negative mobility occurs. They form a band-like structure. The stripes of negative velocity are interspersed with the stripes of positive velocity and the difference in its magnitude in the neighbouring regions can be significant. This suggests that the system may be very sensitive to a small change of values of parameters. It can be observed that larger values of  $f$  lead to reduction of the negative mobility areas towards the lower  $\omega$  and  $a$ . At the same time the bands of negative velocity become wider and more intense. In contrast, the regions of positive mobility increase population and supersede their negative counterparts. Overall, as the bias  $f$  is increased the band structure shrinks and finally disappears, and the averaged velocity is positive. For large values of  $f$  the velocity  $\langle v \rangle$  exhibits Ohmic-like behaviour being a monotonically increasing function of  $f$ . In Fig. 2 we depict the same characteristic but for different values of thermal noise intensity  $D$  with fixed  $m = 0.1$  and  $f = 0.5$ . One can expect that thermal noise perturbs deterministic dynamics. We observe that larger areas of negative mobility are relatively stable with respect to increasing temperature, while the smaller ones disappear more quickly. Thermal noise first blurs the band-like structure of negative mobility areas, erasing the finer details of the regions visible in the deterministic case  $D = 0$ . It seems to be obvious since thermal noise enables random transitions between deterministically coexisting basins of attraction. For high enough temperatures, negative mobility disappears completely. A careful inspection of Fig. 2 reveals that there are regions in the parameter space where the directed velocity  $\langle v \rangle$  is zero or positive in the deterministic case, but becomes negative upon the introduction of noise. This fact suggests that thermal fluctuations may induce negative mobility or reverse its sign even for the strongly damped Brownian particle. Most likely for these parameter regimes there exists a large number of unstable periodic orbits transporting the particle in both positive and negative directions and influencing the relaxation dynamics from points lying far from the stable solutions. In the presence of thermal noise the particle is constantly kicked out from the stable solutions in the way which favour the unstable orbits transporting the particle to the negative direction. Finally, in Fig. 3 we present

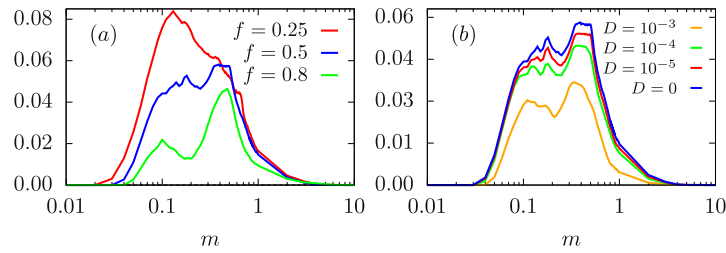


**Fig. 4.** Fraction of the negative mobility area in the analysed parameter space,  $a \in [0, 20]$ ,  $\omega \in [0, 20]$  is presented in panel (a) for  $D = 0$  and different values of the bias  $f$  and (b) for  $f = 0.5$  and various temperatures  $D$ .

the directed velocity  $\langle v \rangle$  versus the amplitude  $a$  and the angular frequency  $\omega$  for different values of the mass  $m$  with  $D = 0$  and  $f = 0.5$ . The stripes of negative mobility move towards lower values of  $\omega$  and higher values of  $a$  as  $m$  is increased. The band-like structure changes its inclination and the regions becomes more horizontally oriented. Moreover, for larger masses  $m$  some new negative mobility bands appear, while at the same time the negative velocity tends to disappear in other regions. This effect suggests that there should exist an optimal mass  $m$  for which the occurrence of negative mobility is mostly pronounced.

#### 4.2. Optimal mass for the presence of negative mobility

Since the impact of the mass  $m$  seems to be non-trivial, an interesting task is to find the value of  $m$  for which the presence of negative mobility is the most common. Our numerical scans of the parameter space allowed us to determine this value. The result is shown in Fig. 4. In panel (a) we depict fraction of the negative mobility area in the analysed parameter space for the deterministic system  $D = 0$  and different values of the bias  $f$ . A perhaps surprising finding is that for the small values of the static load  $f = 0.25$  the optimal mass for the presence of negative mobility is  $m \approx 0.13$ . It is significantly less than the magnitude of dimensionless friction coefficient, which for the employed scaling is equal to unity  $\gamma = 1$ . This fact indicates that the friction plays prevalent role for the emergence of negative mobility. Moreover, even for the very strongly damped Brownian particle  $m \ll \gamma = 1$  the area of negative mobility is non-zero and relatively large. In both limiting regimes of the overdamped  $m \rightarrow 0$  and the underdamped  $m \rightarrow \infty$  motion there are no regions of negative mobility. Ipso facto we confirmed numerically the no-go theorem formulated in Ref [19]. This conclusion is valid also for larger values of the bias  $f$ , however, then the optimal mass  $m$  for the presence of negative mobility becomes shifted towards higher, e.g.  $m \approx 0.47$  for  $f = 0.8$ . Moreover, as the static load  $f$  is increased the overall occurrence of negative mobility in the analysed parameter space is decreased and the presented curves come to be more flattened. In panel (b) we show the same characteristic but for the fixed bias  $f = 0.5$  and different values of thermal noise intensity  $D$ . As temperature grows the regions of negative mobility in the parameter space tend to contract which is illustrated in the figure. Apart from this fact for stronger thermal noise, c.f. the case  $D = 10^{-3}$ , the curve becomes noticeably more bimodal. This observation is most likely due to parameter regimes for which negative mobility is induced by thermal fluctuations.

#### 4.3. The mechanisms of negative mobility

To gain further insight into the nature of negative mobility in this system, as the next step we identify, exemplify and analyse the mechanisms standing behind emergence of this phenomenon. In Fig. 5 we present the regime of parameters for which negative mobility occurs on grounds which are rooted solely in the complex, strongly damped and deterministic chaotic dynamics. Panel (a) depicts the directed velocity  $\langle v \rangle$  versus the external static bias  $f$ . It is a nonlinear function without any obvious relation to the magnitude of the force  $f$ . Clearly, there are two windows of the latter parameter for which negative mobility  $\langle v \rangle < 0$  is observed. The first starts at  $f \approx 0.1$  and ends at  $f \approx 0.7$ . In this interval, the minimal value of  $\langle v \rangle \approx -0.767$  is at the bias value  $f = 0.658$ . The second is present for the bias larger than approximately  $f \approx 0.9$ . In turn, panel (b) presents the directed velocity  $\langle v \rangle$  as a function of thermal noise intensity  $D$  for the fixed bias  $f = 0.66$  for which  $\langle v \rangle \approx -0.26$  in the limit  $D \rightarrow 0$ . In the regime of very low temperatures  $D \rightarrow 0$  the measured directed velocity is less than zero indicating that negative mobility has its origin in the complex deterministic dynamics. For increasing temperature the directed velocity grows as well up to the critical thermal noise intensity  $D \approx 10^{-3}$ , for which the Brownian particle response reverses its sign  $\langle v \rangle > 0$ . In the high temperature limit  $D \rightarrow \infty$  (not depicted) all forces in the right hand side of Eq. (5) become negligible in comparison to thermal noise and thus the directed velocity vanishes completely  $\langle v \rangle = 0$ . Panel (c) of the same figure presents the bifurcation diagram of the latter quantity  $\langle v \rangle$  illustrated as the function of the external bias  $f$  for the deterministic system with  $D = 0$ . Each blue dot represents an attractor for the asymptotic long time directed velocity  $\langle v \rangle$ . For almost all values in the considered range of the bias  $f$  there is the continuum of the directed velocity solutions. This fact suggests that the system is predominantly chaotic in this interval. We confirm this hypothesis in panel (d) where we depict the maximal Lyapunov exponent  $\lambda$  for the deterministic system described by Eq. (5) with  $D = 0$  versus the biasing force  $f$ . Accordingly, this quantity is positive in almost entire considered interval of the parameter  $f$ . In particular, it is so for the values of  $f$  corresponding to negative mobility. Therefore, we conclude that in the presented parameter regime this

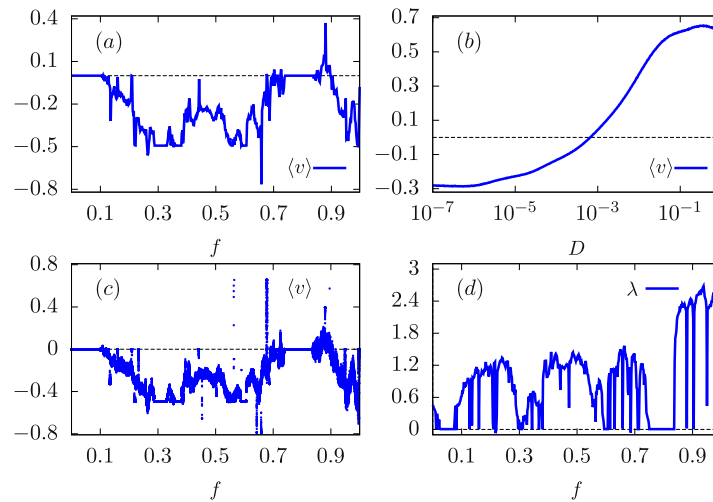


**Fig. 5.** The negative mobility of the strongly damped Brownian particle  $m \ll 1$  induced by the deterministic chaotic dynamics. Panel (a) the directed velocity  $\langle v \rangle$ , (c) bifurcation diagram of the directed velocity  $\langle v \rangle$ , (d) the maximal Lyapunov exponent  $\lambda$  as the function of the external static bias  $f$  with  $D = 0$ . Panel (b) the directed velocity  $\langle v \rangle$  versus thermal noise intensity  $D$  for  $f = 0.66$ . Other parameters are  $m = 0.0555$ ,  $a = 8.55$ ,  $\omega = 12.38$ .

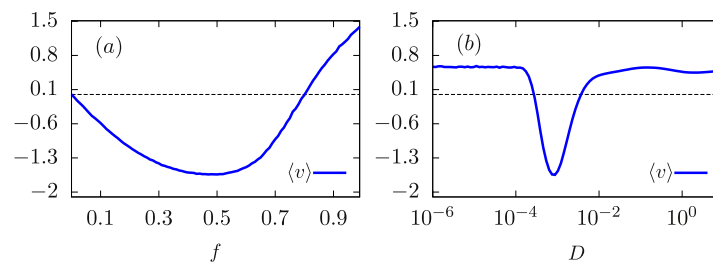


**Fig. 6.** The negative mobility of the strongly damped Brownian particle  $m \ll 1$  induced by thermal equilibrium fluctuations. The directed velocity  $\langle v \rangle$  is presented versus external static bias  $f$  in panel (a) and versus thermal noise intensity  $D$  in panel (b). Parameters are the same as in Fig. 5, except now  $m = 0.1047$ ,  $f = 0.5$  and  $D = 0.0009$ .

phenomenon is induced solely by the chaotic deterministic dynamics of the system given by Eq. (5). Such a mechanism has been already reported in literature [3,19], however, here we prove that it may operate also for the strongly damped Brownian particle  $m \ll \gamma = 1$ .

The second mechanism of the emergence of negative mobility is exemplified in Fig. 6. In panel (a) we present the directed velocity  $\langle v \rangle$  of the strongly damped Brownian particle  $m \ll \gamma = 1$  versus the external static bias  $f$  for thermal fluctuations intensity  $D = 0.0009$ . In this case a very small amount of noise yields negative mobility in the linear response regime, i.e. for small forces  $f$ . For larger values of the bias  $f$  the directed velocity is positive  $\langle v \rangle > 0$  and the particle moves in the direction pointed by the static force  $f$ . Interestingly, there is an optimal value of  $f \approx 0.5$  for which negative mobility is most pronounced. To gain further insight into the origin of the discussed anomaly in the presented regime, in the neighbouring panel (b) we study the directed velocity  $\langle v \rangle$  as a function of thermal noise intensity  $D \propto T$ . Contrary to the previously presented case, here at low temperature  $D \rightarrow 0$  the Brownian particle velocity is positive. The above described negative mobility manifests itself only in finite interval of temperature  $D \in (2.8 \times 10^{-4}, 3.2 \times 10^{-3})$ . Further increase of thermal noise intensity leads to disappearance of this phenomenon. Although a solely noise induced negative mobility can occur only under impact of thermal fluctuations, the underlying relevant mechanism is strongly influenced by the deterministic dynamics as it was already shown in Ref. [3].

Finally, in Fig. 7 we present a case of negative mobility induced by the deterministic *non-chaotic* dynamics of the system. Panel (a) illustrates the directed velocity  $\langle v \rangle$  as a function of the external bias  $f$  for the deterministic case  $D = 0$  and in the strong damping regime  $m \ll 1$ . For very small values of the force  $f$  the directed velocity oscillates around zero. When the bias is of moderate magnitude there is a window for which the particle response is opposite to the applied constant perturbation, so we detect there negative mobility. Further increase of the external force rapidly reverses the particle current and causes its monotonic growth. In panel (b) we study the impact of thermal fluctuations on  $\langle v \rangle$  in the parameter regime with  $f = 0.5$  corresponding to the minimal plateau depicted in the plot (a). Indeed, for the deterministic limit of the dynamics  $D \rightarrow 0$  the directed velocity  $\langle v \rangle$  is negative suggesting that the observed phenomenon of negative mobility has the deterministic origin. An increase of thermal noise intensity ceases this effect. For this parameter regime there is a surprisingly simple structure of attractors for the directed velocity which is visualized in the panel (c) in the deterministic case with  $D = 0$ . In the considered interval of the external force  $f$  there are two asymptotically stable solutions corresponding to  $\langle v \rangle = \pm 2$ . Notably, in the bias window where negative mobility is observed only the attractor  $\langle v \rangle = -2$  survives. This unexpected simplicity

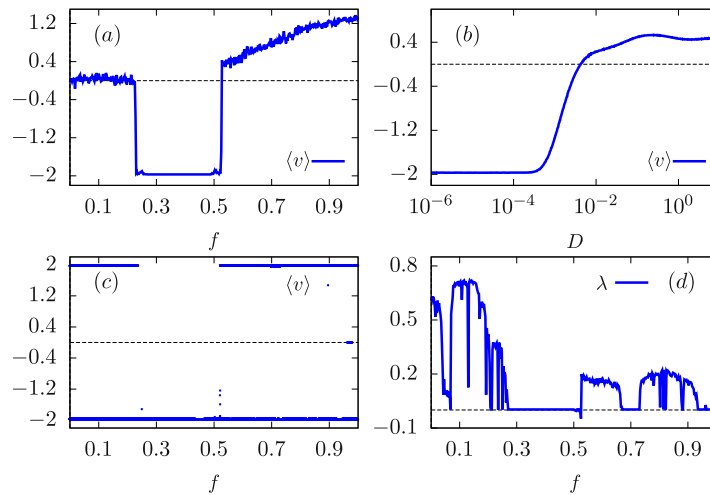


**Fig. 7.** The negative mobility of the strongly damped Brownian particle  $m \ll 1$  induced by the deterministic non-chaotic dynamics. Panel (a) the directed velocity  $\langle v \rangle$ , (c) bifurcation diagram of the directed velocity  $\langle v \rangle$ , (d) the maximal Lyapunov exponent  $\lambda$  as the function of the external static bias  $f$  with  $D = 0$ . Panel (b) the directed velocity  $\langle v \rangle$  versus thermal noise intensity  $D$  for  $f = 0.5$ . Other parameters are the same as in Fig. 5 and  $m = 0.1$ .

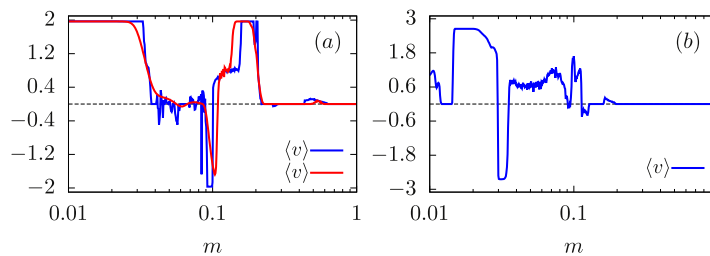


**Fig. 8.** The directed velocity  $\langle v \rangle$  of the driven Brownian particle versus its inertia  $m$ . Panel (a):  $a = 8.55$ ,  $\omega = 12.38$  and  $f = 0.5$ . The blue curve is for the deterministic case  $D = 0$  and the red curve is for the noisy system with  $D = 0.0009$ . Panel (b):  $a = 9.845$ ,  $\omega = 16.64$ ,  $f = 0.25$  and  $D = 10^{-5}$ . (For interpretation of the references to color in this figure legend, the reader is referred to the web version of this article.)

of solutions suggests that in the considered parameter regime the deterministic dynamics is non-chaotic, nonetheless still exhibits negative mobility. Our finding is confirmed in panel (d) where we depict the maximal Lyapunov exponent  $\lambda$  versus the bias  $f$  for the system with  $D = 0$ . An interesting observation is that the dynamics is generally chaotic ( $\lambda > 0$ ) when two attractors  $\langle v \rangle = \pm 2$  coexist and it is non chaotic with  $\lambda = 0$  in the window where negative mobility emerges. To the best of the authors knowledge such a mechanism has never been reported. It may potentially open a possibility of observation of the negative mobility phenomenon for the discontinuous or non-ergodic one-dimensional nonequilibrium overdamped dynamics, corresponding to the formal substitution  $m = 0$  in Eq. (5) [19].

#### 4.4. Impact of inertia

To conclude this section we present in Fig. 8 the representative dependence of the directed velocity  $\langle v \rangle$  on the inertia  $m$  for the deterministic and noisy system. In panel (a) the amplitude  $a$  and frequency  $\omega$  of the periodic driving are the same as in the previous Figs. 5–7. Here, the most pronounced negative mobility is observed for the mass  $m \approx 0.1$ . For specifically tailored parameter sets this phenomenon could be detected for even smaller mass. We exemplify this situation in panel (b) where it is observed for  $m \approx 0.03$  which is indeed the regime of very strong damping.

We observe that the system response is very sensitive to even smallest changes of the particle mass  $m$ . Moreover, there are multiple reversals of the sign of the directed velocity which are characteristic for a massive setup driven by the external harmonic force [44,45]. This finding can be utilized to particle sorting [46]. For instance, one can see from the above figure that particles with different masses can easily be guided into opposite direction by a suitable choice of the system parameters. In addition, we want to point out that the occurrence of the three presented mechanisms of negative mobility are controlled by the magnitude of the particle inertia. Depending on its value the deterministic chaotic, thermal noise induced and the deterministic non-chaotic anomalous transport can be observed. It is worth to explicitly note that a tiny change from  $m = 0.1$  to  $m = 0.1047$  transforms the nature of negative mobility effect from deterministic non-chaotic to thermal noise induced, c.f. Figs. 6 and 7. Therefore, the outlined mechanisms of the occurrence of negative mobility are also very sensitive to alteration of the particle inertia.

## 5. Conclusion

In this work we investigated the impact of inertia on transport properties of a Brownian particle moving in a periodic symmetric structure, which in addition is exposed to a harmonic ac driving as well as a constant bias. The parameter space is 5-dimensional and its complete numerical exploration is far beyond the scope of this work. We first analysed the general behaviour of the directed velocity ( $v$ ) as a function of the amplitude  $a$  and the angular frequency  $\omega$  of the driving, for selected values of the remaining system parameters: the particle inertia  $m$ , the external bias  $f$  and thermal noise intensity  $D$ . These results reveal especially that the negative mobility phenomenon emerges also for the strongly damped motion of a Brownian particle when the dissipation dominates over inertia. Our scans of the parameter space allowed us to determine the optimal mass  $m \approx 0.35$  for the presence of the negative mobility phenomenon. By observing that the fraction of the negative mobility area in the analysed parameter space disappears for both the limiting cases of the overdamped  $m \rightarrow 0$  and underdamped  $m \rightarrow \infty$  motion, we confirmed with precise numerics the no-go theorem formulated in Ref. [19]. We gained further insights into the origin of negative mobility in this system by revealing three classes of mechanisms responsible for this anomalous transport process. It can be (i) caused by the complex deterministic chaotic dynamics of the system or (ii) induced by the thermal noise, or (iii) associated with the deterministic, yet non-chaotic system evolution. In particular, according to the best of authors knowledge, the latter origin has never been reported before. It may provide guidance to the possibility of observation of the negative mobility phenomenon for the discontinuous or non-ergodic one-dimensional nonequilibrium overdamped dynamics when the particle inertia is fixed to zero  $m = 0$ . This case is of fundamental importance from the point of view of biological systems, all of which in situ operate in strongly fluctuating environments. Finally, we depict the illustrative impact of the particle inertia on its transport properties to unravel its spectacular sensitiveness to variation of this parameter. We detect the phenomenon of multiple velocity reversals which may constitute a cornerstone of particle sorting. Moreover, a small change in the particle inertia can radically alter the mechanism of negative mobility.

Our results can readily be experimentally tested with a single Josephson junction device or cold atoms moving in a dissipative optical lattice. Suitable parameter values, for which the above effects are predicted to occur, are accessible experimentally.

## Acknowledgement

The work was supported by the NCN grant 2015/19/B/ST2/02856 (J. S. & J. Ł.).

## References

- [1] Denisov S, Flach S, Hänggi P. Tunable transport with broken space-time symmetries. *Phys Rep* 2014;538:77–120.
- [2] Hänggi P, Marchesoni F. Artificial Brownian motors: controlling transport on the nanoscale. *Rev Mod Phys* 2009;81:387.
- [3] Machura L, et al. Absolute negative mobility induced by thermal equilibrium fluctuations. *Phys Rev Lett* 2007;98:40601.
- [4] Nagel J, et al. Observation of negative absolute resistance in a Josephson junction. *Phys Rev Lett* 2008;100:217001.
- [5] Kostur M, Łuczka J, Hänggi P. Negative mobility induced by colored thermal fluctuations. *Phys Rev E* 2009;80:051121.
- [6] Spiechowicz J, Łuczka J, Hänggi P. Absolute negative mobility induced by white Poissonian noise. *J Stat Mech* 2013:P02044.
- [7] Spiechowicz J, Łuczka J, Machura L. Efficiency of transport in periodic potentials: dichotomous noise contra deterministic force. *J Stat Mech* 2016;054038.
- [8] Hennig D. Current control in a tilted washboard potential via time-delayed feedback. *Phys Rev E* 2009;79:041114.
- [9] Du L, Mei D. Time delay control of absolute negative mobility and multiple current reversals in an inertial Brownian motor. *J Stat Mech* 2011:P11016.
- [10] Mulhern C. Persistence of uphill anomalous transport in inhomogeneous media. *Phys Rev E* 2013;88:022906.
- [11] Dandogbessi B, Kenfack A. Absolute negative mobility induced by potential phase modulation. *Phys Rev E* 2015;92:062903.
- [12] Du L, Mei D. Absolute negative mobility in a vibrational motor. *Phys Rev E* 2012;85:011148.
- [13] Januszewski M, Łuczka J. Indirect control of transport and interaction-induced negative mobility in an overdamped system of two coupled particles. *Phys Rev E* 2011;83:051117.
- [14] Machura L, et al. Two coupled Josephson junctions: dc voltage controlled by biharmonic current. *J Phys Condens Matter* 2012;24:085702.
- [15] Ghosh PK, Hänggi P, Marchesoni F, Nori F. Giant negative mobility of Janus particles in a corrugated channel. *Phys Rev E* 2014;89:062115.
- [16] Malgaretti P, Pagonabarraga I, Rubi JM. Entropic electrokinetics: recirculation, particle separation, and negative mobility. *Phys Rev Lett* 2014;113:128301.
- [17] Sarracino A, Cecconi F, Puglisi A, Vulpiani A. Nonlinear response of inertial tracers in steady laminar flows: differential and absolute negative mobility. *Phys Rev Lett* 2016;117:174501.
- [18] Bressloff PC, Newby JM. Stochastic models of intracellular transport. *Rev Mod Phys* 2013;85:135.
- [19] Speer D, Eichhorn R, Reimann P. Transient chaos induces anomalous transport properties of an underdamped Brownian particle. *Phys Rev E* 2007;76:051110.
- [20] Risken H. *The Fokker–Planck Equation*. Berlin: Springer-Verlag; 1984.
- [21] Magnasco MO. Forced thermal ratchets. *Phys Rev Lett* 1993;71:1477.
- [22] Sarracino A. Time asymmetry of the Kramers equation with nonlinear friction: fluctuation-dissipation relation and ratchet effect. *Phys Rev E* 2013;88(8):052124.
- [23] Gnoli A, et al. Brownian ratchet in a thermal bath driven by Coulomb friction. *Phys Rev Lett* 2013;110:120601.
- [24] Łuczka J, Bartussek R, Hänggi P. White noise induced transport in periodic structures. *Europhys Lett* 1995;31:431–6.
- [25] Spiechowicz J, Hänggi P, Łuczka J. Brownian motors in the microscale domain: enhancement of efficiency by noise. *Phys Rev E* 2014;90:032104.
- [26] Spiechowicz J, Łuczka J, Hänggi P. Transient anomalous diffusion in periodic systems: ergodicity, symmetry breaking and velocity relaxation. *Sci Rep* 2016;6:30948.
- [27] Spiechowicz J, Kostur M, Łuczka J. Brownian ratchets: how stronger thermal noise can reduce diffusion. *Chaos* 2017;27:023111.
- [28] Dechant A, et al. Gaussian white noise as a resource for work extraction. *Phys Rev E* 2017;95:032132.
- [29] Marconi UMB, Puglisi A, Rondoni L, Vulpiani A. Fluctuation-dissipation: response theory in statistical physics. *Phys Rep* 2008;461:111–95.
- [30] Blackburn JA, Cirillo M, Gronbech-Jensen N. A survey of classical and quantum interpretations of experiments on Josephson junctions at very low temperatures. *Phys Rep* 2016;611(1).

- [31] Lutz E, Renzoni F. Beyond Boltzmann–Gibbs statistical mechanics in optical lattices. *Nat Phys* 2013;9(615).
- [32] Fulde P, et al. Problem of Brownian motion in a periodic potential. *Phys Rev Lett* 1975;35:1776.
- [33] Coffey W, Kalmykov Y, Waldron J. *The Langevin Equation*. Singapore: World Scientific; 2004.
- [34] Gruner G, Zawadowski A, Chaikin P. Nonlinear conductivity and noise due to charge-density-wave depinning in  $nbse_3$ . *Phys Rev Lett* 1981;46:511.
- [35] Guantes R, Vega J, Miret-Artés S. Chaos and anomalous diffusion of adatoms on solid surfaces. *Phys Rev B* 2001;64:245415.
- [36] Machura L, Kostur M, Łuczka J. Transport characteristics of molecular motors. *BioSystems* 2008;05:033.
- [37] Jung P. Periodically driven stochastic systems. *Phys Rep* 1993;234:175.
- [38] Kautz RL. Noise, chaos and the Josephson voltage standard. *Rep Prog Phys* 1996;59:935.
- [39] Shapiro S, et al. Effect of microwaves on Josephson currents in superconducting tunneling. *Rev Mod Phys* 1964;36:223.
- [40] Baker GL, Gollub JP. *Chaotic Dynamics: An Introduction*. Cambridge: Cambridge University Press; 1996.
- [41] Boffetta G, Cencini M, Falcioni M, Vulpiani A. Predictability: a way to characterize complexity. *Phys Rep* 2002;356:367.
- [42] Spiechowicz J, Kostur M, Machura L. GPU accelerated Monte Carlo simulation of Brownian motor dynamics with CUDA. *Comp Phys Commun* 2015;191:140.
- [43] Chi CC, Vanneste C. Onset of chaos and dc current-voltage characteristics of rf-driven Josephson junctions in the low-frequency regime. *Phys Rev B* 1990;42:9875.
- [44] Bartussek R, Hänggi P, Kissner JG. Periodically rocked thermal ratchets. *Europhys Lett* 1994;28:459.
- [45] Jung P, Kissner JG, Hänggi P. Regular and chaotic transport in asymmetric periodic potentials: inertia ratchets. *Phys Rev Lett* 1996;76:3436.
- [46] Eichhorn R, Regtmeier J, Anselmetti D, Reimann P. Negative mobility and sorting of colloidal particles. *Soft Matter* 2010;6:1858.



## Tunable Mass Separation via Negative Mobility

A. Słapik,<sup>1</sup> J. Łuczka,<sup>1</sup> P. Hänggi,<sup>2,3</sup> and J. Spiechowicz<sup>1,2</sup><sup>1</sup>*Institute of Physics and Silesian Center for Education and Interdisciplinary Research, University of Silesia, 41-500 Chorzów, Poland*<sup>2</sup>*Institute of Physics, University of Augsburg, D-86135 Augsburg, Germany*<sup>3</sup>*Nanosystems Initiative Munich, Schellingstraße 4, D-80799 München, Germany* (Received 19 September 2018; revised manuscript received 22 November 2018; published 21 February 2019)

A prerequisite for isolating diseased cells requires a mechanism for effective mass-based separation. This objective, however, is generally rather challenging because typically no valid correlation exists between the size of the particles and their mass value. We consider an inertial Brownian particle moving in a symmetric periodic potential and subjected to an externally applied unbiased harmonic driving in combination with a constant applied bias. In doing so, we identify a most efficient separation scheme which is based on the anomalous transport feature of negative mobility, meaning that the immersed particles move in the direction opposite to the acting bias. This work is the first of its kind in demonstrating a *tunable* separation mechanism in which the particle mass targeted for isolation is effectively controlled over a regime of nearly 2 orders of mass magnitude upon changing solely the frequency of the external harmonic driving. This approach may provide mass selectivity required in present and future separation of a diversity of nano- and microsized particles of either biological or synthetic origin.

DOI: [10.1103/PhysRevLett.122.070602](https://doi.org/10.1103/PhysRevLett.122.070602)

The objective of separating and sorting particles of small size is attracting growing interest [1–20], opening the way towards the precise analysis of biophysical and synthetic processes on the microscale. In this regime of sizes the omnipresent Brownian jitter dynamics is of relevant impact. Nowadays, effective isolation and separation techniques are of essential importance in a wide range of areas including both research and industrial applications. Particularly, such techniques carry a large potential to study selective transport of biological particles such as whole cells, organelles, or DNA complexes. It has been found that several diseases alter physical properties of cells and therefore their sorting has great significance in health care [21]. So far, much emphasis has been placed on size based isolation techniques [6,7,10–13,15–18,20]. However, another aspect representing one of the most important factors for specifically identifying a bioparticle presents its own mass. For instance, cancer cells are found to differ in mass as compared to healthy ones [21]. This fact suggests that mass heterogeneity might be an important factor associated with disease initiation and progression. A reliable and effective approach to separating particles by their masses is therefore much in demand and hence one needs to learn more about various mechanisms for separating different masses on the Brownian scale [14,22,23]. As is commonly appreciated, the task is challenging because of the fact that heavier objects do not necessarily imply also larger sizes. This very feature thereby excludes passive mechanical separation techniques such as filtration in artificial sieves [24].

In the following, we demonstrate a nonintuitive, yet efficient, mass-based separation strategy taking advantage of a paradoxical mechanism of negative mobility (NM) [3,25–29]. In a regime of NM the particles move in a direction opposite to the net acting force. This phenomenon rests on two main ingredients: (i) a spatially periodic nonlinear structure together with (ii) an inertial nonequilibrium stochastic dynamics created, for example, via a time-periodic varying driving force of vanishing mean value. We demonstrate that under an additional action of an applied constant bias only particles of a given mass migrate in the direction opposite to this net force, whereas the others move concurrently towards it. This opens the possibility of steering different particle species in opposite directions under identical experimental conditions. Moreover, we demonstrate that the mass targeted for separation can be tuned by nearly 2 orders of magnitude by changing only the frequency of external time-periodic driving. The proof of principle experiment of a similar separation scheme but based rather on the particle size has been already demonstrated in Refs. [30,31], using a lab-on-a-chip device, consisting of insulator dielectrophoresis in a nonlinear, symmetric microfluidic structure with electrokinetically induced transport. This system was built employing a photolithographic device fabrication strategy without the need of making use of more complex nanofabrication techniques. Very recently, it allowed one to induce not only for colloidal particles but even for a biological compound in the form of mouse liver mitochondrion [32]. Therefore, the separation scheme proposed here

may provide mass selectivity required for individual isolation of nano- and microparticles, proteins, organelles, and cells. Yet other suitable setups which allow one to test our theoretical predictions would be based on cold atoms dwelling in optical lattices [33,34].

Let us consider a classical inertial Brownian particle dynamics of mass  $M$  moving in a spatially periodic one-dimensional potential  $U(x) = U(x + L)$  of period  $L$  which is subjected to an unbiased time-periodic force  $A \cos(\Omega t)$  of amplitude  $A$  and angular frequency  $\Omega$ , as well as an external static force  $F$ . The Brownian dynamics of such a particle is described by the Langevin equation [35]

$$M\ddot{x} + \Gamma\dot{x} = -U'(x) + A \cos(\Omega t) + F + \sqrt{2\Gamma k_B T} \xi(t). \quad (1)$$

The parameter  $\Gamma$  denotes the friction coefficient and  $k_B$  is the Boltzmann constant. The periodic potential  $U(x)$  is taken to possess *reflection symmetry* with period  $L$  and a potential height  $2\Delta U$ , i.e.,

$$U(x) = \Delta U \sin\left(\frac{2\pi}{L}x\right). \quad (2)$$

The interaction with a heat bath of temperature  $T$  is described by thermal fluctuations modeled by Gaussian white noise of zero mean and unit intensity, i.e.,

$$\langle \xi(t) \rangle = 0, \quad \langle \xi(t)\xi(s) \rangle = \delta(t-s). \quad (3)$$

Despite the apparent simplicity of this model setup it exhibits peculiar transport behaviors including, e.g., a nonequilibrium noise enhanced transport efficiency [28], anomalous diffusion [36], amplification of normal diffusion [37,38], or also a nonmonotonic temperature dependence of normal diffusion [39].

For our analysis we first recast Eq. (1) into its dimensionless form, i.e.,

$$m\ddot{\hat{x}} + \dot{\hat{x}} = -\hat{U}'(\hat{x}) + a \cos(\omega \hat{t}) + f + \sqrt{2D}\hat{\xi}(\hat{t}), \quad (4)$$

where  $\hat{x} = x/L$ ,  $\hat{t} = t/\tau_0$ , and  $\tau_0 = \Gamma L^2/\Delta U$ . The dimensionless mass  $m$  is given by the ratio of two characteristic timescales, reading

$$m = \frac{\tau_1}{\tau_0} = \frac{M\Delta U}{\Gamma^2 L^2}, \quad (5)$$

where  $\tau_1 = M/\Gamma$ . We here emphasize the fact that the dimensionless mass  $m$  depends not only on the actual physical mass of the particle  $M$  but also on the friction coefficient  $\Gamma$  as well as the parameters of the potential, i.e., on half of its barrier height  $\Delta U$  and the period  $L$ . The strength of friction  $\Gamma$  enters inversely the scaled mass value and it implies

that the rescaled mass assumes in the regime of viscous moderate-large friction (i.e., operating at low Reynolds numbers, being typical for microsized particles immersed in solution [40,41]) a rather small value. The dimensionless noise intensity reads  $D = k_B T/\Delta U$ . The remaining quantities are explicitly defined as detailed in Ref. [35]. From here on, we stick throughout to these dimensionless variables. In order to simplify the notation, we will also omit the *hat* notation in Eq. (4).

The observable of main interest for mass separation is the directed velocity  $\langle v \rangle$  of the particle, reading [35]

$$\langle v \rangle = \lim_{t \rightarrow \infty} \frac{1}{t} \int_0^t ds \langle \dot{x}(s) \rangle, \quad (6)$$

where  $\langle \cdot \rangle$  indicates averaging over the thermal noise realizations as well as over the initial conditions for the position  $x(0)$  and velocity  $\dot{x}(0)$  of the Brownian particle. The latter is required in the deterministic limit  $D \propto T \rightarrow 0$  when the dynamics may turn out to be nonergodic and dependent on specific choice of these initial conditions [42].

Knowingly, the Fokker-Planck equation corresponding to the Langevin Eq. (4) cannot be solved analytically in closed form. The task is thus to systematically analyze by comprehensive numerical means the emerging and rich variety of possible transport behaviors. The setup comprises a complex five-dimensional parameter space  $\{m, a, \omega, f, D\}$ . We nonetheless succeeded in performing the numerical analysis with unprecedented resolution. Overall, we considered nearly  $10^9$  different parameter sets. The high precision was made possible solely due to an innovative computational method which is based on employing GPU supercomputers, for details see in Ref. [43].

The underlying symmetries of the Langevin dynamics in Eq. (4) imply that the directed velocity  $\langle v \rangle$  behaves odd as a function of the external static bias  $f$ , i.e.,  $\langle v \rangle(-f) = -\langle v \rangle(f)$  so that  $\langle v \rangle(f=0) \equiv 0$  [3]. Generally,  $\langle v \rangle$  is an increasing function in the direction of the static bias  $f$  as one commonly would expect. The resulting particle transport velocity thus follows in the direction of the acting bias  $f$ ,  $\langle v \rangle = \mu(f)f$ , with a positive-valued nonlinear mobility  $\mu(f) > 0$ . However, in the parameter space there occur also regimes for which the particle moves on average in the opposite direction to the applied bias; i.e.,  $\langle v \rangle < 0$  for  $f > 0$  thus exhibiting anomalous transport in the form of NM with  $\mu(f) < 0$  [26–29]. The key prerequisite for the occurrence of the latter phenomenon is that the system (i) is driven far from thermal equilibrium into a time-dependent *nonequilibrium* state, whose inertial dynamics does exhibit (ii) zero crossings of  $\langle v \rangle$  [26,27]. In our case this condition is induced by the presence of the external time-periodic driving  $a \cos(\omega t)$  which in turn *overrides* the limiting response behavior encoded with the Le Chatélier–Braun equilibrium principle [44], stating that at finite  $f$  the response occurs into the

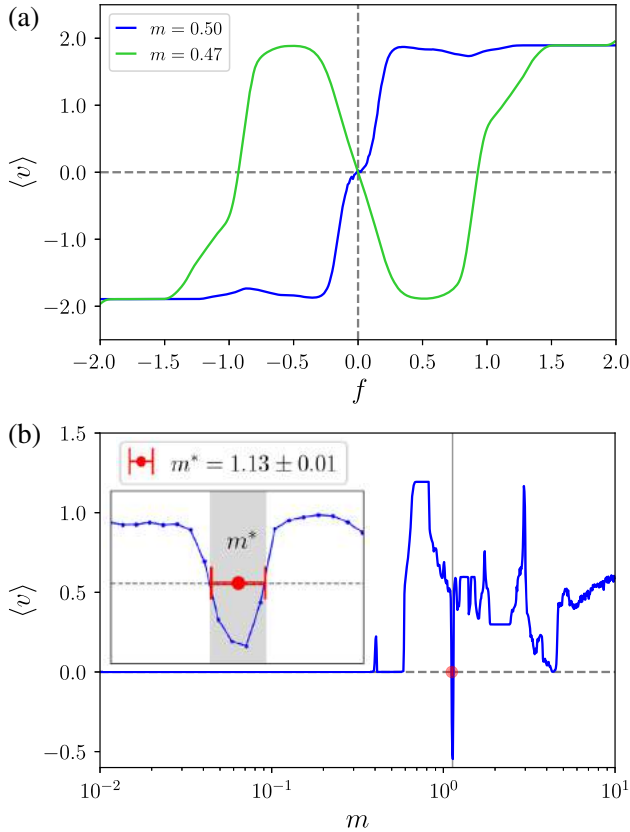


FIG. 1. (a) The force-directed velocity curve  $\langle v \rangle(f)$  is depicted for the two parameter regimes corresponding to normal (blue) and anomalous (green) transport behavior in the form of NM. Note the sensitivity of the latter effect with respect to changes of the dimensionless mass  $m$ . The chosen parameters are  $a = 10$ ,  $\omega = 5.95$ , and  $D = 0.001$ . (b) The directed velocity  $\langle v \rangle$  versus mass  $m$ . In the inset we present the blow up (red region) showing the interval of the NM phenomenon as marked by the gray area. Parameters are  $a = 5.125$ ,  $\omega = 3.75$ ,  $f = 1$ ,  $D = 0.0001$ .

direction of the applied force towards a new, displaced equilibrium.

With panel (a) of Fig. 1 we exemplify two force-velocity characteristics,  $\langle v \rangle(f)$ , corresponding to normal and NM transport behavior. Please note the sensitivity of the latter effect with respect to minute changes in the dimensionless mass  $m$ . A tiny change in mass by  $\Delta m = 0.03$  is accompanied with the reverse of the particle response (note the blue line versus the green line behavior). There is seemingly no clear relationship detectable among the set of parameter values and the occurrence of this NM phenomenon. A small displacement in the parameter space may either cause a sudden emergence of NM or its rapid absence. One important observation is that typically it occurs in regimes for which the values of the parameters are *a priori* unknown. The interested reader is referred to the animation of the maps  $\langle v \rangle(\omega, m)$  for several different magnitudes of the ac-driving amplitude  $a$  which can be inspected on the web [45].

Among the regimes of NM in the parameter space there are tailored ones for which the latter phenomenon appears only for a very narrow interval of the mass  $m$ . This is illustrated with panel (b) of Fig. 1 where we depict the directed velocity  $\langle v \rangle$  of the Brownian particle versus the mass  $m$ . An interesting transport property can be detected: among many particles with masses from a wide interval  $m \in [10^{-2}, 10^1]$  only those with a mass  $m \approx 1.13$  will move in the opposite direction  $\langle v \rangle < 0$  to the acting bias  $f = 1$ . All other particles with positive velocity  $\langle v \rangle$  will follow towards the direction of the bias. As a result, the particles with mass very close to  $m \approx 1.13$  will be separated from all the others. This process of mechanical separation seems to be very promising provided that one would be able to control the mass  $m^*$  of particles which are intended to be separated. The half-width  $\delta m \approx 0.01$  of the interval where the NM occurs is indicated in the inset of the panel (b). It can be viewed as the resolution capacity for separation. However, we stress that typically NM in these intervals is sharply peaked, meaning that due to the clear difference between the magnitude of the negative velocity indeed only the particles with the precisely defined mass  $m^*$  will be pronouncedly isolated from the others moving in the same or the opposite direction. We in turn undertook the attempt to search for such parameter regimes of the Langevin equation (4) that would enable us to control the occurrence of the NM by tuning just one parameter.

After this comprehensive numerical analysis we identified practically all sets of parameters  $\{a, \omega, f, D\}$  for which NM emerges only for a narrow interval of mass  $[m^* - \delta m, m^* + \delta m]$ . Among selected parameter regimes, we focused on those which reveal a specific functional dependence between the isolated mass  $m^*$  and the

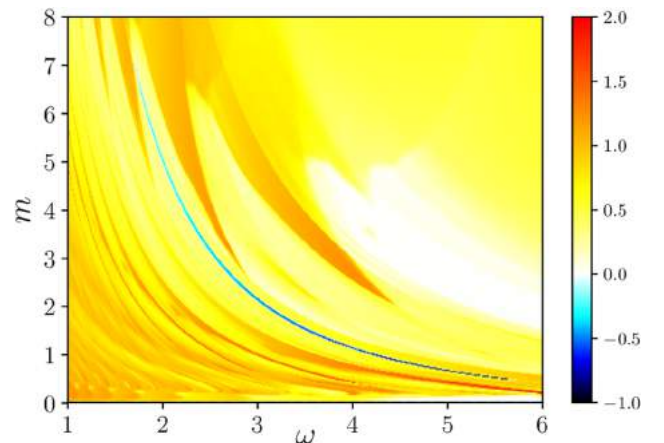


FIG. 2. Two-dimensional map of the directed velocity  $\langle v \rangle$  of the Brownian particle as a function of the externally applied periodic driving frequency  $\omega$  and mass  $m$ . The magnitude of velocity  $\langle v \rangle$  is indicated by the color code with blue indicating regimes with NM. Chosen remaining parameters are set at  $a = 5.9375$ ,  $f = 1$ ,  $D = 0.0001$ .

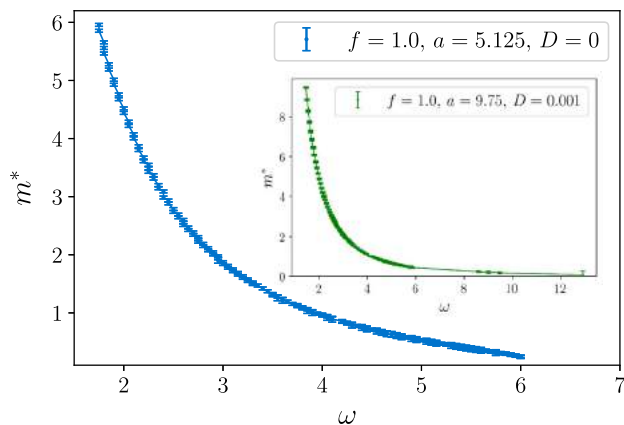


FIG. 3. The dependence of the mass  $m^*$  tailored for separation as a function of the external driving frequency  $\omega$  for zero temperature  $D \propto T = 0$  with fixed  $a = 5.125$  and  $f = 1$ . In the inset we present a different regime with  $D = 0.001$  allowing for efficient and tunable mass separation via negative mobility.

parameter  $a$ ,  $\omega$ ,  $f$ , or  $D$ . In Fig. 2 we present such an example of the directed velocity  $\langle v \rangle$  map as a function of the external driving frequency  $\omega$  and scaled mass  $m$ . The magnitude of the velocity  $\langle v \rangle$  is indicated with a corresponding color code. The blue regime corresponds to NM. It can be observed that for a given value of the frequency  $\omega$  NM is present *solely* for a particular value of mass  $m^*$ . Therefore, using those tailored parameters read off from Fig. 2 we are able to tune the NM to the particle of a given mass  $m^*$  by changing the value of the external driving frequency  $\omega$  at fixed periodic driving strength. Doing so allows for efficient mass separation from an interval covering nearly 2 orders of magnitude.

In order to examine our results even more accurately we isolated the NM area from corresponding two parameter maps into a graph of the target mass  $m^*$  versus the external driving frequency  $\omega$ . The result is depicted in Fig. 3 for zero temperature  $D \propto T = 0$ . A change of thermal noise intensity from  $D = 0$  up to temperature  $D \approx 0.0003$  does not significantly alter the desired characteristics which is quite robust with respect to temperature variation. Because NM derives from the complex deterministic dynamics, strong thermal noise of sufficient intensity is expected to cause a blurring of the phenomenon [35]. Interestingly, however, increasing thermal noise strength produces a shrinking of corresponding NM intervals, thereby optimizing the range  $\delta m$ . This feature implies an improvement of the selectivity for separation. In the inset of Fig. 3 we additionally depict different parameter regime allowing tunable mass separation for even higher temperature  $D = 0.001$ . Moreover, our method of mass separation is stable against a variation of the amplitude strength  $a$  (not depicted). The effect is present for a wide range of amplitudes  $a \in [4, 8]$ . At this

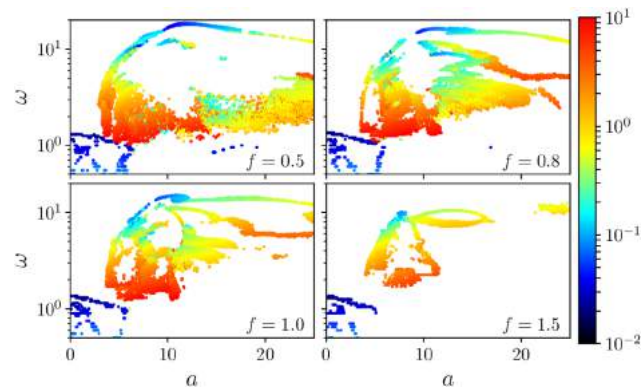


FIG. 4. The mass  $m^*$  targeted for separation (color coded scale) via the NM effect as a function of the external ac-driving strength  $a$  and frequency  $\omega$  for different values of the bias  $f$ . Thermal noise intensity is set to zero  $D = 0$ .

point we remark that the effect of mass separation upon harvesting the NM phenomenon is also present for the dependence  $m^*(a)$  and alike for  $m^*(f)$ ; the range of tunable mass separation proves, however, somewhat smaller.

Finally, we consider yet a further issue: Let us assume that we deal with a given mass  $m^*$  which we want to separate from the rest. The question then is, for how many different masses  $m^*$  taken from the extended interval  $m^* \in [10^{-2}, 10^1]$  is it possible to isolate the sought-after parameter set  $\{a, \omega, f, D\}$  for which only this very specific mass value  $m^*$  displays NM, thereby allowing its separation in a most efficient unique manner. We note that for a single mass  $m^*$  there might be several parameter regimes obeying this condition. The answer to this question is summarized with Fig. 4. There, the distribution of the mass  $m^*$  targeted for separation via the NM phenomenon in the parameter plane of the ac-driving amplitude  $a$  and frequency  $\omega$  is depicted for different values of the static bias  $f$ . We observe that small masses can be isolated with low values of  $a$  and  $\omega$ . Medium and large masses are separated when the amplitude and frequency assume moderate magnitudes. We detected that with this method and for a fixed bias value  $f = 1$  nearly all masses from the considered interval can be isolated. We also find that the overall distribution of the mass  $m^*$  targeted for separation depicted (in color) in Fig. 4 is robust with respect to a variation of bias  $f$ , noting that for smaller values of  $f$  it undergoes a stretching.

In conclusion, this work provides an effective solution for the objective of the tunable mass separation. In our scheme, mass targeted for isolation can be controlled by nearly 2 orders of magnitude by merely changing the frequency  $\omega$  of the external harmonic driving. This task apparently cannot be accomplished with similar quality by use of alternative methods such as filtration techniques or schemes which are based on fluid-driven Brownian motor methodology [1,46,47]. The approach presented here uses

only a spatially periodic nonlinear structure in combination with unbiased external time-periodic driving. Our method can further be adapted to the needs by proper fabrication of the nonlinear landscape described by its barrier height  $\Delta U$  and period  $L$ . Other advantages are (i) as a representative of active techniques it offers an improved averaged migration speed as compared to alternative approaches [32], (ii) in contrast to microfluidic methods it allows the possibility to not only deflect different particle species along different transport angles, but even to steer them in opposite directions, (iii) use of small size of a lab-on-a-chip device technology together with advantageous fabrication costs allows for massive parallelization which makes high-throughput separation possible. We envision that the separation strategy proposed here provides mass selectivity required in present and future isolation of nano and micro particles, proteins, organelles and cells.

This work was supported by the Grants No. NCN 2017/26/D/ST2/00543 (J.S.) and No. NCN 2015/19/B/ST2/02856 (J.Ł.)


- 
- [1] P. Hänggi and F. Marchesoni, *Rev. Mod. Phys.* **81**, 387 (2009).
- [2] P. Reimann, *Phys. Rep.* **361**, 57 (2002).
- [3] S. Denisov, S. Flach, and P. Hänggi, *Phys. Rep.* **538**, 77 (2014).
- [4] M. J. Skaug, Ch. Schwemmer, S. Fringes, C. D. Rawlings, and A. W. Knoll, *Science* **359**, 1505 (2018).
- [5] Ch. Schwemmer, S. Fringes, U. Duerig, Y. K. Ryu Cho, and A. Knoll, *Phys. Rev. Lett.* **121**, 104102 (2018).
- [6] M. Masaeli, E. Sollier, H. Amini, W. Mao, K. Camacho, N. Doshi, S. Mitragotri, A. Alexeev, and D. Di Carlo, *Phys. Rev. X* **2**, 031017 (2012).
- [7] D. Reguera, A. Luque, P. S. Burada, G. Schmid, J. M. Rubi, and P. Hänggi, *Phys. Rev. Lett.* **108**, 020604 (2012).
- [8] S. Meinhardt, J. Smiatek, R. Eichhorn, and F. Schmid, *Phys. Rev. Lett.* **108**, 214504 (2012).
- [9] L. Bogunovic, M. Fliedner, R. Eichhorn, S. Wegener, J. Regtmeier, D. Anselmetti, and P. Reimann, *Phys. Rev. Lett.* **109**, 100603 (2012).
- [10] P. Margaretti, I. Pagonabarraga, and J. M. Rubi, *Phys. Rev. Lett.* **113**, 128301 (2014).
- [11] S. Bo and R. Eichhorn, *Phys. Rev. Lett.* **119**, 060603 (2017).
- [12] D. Matsunaga, F. Meng, A. Zöttl, R. Golestanian, and J. M. Yeomans, *Phys. Rev. Lett.* **119**, 198002 (2017).
- [13] Q. Vagne and P. Sens, *Phys. Rev. Lett.* **120**, 058102 (2018).
- [14] A. K. Mukhopadhyay, B. Liebchen, and P. Schmelcher, *Phys. Rev. Lett.* **120**, 218002 (2018).
- [15] K. K. Zeming, S. Ranjan, and Y. Zhang, *Nat. Commun.* **4**, 1625 (2013).
- [16] Z. Wang, A. Knebel, S. Grosjean, D. Wagner, S. Bräse, Ch. Wöll, J. Caro, and L. Heinke, *Nat. Commun.* **7**, 13872 (2016).
- [17] G. Guan, L. Wu, A. A. Bhagat, Z. Li, P. C. Y. Chen, S. Chao, Ch. J. Ong, and J. Han, *Sci. Rep.* **3**, 1475 (2013).
- [18] J. Zhang, S. Yan, R. Sluyter, W. Li, G. Alici, and N.-T. Nguyen, *Sci. Rep.* **4**, 4527 (2014).
- [19] H. Jeon, Y. Kim, and G. Lim, *Sci. Rep.* **6**, 19911 (2016).
- [20] Y. Li, H. Zhang, Y. Li, X. Li, J. Wu, S. Qian, and F. Li, *Sci. Rep.* **8**, 3618 (2018).
- [21] S. Suresh, *Acta Mater.* **55**, 3989 (2007).
- [22] B. Lindner, L. Schimansky-Geier, P. Reimann, P. Hänggi, and M. Nagaoka, *Phys. Rev. E* **59**, 1417 (1999).
- [23] M. Borromeo and F. Marchesoni, *Phys. Rev. Lett.* **99**, 150605 (2007).
- [24] P. Sajeesh and A. K. Sen, *Microfluid. Nanofluid.* **17**, 1 (2014).
- [25] R. Eichhorn, P. Reimann, and P. Hänggi, *Phys. Rev. Lett.* **88**, 190601 (2002).
- [26] Ł. Machura, M. Kostur, P. Talkner, J. Łuczka, and P. Hänggi, *Phys. Rev. Lett.* **98**, 040601 (2007).
- [27] D. Speer, R. Eichhorn, and P. Reimann, *Phys. Rev. E* **76**, 051110 (2007).
- [28] J. Spiechowicz, P. Hänggi, and J. Łuczka, *Phys. Rev. E* **90**, 032104 (2014).
- [29] J. Nagel, D. Speer, T. Gaber, A. Sterck, R. Eichhorn, P. Reimann, K. Ilin, M. Siegel, D. Koelle, and R. Kleiner, *Phys. Rev. Lett.* **100**, 217001 (2008).
- [30] A. Ros, R. Eichhorn, J. Regtmeier, T. T. Duong, P. Reimann, and D. Anselmetti, *Nature (London)* **436**, 928 (2005).
- [31] R. Eichhorn, J. Regtmeier, D. Anselmetti, and P. Reimann, *Soft Matter* **6**, 1858 (2010).
- [32] J. Luo, K. Muratore, E. Arriaga, and A. Ros, *Anal. Chem.* **88**, 5920 (2016).
- [33] M. Schiavoni, L. Sanchez-Palencia, F. Renzoni, and G. Grynberg, *Phys. Rev. Lett.* **90**, 094101 (2003).
- [34] E. Lutz and F. Renzoni, *Nat. Phys.* **9**, 615 (2013).
- [35] A. Słapik, J. Łuczka, and J. Spiechowicz, *Commun. Non-linear Sci. Numer. Simul.* **55**, 316 (2018).
- [36] J. Spiechowicz and J. Łuczka, *Sci. Rep.* **7**, 16451 (2017).
- [37] P. Reimann, C. Van den Broeck, H. Linke, P. Hänggi, J. M. Rubi, and A. Pérez-Madrid, *Phys. Rev. Lett.* **87**, 010602 (2001).
- [38] B. Lindner and I. M. Sokolov, *Phys. Rev. E* **93**, 042106 (2016).
- [39] J. Spiechowicz, P. Talkner, P. Hänggi, and J. Łuczka, *New J. Phys.* **18**, 123029 (2016).
- [40] F. M. Purcell, *Am. J. Phys.* **45**, 3 (1977).
- [41] E. Lauga, *Soft Matter* **7**, 3060 (2011).
- [42] J. Spiechowicz, J. Łuczka, and P. Hänggi, *Sci. Rep.* **6**, 30948 (2016).
- [43] J. Spiechowicz, M. Kostur, and Ł. Machura, *Comput. Phys. Commun.* **191**, 140 (2015).
- [44] L. D. Landau and E. M. Lifshitz, *Statistical Physics, Part 1*, 3rd ed. (Pergamon Press, Oxford, 1980).
- [45] <https://github.com/jspiechowicz/mass-separation>.
- [46] C. Kettner, P. Reimann, P. Hänggi, and F. Müller, *Phys. Rev. E* **61**, 312 (2000).
- [47] S. Matthias and F. Müller, *Nature (London)* **424**, 53 (2003).

## Temperature-Induced Tunable Particle Separation

A. Słapik,<sup>1</sup> J. Łuczka<sup>1,\*</sup>, and J. Spiechowicz<sup>1,2</sup>

<sup>1</sup>*Institute of Physics and Silesian Center for Education and Interdisciplinary Research, University of Silesia, 41-500 Chorzów, Poland*

<sup>2</sup>*Institute of Physics, University of Augsburg, 86135 Augsburg, Germany*

 (Received 19 August 2019; revised manuscript received 10 October 2019; published 1 November 2019)

An effective approach to isolation of submicrometer-sized particles is desired to separate cancer cells and healthy cells or in therapy for Parkinson's disease and Alzheimer's disease. However, since bioparticles span a large size range covering several orders of magnitude, the development of an adequate separation method is a challenging task. We consider a collection of noninteracting Brownian particles of various sizes moving in a symmetric periodic potential and subjected to external unbiased harmonic driving as well as a constant bias. We reveal a nonintuitive, yet efficient, separation mechanism based on a thermal-fluctuation-induced negative-mobility phenomenon in which particles of a given size move in a direction opposite to the applied bias. By varying solely the temperature of the system, one can separate particles of various strictly defined sizes. This approach may be an important step toward the development of point-of-care lab-on-a-chip devices.

DOI: [10.1103/PhysRevApplied.12.054002](https://doi.org/10.1103/PhysRevApplied.12.054002)

### I. INTRODUCTION

Separation and fractionation of micrometer-sized and submicrometer-sized particles has ever-growing importance in both research and industrial applications, including chemical and biological research as well as medical diagnostics [1]. For example, detection and treatment of HIV infection relies on the isolation of human T lymphocytes from whole blood [2]. Similarly, separation of neuronal cells plays a pivotal role in cell-replacement therapy for neurodegenerative disorders such as Parkinson's disease and Alzheimer's disease [3]. The bioparticle size is often a signature of abnormal biological properties leading to disease. This is apparent, for example, for mitochondria and lipid droplets, where anomalous size indicates Huntington's disease [4] or leukemia [5]. In some cases cancer cells are found to differ in size as compared with healthy ones [6]. Therefore, efficient strategies for separation of bioparticles are required to investigate variations of biomolecular signatures.

Unfortunately, bioparticles span a large size range covering several orders of magnitude from hundreds of nanometers to tens of micrometers [7,8]. For such a submicrometer scale, thermal fluctuations are lead actors and isolation techniques are rather scarce [9,10]. An ideal solution would be a tunable method that allows one to change the bioparticle size targeted for separation by controlling one of its parameters. In the following we demonstrate a nonintuitive, yet efficient, separation strategy taking

advantage of a paradoxical mechanism of thermal-noise-induced absolute negative mobility (ANM) [11–13]. Its main advantage is that it combines the benefits of both active and passive separation techniques. The method uses an external driving force as well as a constant bias, so the particle-sorting efficiency and throughput are expected to be higher than for alternative passive and some active (e.g., ratchet) techniques. On the other hand, since the separation process is induced and controlled by thermal fluctuations, it can be applied also to electrically neutral objects that carry no charge or dipole. Moreover, this scheme allows one not only to deflect different particle species along different transport angles but also to steer them in opposite directions, and therefore it is ideal for separation and fractionation purposes. Finally, the same setup can be applied to segregate particles with respect to their mass [14].

A key finding of this development is that the omnipresent thermal fluctuations are not necessarily a redundant nuisance but rather may provide a tunable mechanism for particle separation at the submicrometer scale. It requires only two ingredients: (i) a *symmetric* spatially periodic nonlinear structure and (ii) a *nonequilibrium* state created by, for example, a time-periodic driving force of vanishing mean value. We show that under the additional action of a constant bias, thermal fluctuations guide particles of a given size in the direction opposite to this net force, whereas the others move concurrently toward it, all under identical experimental conditions. Moreover, we demonstrate that by changing only the temperature of the system, one is able to tune the negative-mobility effect solely for a precisely defined size of the particle, therefore

\*jerzy.luczka@us.edu.pl

allowing its separation from the other particles of different sizes.

Our setup can be experimentally realized using a lab-on-a-chip device consisting of a microfluidic structure. The oscillating force driving the system out of equilibrium may be induced through hydrodynamic flow, but electrophoresis, electro-osmosis, or dielectrophoresis can also be used [10]. In particular, a proof-of-principle experiment of a similar separation scheme was performed with insulator dielectrophoresis in a nonlinear, symmetric microfluidic structure with electrokinetically activated transport [15,16]. Recently, such a setup allowed the induction of ANM not only for a colloidal particle but also for a biological compound in the form of mouse-liver mitochondria [17]. However, these experiments used for separation purposes the deterministic ANM, whereas here we present an essentially different approach based on the thermal-noise-induced phenomenon. Temperature-driven tunability of the proposed particle-separation process can be achieved solely for this latter fundamentally distinct mechanism of ANM.

## II. MODEL

We study a collection of noninteracting classical Brownian particles of various sizes that move in a spatially periodic potential  $U(x) = U(x + L)$  of period  $L$  and are additionally subjected to an unbiased time-periodic force  $A \cos \Omega t$  of amplitude  $A$  and angular frequency  $\Omega$ , as well as an external static force  $F$ . The dynamics of a single particle of mass  $M$  is described by the following Langevin equation [18]:

$$M\ddot{x} + \Gamma\dot{x} = -U'(x) + A \cos \Omega t + F + \sqrt{2\Gamma k_B T} \xi(t), \quad (1)$$

where the dot and the prime denote differentiation with respect to time  $t$  and the particle coordinate  $x$ , respectively. The coupling of the particle with a thermal bath of temperature  $T$  is modeled by Gaussian white noise of zero mean and unity intensity; that is,

$$\langle \xi(t) \rangle = 0, \quad \langle \xi(t) \xi(s) \rangle = \delta(t - s). \quad (2)$$

The parameter  $k_B$  is the Boltzmann constant and  $\Gamma$  is the friction coefficient. The potential  $U(x)$  is assumed to be *symmetric* and in the simplest form; namely,

$$U(x) = \Delta U \sin\left(\frac{2\pi}{L}x\right). \quad (3)$$

Despite its apparent simplicity, the model studied serves as a paradigmatic example exhibiting peculiar transport behavior, including noise-enhanced transport efficiency [13,19], anomalous diffusion [20], amplification of normal

diffusion [21–23], and a nonmonotonic temperature dependence of normal diffusion [24,25].

We first recast Eq. (1) in its dimensionless form. This procedure ensures that the results obtained later are independent of the setup, which is essential to facilitate the choice in realizing the best setup for the testing our theory by experimentalists. We rescale the particle coordinate and time as

$$\hat{x} = \frac{x}{L}, \quad \hat{t} = \frac{t}{\tau_\gamma}, \quad \tau_\gamma = L\sqrt{\frac{M}{\Delta U}}, \quad (4)$$

which transform Eq. (1) to the form

$$\ddot{\hat{x}} + \gamma\dot{\hat{x}} = -\hat{U}'(\hat{x}) + a \cos \omega \hat{t} + f + \sqrt{2D}\hat{\xi}(\hat{t}). \quad (5)$$

The *dimensionless friction coefficient*  $\gamma$  is the ratio of the two characteristic time scales:

$$\gamma = \frac{\tau_\gamma}{\tau_0} = \frac{\Gamma L}{\sqrt{M\Delta U}}, \quad (6)$$

where  $\tau_0 = M/\Gamma$ . The parameter  $\gamma$  is crucial for the proposed size-based separation because it depends, via the Stokes formula, on the linear size  $R$  of the particle. For example, for a spherical particle  $\Gamma = 6\pi\eta R$ , where  $\eta$  is the viscosity of the surrounding medium and  $R$  is the radius of the spherical particle. A (sub)micrometer-sized particle typically has a rather small physical mass  $M$ , and therefore the rescaled friction coefficient  $\gamma$  is expected to be of moderate to large magnitude as compared with the dimensionless mass  $m$ , which in this scaling is set to unity,  $m = 1$ . Other parameters are  $a = (L/\Delta U)A$ ,  $\omega = \tau_\gamma\Omega$ , and  $f = (L/\Delta U)F$ . The rescaled potential is  $\hat{U}(\hat{x}) = U(L\hat{x})/\Delta U = \sin 2\pi\hat{x}$  and has the unit period  $\hat{U}(\hat{x}) = \hat{U}(\hat{x} + 1)$ . The dimensionless thermal noise  $\hat{\xi}(\hat{t})$  has the same statistical properties as  $\xi(t)$ , and  $D = k_B T/\Delta U$  is the ratio of the thermal energy to half of the nonrescaled potential barrier. From now on, only the dimensionless variables are used in this study, and therefore to simplify the notation, the hat symbol is omitted.

## A. Methods

The observable of foremost interest in this study is the stationary averaged velocity  $\langle v \rangle$ , which can be expressed as

$$\langle v \rangle = \lim_{t \rightarrow \infty} \frac{1}{t} \int_0^t ds \langle \dot{x}(s) \rangle, \quad (7)$$

where  $\langle \rangle$  indicates averaging over all realizations of the thermal noise as well as over the initial conditions for the particle position  $x(0) \in [0, 1]$  and its velocity  $\dot{x}(0) \in [-2, 2]$  being uniformly distributed. The latter is obligatory for the deterministic limit  $D \propto T \rightarrow 0$  when the dynamics

may be nonergodic and the results can be affected by the specific choice of the initial conditions [26].

Unfortunately, the Fokker-Planck equation corresponding to the Langevin equation (5) cannot be solved in a closed form. For this reason we are forced to perform comprehensive numerical simulations. The dynamics described by Eq. (5) is characterized by a five-dimensional parameter space  $\{\gamma, a, \omega, f, D\}$ , the detailed exploration of which is a very challenging task. We perform numerical simulations of Eq. (5) over a parameter domain in the area  $\gamma \times a \times \omega \in [0.1, 10] \times [0, 25] \times [0, 20]$  at a resolution of 400 points per dimension for several values of the force  $f$  taken from the interval  $[0, 2]$  and thermal-noise intensity  $D \in [0, 10^{-1}]$ . Overall, we consider nearly  $10^9$  different parameter sets. This exceptional precision is possible only because of our innovative simulation method, which is based on the use of graphics-processing-unit supercomputers; for details see Ref. [27]. In particular, we use a weak second-order predictor-corrector method [28] with the time step scaled by the fundamental period  $T = 2\pi/\omega$  of the external driving force (i.e.,  $h = 10^{-2} \times T$ ). Since we are interested in the asymptotic long-time state of the system, numerical stability is an extremely important problem to obtain reliable results. Fortunately, the predictor-corrector algorithm is similar to implicit methods but it does not require the solution of the algebraic equation at each step. It offers good numerical stability, which it inherits from the implicit counterpart of its corrector. The stationary averaged velocity  $\langle v \rangle$  is averaged over the ensemble of  $2^{10} = 1024$  trajectories, each starting with different initial conditions according to the distribution presented above. The number of realizations of stochastic dynamics is not accidental but is chosen to maximize the numerical simulation performance. The quantity of interest is calculated after it reaches its asymptotic stationary value, which typically occurs after  $10^4$  periods of the external harmonic driving  $T = 2\pi/\omega$ .

### III. RESULTS

Our idea how to separate submicrometer-sized particles is as follows. The stationary averaged velocity  $\langle v \rangle$  depends, via dynamics determined by Eq. (5), on the friction coefficient  $\gamma = \gamma(R)$ , which in turn is a function of the particle size  $R$ . Assume that there is a collection of, for example, four types of particles with  $R_1 < R_2 < R_3 < R_4$ . We want to separate only particles with radius  $R_2$ . To this aim we should find such a parameter regime  $\{a, \omega, f, D\}$  in which the particles of sizes  $R_1, R_3$ , and  $R_4$  move in the positive direction,  $\langle v \rangle > 0$ , whereas particles with radius  $R_2$  travel in the negative direction,  $\langle v \rangle < 0$ . Then only particles of size  $R_2$  will be separated from the rest. We now look for parameter regimes permitting such an isolation process by using the ANM phenomenon.

In the normal transport regime (outside the parameter range for ANM), for sufficiently small values of the external perturbing bias  $f$ , the Green-Kubo linear response theory holds true and the standard response of the system is that the average particle velocity is an increasing function of the static force (i.e.,  $\langle v \rangle = \mu f$ ). However, there are also regimes for which particles move on average in the direction *opposite* to the applied bias, namely,  $\langle v \rangle < 0$  for  $f > 0$ , exhibiting anomalous behavior in the form of *negative mobility*,  $\mu < 0$  [12,29,30]. The key ingredient for the occurrence of the latter effect is that the system is driven far away from thermal equilibrium into a time-dependent nonequilibrium state [12,18,29]. In our case this condition is guaranteed by the presence of the external harmonic driving  $a \cos \omega t$ .

In Fig. 1(a) we demonstrate the ANM phenomenon. For  $\gamma = 2.135$ , the average velocity  $\langle v \rangle$  assumes the same sign as the force  $f$ , which results in typical transport behavior, consistent with the direction of the applied bias. For  $\gamma = 1.935$ , however, the average response of the system is opposite to the acting static bias  $f$  (i.e.,  $\langle v \rangle < 0$  for small  $f > 0$ ), indicating the ANM phenomenon. No relationship

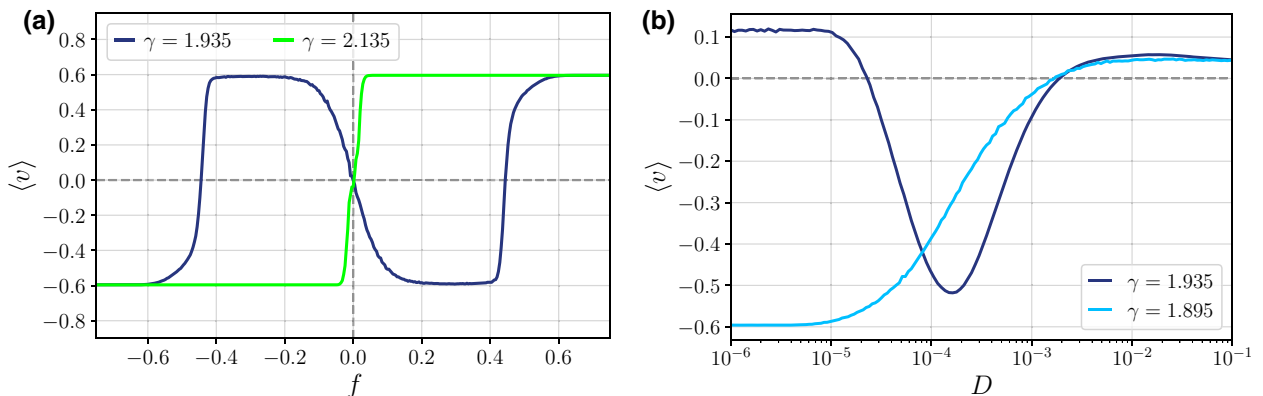


FIG. 1. (a) Average velocity  $\langle v \rangle$  as a function of the static force  $f$  for two different values of the friction  $\gamma$ . (b) Average velocity  $\langle v \rangle$  versus thermal-noise intensity  $D \propto T$  for different values of  $\gamma$ . The other parameters are  $a = 5.75$ ,  $\omega = 3.75$ ,  $f = 0.1$ , and  $D = 0.0002$ .



is detectable between the set of parameter values and the occurrence of the ANM effect, and therefore the values of the friction coefficient chosen here are just exemplary ones. It was shown that there exist two fundamentally different mechanisms responsible for the emergence of ANM in our setup: (i) it can be generated by the deterministic chaotic dynamics [29] or (ii) it can be induced by thermal-equilibrium fluctuations [12]. Very recently, a third mechanism generating the ANM effect was discovered. Accordingly, the ANM phenomenon may emerge as well within deterministic and nonchaotic parameter regimes [31].

In Fig. 1(b) we study the temperature dependence of the average velocity  $\langle v \rangle$  in the exemplary parameter regime corresponding to the ANM effect. For  $\gamma = 1.895$ , the ANM phenomenon is observed even in the limit of vanishing thermal-noise intensity  $D \propto T \rightarrow 0$ , indicating that in this regime the latter effect is caused purely by the deterministic dynamics of the system. This mechanism is the most populated in the parameter space. As illustrated in Fig. 1(b), in such a case thermal fluctuations typically have a destructive impact (i.e., when the thermal-noise intensity increases, the ANM disappears). On the other hand, for  $\gamma = 1.935$ , the ANM is induced by thermal fluctuations. This means that there is a finite window of temperature  $D \propto T$  in which the average velocity  $\langle v \rangle < 0$  with  $f > 0$ , and this effect is not observed in the limit of vanishing thermal-noise intensity  $D \rightarrow 0$ .

We now attempt to find a parameter regime for which particles differing in size could be isolated by an appropriate dose of thermal fluctuations  $D \propto T$ . Motivated by the large size range typically encountered in biochemical applications, we aim to develop a tunable scheme that allows us to control the particle size targeted for isolation by changing solely the temperature of the system. In doing so we are automatically restricted to parameter sets corresponding to thermal-noise-induced ANM as for

the deterministic mechanism temperature has a destructive influence on the latter effect. These regimes are significantly less populated in the parameter space than the deterministic ones, and therefore this task is highly challenging.

As the first step of our analysis, we isolate all parameter regimes  $\{a, \omega, f, D\}$  for which the ANM effect is induced by thermal fluctuations and observed for only one narrow interval of the friction coefficient  $\gamma$ . We exemplify this procedure in Fig. 2, where we depict the average velocity  $\langle v \rangle$  versus the friction  $\gamma$ , which can be identified with the particle size  $R$ . Among many particles of sizes corresponding to the friction in a wide interval  $\gamma \in [10^{-1}, 10]$ , only those with friction coefficient  $\gamma^* = 1.59$  will move in the opposite direction  $\langle v \rangle < 0$  to the applied bias  $f > 0$ . Other particles will move toward the direction of the bias. As a consequence, only those particles with  $\gamma^* \approx 1.59$  will be separated from the others. In Fig. 2(b) we magnify the interval in which the ANM phenomenon occurs. It can be viewed as the resolution capacity of this method. In the case presented it reads  $\delta\gamma \approx 0.1$ . However, as illustrated, typically negative velocity  $\langle v \rangle$  is noticeably peaked in such a region and therefore the particles of the precisely defined size  $\gamma^*$  for which the velocity is minimal  $\langle v \rangle_{\min} = \langle v \rangle(\gamma^*)$  will be pronouncedly isolated from the others. We stress that the dimensionless friction coefficient  $\gamma$  in Eq. (6) depends not only on the actual friction  $\Gamma \propto R$  but also on the parameters of the potential  $\Delta U$  and  $L$ . Therefore, experimentalists may exploit these characteristics of the periodic substrate to further adapt the particle size targeted for separation.

Given the target audience of this journal, we now provide the exemplary set of the model parameters expressed in real, physical units corresponding to the regime presented in Fig. 2. In doing so we use the data for the microfluidic system reported in Ref. [17] that was successfully used to separate colloidal particles and mouse-liver mitochondria by use of the ANM effect. In particular, for

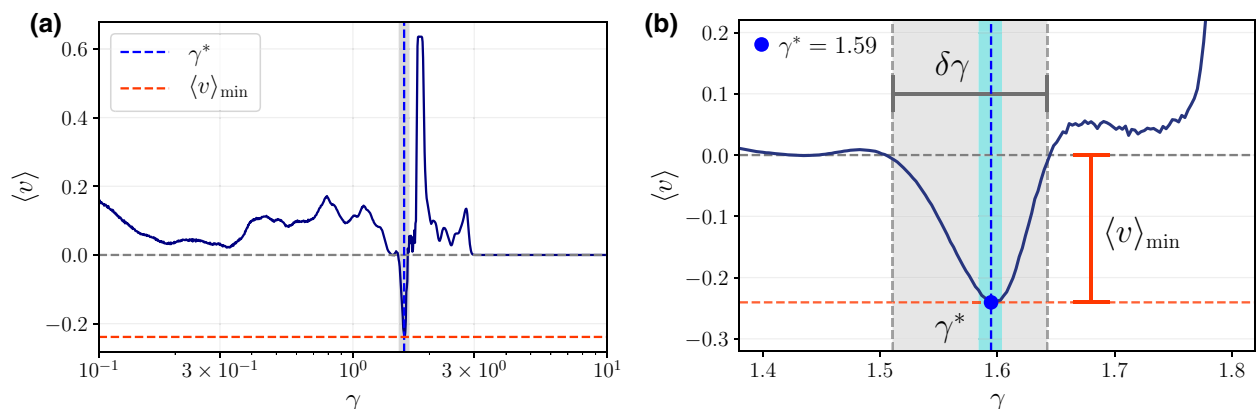


FIG. 2. (a) Average velocity  $\langle v \rangle$  versus the friction coefficient  $\gamma$ . ANM is observed only for a narrow interval marked in gray. (b) An enlargement of this region. The parameter values are as follows:  $a = 5.75$ ,  $\omega = 4.0$ ,  $f = 0.1$ , and  $D = 0.0006$ .

a realistic colloidal particle of radius  $R = 2.2 \mu\text{m}$ , for which the negative-mobility effect is tailored, suspended in an aqueous solution with viscosity  $\eta = 8.9 \times 10^{-4} \text{ Pa s}$  at temperature  $T = 25^\circ\text{C}$ , the characteristic timescales are  $\tau_\gamma = 0.4 \text{ s}$  and  $\tau_0 = 0.25 \text{ s}$ . These imply that the potential barrier  $\Delta U = 43 \text{ eV}$  and the spatial period of the potential  $L = 11 \mu\text{m}$ . Consequently, the conservative force  $-U'(x)$  is of the order of  $\Delta U/L = 0.63 \text{ pN}$ . The amplitude and the frequency of the external driving read  $A = 3.6 \text{ pN}$  and  $\Omega = 10 \text{ Hz}$ , respectively. Finally, the constant bias  $F$  is  $0.063 \text{ pN}$ . All characteristic timescales,  $\tau_\gamma = 0.4 \text{ s}$ ,  $\tau_0 = 0.25 \text{ s}$ , and  $T = 2\pi/\Omega = 0.628 \text{ s}$ , are of the same order of magnitude, which is typical for the parameter regimes in which the ANM effect is observed. Moreover, the order of magnitude of piconewtons appearing here is adequate for the biomolecular scale as, for example, the Brownian-motion force on an *Escherichia coli* bacterium averaged over  $1 \text{ s}$  is  $0.01 \text{ pN}$  and the propulsion developed by a molecular motor is  $5 \text{ pN}$  [32].

As the second step of the analysis we focus on the parameter regimes  $\{a, \omega, f\}$  for which a specific functional

dependence between the friction  $\gamma^*$  (equivalently the size  $R^*$  of the particle) intended for isolation and temperature  $D \propto T$  can be revealed. In Figs. 3(a)–3(c) we present three exemplary curves  $\gamma^*(D)$  for different values of the external harmonic driving amplitude  $a$  and the frequency  $\omega$ . They are obtained from characteristics  $\langle v \rangle(\gamma)$  computed for many different temperatures  $D \propto T$ ; see Fig. 2(a). Each blue dot in the plot represents the friction coefficient  $\gamma^*$  for which the Brownian-particle velocity attains its global minimum value at fixed thermal-fluctuation intensity. The gray bars indicate the friction-coefficient interval  $\delta\gamma$  where the ANM effect occurs; see Fig. 2(b). The conclusion is that there is no single parameter regime covering a wide range of the particle size  $R^* \propto \gamma^*$  targeted for separation by changing solely the temperature  $D \propto T$ . However, the parameters  $a$ ,  $\omega$ , and  $f$  give enough freedom to cover by parts a physically significant interval of moderate to large friction that is characteristic for small particles at low Reynolds numbers; for example, for Fig. 3(a)  $\gamma^* \in [0.84, 0.96]$ , for Fig. 3(b)  $\gamma^* \in [0.55, 0.58]$ , and for Fig. 3(c)  $\gamma^* \in [0.58, 0.75]$ . Using one of these

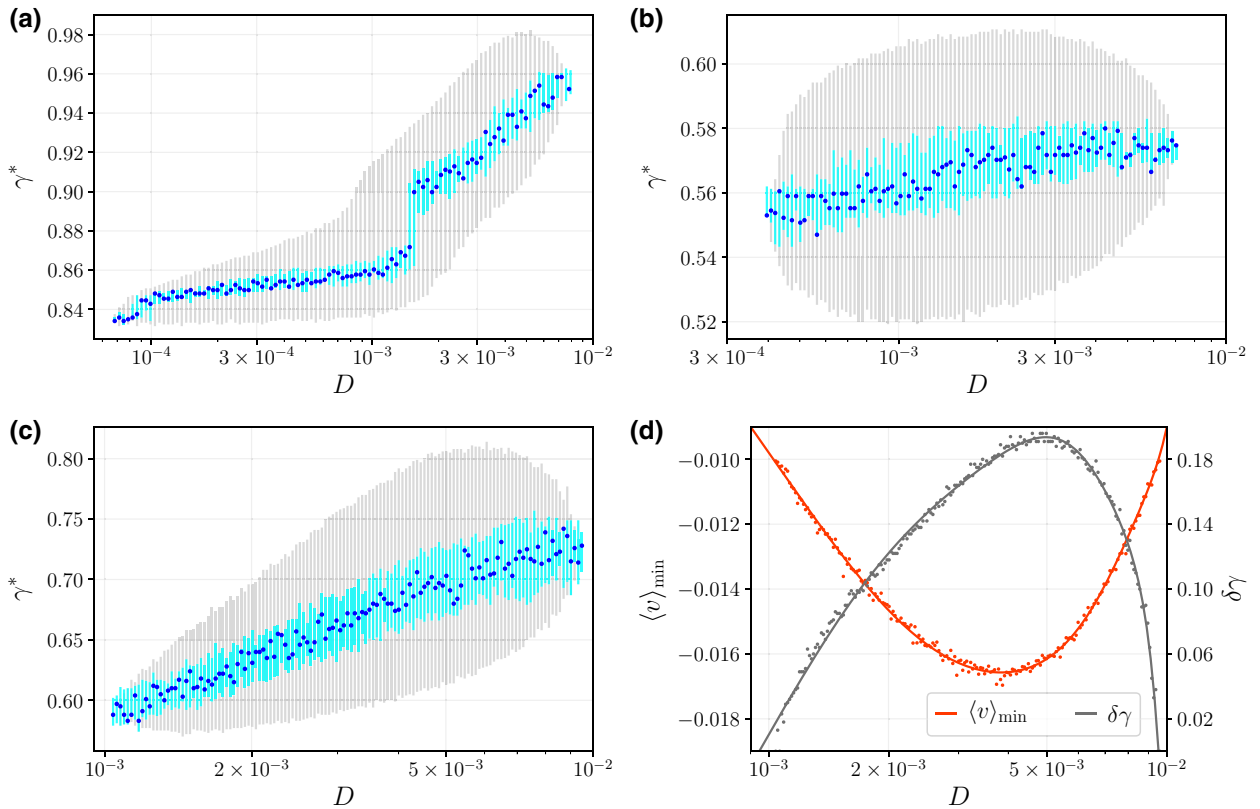


FIG. 3. (a)–(c) Friction coefficient (proportional to the particle size)  $\gamma^* \propto R$  for which the Brownian-particle velocity attains its global minimum  $\langle v \rangle_{\min} \equiv \langle v \rangle(\gamma^*)$  as a function of temperature  $D \propto T$ . The gray bars represent the friction-coefficient interval  $\delta\gamma$  in which the ANM effect occurs [see Fig. 2(b)]. The cyan region marks the range of the particle size  $\gamma \propto R$  corresponding to the vicinity of the minimum; that is,  $[(v)_{\min} - 0.05(v)_{\min}, (v)_{\min}]$ . The other parameters are as follows: (a)  $a = 5.55$ ,  $\omega = 1.5$ ; (b)  $a = 5.75$ ,  $\omega = 1.65$ ; (c)  $a = 5.75$ ,  $\omega = 5.65$ . In (a)–(c) the bias  $f = 0.1$ . (d) The minimal velocity  $\langle v \rangle_{\min}$  (left axis) as well as the resolution capacity  $\delta\gamma$  (right axis) versus temperature  $D$  for the parameter regime corresponding to (c).

exemplary tailored parameter regimes, one is able to tune the ANM to the particle of a given size  $R^* \propto \gamma^*$  by changing solely the temperature  $D \propto T$  of the system. Doing this allows us to separate particles with respect to their size in an efficient and tunable way.

#### IV. DISCUSSION

At first glance the magnitude of the intervals  $\delta\gamma$  where the ANM occurs that are represented in Figs. 3(a)–3(c) by the gray bars may look alarming. However, this fact should be considered as an *intrinsic feature* rather than a bug. First, we discuss the typical dependence of the resolution capacity  $\delta\gamma$  on temperature  $D$ . This function is depicted in Fig. 3(d) (right axis) for the parameter regime corresponding to Fig. 3(c). The reader may observe there the nonmonotonic dependence of  $\delta\gamma$  on temperature  $D$ , which is very characteristic for the negative-mobility phenomenon induced by thermal fluctuations. The anomalous transport effect emerges at the minimal temperature  $D_{\min}$ , and then  $\delta\gamma$  initially increases, passes through its maximum observed for an appropriate dose of thermal noise, and then starts to decrease until it reaches the maximal temperature  $D_{\max}$ . In Fig. 3(d) we depict also the dependence of the minimal velocity  $\langle v \rangle_{\min} = \langle v \rangle(\gamma^*)$ , corresponding to the particle size  $\gamma^*$  for which the negative mobility is tailored, on temperature  $D$ . Luckily, we observe that initially thermal noise not only increases the interval  $\delta\gamma$  where the ANM is detected but at the same time increases the absolute value of the global minimum of the Brownian-particle velocity  $\langle v \rangle_{\min}$ . Moreover, we notice that there is a temperature for which the resolution capacity  $\delta\gamma$  is maximal and the velocity  $\langle v \rangle_{\min}$  is minimal. This means that even though as thermal noise increases the ANM peaks in characteristics  $\langle v \rangle(\gamma)$  become wider and more pronounced; see Fig. 2(b). This fact guarantees that the particle size  $\gamma^*$  for which the ANM is tailored will be well distinguished from the others. For this reason, in Figs. 3(a)–(c) we additionally mark in cyan the region of the particle size  $\gamma$  corresponding to the vicinity of the minimum; that is,  $[\langle v \rangle_{\min} - 0.05\langle v \rangle_{\min}, \langle v \rangle_{\min}]$ . In this range  $\delta\gamma$  typically equals several percent of the value of  $\gamma^*$ , which is reasonable for separation purposes. Since this interval is a projection of the window  $[\langle v \rangle_{\min} - 0.05\langle v \rangle_{\min}, \langle v \rangle_{\min}]$  onto the  $\gamma$  axis, the so-obtained  $\delta\gamma$  is not necessarily symmetric around  $\gamma^*$ .

Second, taking into account the above discussion, we point out that even though there will be two particle species differing in size  $\gamma_1 \propto R_1$  and  $\gamma_2 \propto R_2$  both in the range where ANM occurs [see the gray area in Fig. 2(b)], typically they will still be separated from each other since usually  $\langle v \rangle(\gamma_1) \neq \langle v \rangle(\gamma_2)$ . This means that, unfortunately, they will both travel in the direction opposite the applied constant force  $f$  but there will be a gap between them because of the difference in their velocities. This opens

up an intriguing possibility for simultaneous separation of several particle species under identical experimental conditions.

We now comment on the salient difference between this work and our previous work [14]. The obvious one is that here we discuss the separation scheme with respect to the particle size  $\gamma \propto R$  rather than its mass  $m$ . Moreover, in our previous paper we used the negative-mobility effect, whose roots lie solely in the deterministic dynamics of the system; see Fig. 1(b). As the latter mechanism is significantly more populated in the parameter space of the model than the thermal-noise-induced one, it allows us to find a unique parameter set for which the particle mass intended for separation is effectively controlled over a regime of nearly 2 orders of mass magnitude on changing solely the frequency  $\omega$  of the external harmonic driving. Another difference is that typically the deterministic ANM is quickly destroyed by temperature increase, meaning that the mentioned parameter regime works effectively only for low thermal-noise intensities. As a consequence, the ANM peaks in the characteristics  $\langle v \rangle(m)$  are much steeper, the resolution capacity  $\delta m$  is significantly greater, and the overall selectivity of the method is superior. On the other hand, here the negative-mobility effect is induced by thermal fluctuations, meaning that one is able to find a parameter set allowing one to observe the ANM in a temperature regime as high as  $D = 10^{-2}$  [see Fig. 3(c)], which is not the case for the deterministic mechanism. Moreover, only because of this different origin the negative-mobility effect can be controlled by thermal fluctuations. This fact combined with an appropriate experimental implementation opens the opportunity to separate particles that carry no charge or dipole, or can hardly be manipulated by means of an external field or force. The price that needs to be paid for this possibility is a slight loss of accuracy in the separation process.

Finally, we comment briefly on the hydrodynamic corrections that may play a key role in experimental reality. We take into account only the simplest hydrodynamic effect expressed by the Stokes term in the model equation (1) and ignore a number of additional phenomena that may prove experimentally important. In particular, when the particle travels in a system with geometrical constraints, which is typically the case, for example, in a microfluidic device, its boundaries significantly modify the particle dynamics. The geometry usually increases the hydrodynamic drag. This effect is notoriously difficult to treat analytically and numerically [33], and certainly lies beyond the scope of this paper. Nevertheless, for some systems it appears to be extremely important and may cause significant underestimation of the results [34]. It can be accurately incorporated by a phenomenological modification based on the experimentally measured quantities and appropriate rescaling of the model parameters [34]. Since the hydrodynamic drag is increased for such

systems, we expect that this effect is likely to hamper the direct observation of the ANM phenomenon. Our preliminary results show that the latter anomalous transport effect notably decreases with the increase of friction (drag) (not depicted). Moreover, simultaneously the ANM becomes less populated in the parameter space, which makes it even harder to detect (not shown). Therefore, we are aware that our theoretical predictions following from Eq. (5) should be used as a guide toward “physical reality” indicating the direction for future experimental and theoretical research rather than taken as granted without approximations.

## V. CONCLUSION

In conclusion, this work provides an effective method for tunable size-based particle separation. In this scheme the particle size intended for isolation can be controlled by changing solely the temperature of the system without modifying the setup. It requires a symmetric spatially periodic nonlinear structure, external time-periodic driving, and a constant bias. Our approach can be readily realized with a lab-on-a-chip device [17] by using current lithographic techniques to develop robust separation applications. These may be further enhanced by advances in three-dimensional-printing technologies, which were recently exploited down to the nanometer range [35]. For this reason we envision that the method investigated can be adapted to a wide range of separation problems in which size selectivity is required, hopefully leading to, for example, new diagnostic applications with commercial potential [36].

## ACKNOWLEDGMENT

This work was supported by Polish National Science Center (NCN) NCN Grant No. 2017/26/D/ST2/00543 (J.S.).

- 
- [1] P. Yager, T. Edwards, E. Fu, K. Helton, and K. Nelson, Microfluidic diagnostic technologies for global public health, *Nature* **442**, 412 (2006).
- [2] X. Cheng, D. Irimia, M. Dixon, K. Sekine, U. Demirci, L. Zamir, R. G. Tompkins, W. Rodriguez, and M. Toner, A microfluidic device for practical label-free CD4(+) T cell counting of HIV-infected subjects, *Lab Chip* **7**, 170 (2007).
- [3] J. A. Korecka, J. Verhaagen, and E. M. Hol, Cell-replacement and gene-therapy strategies for Parkinson’s and Alzheimer’s disease, *Regen. Med.* **2**, 425 (2007).
- [4] R. R. Heffner and S. A. Barron, The early effects of ischemia upon skeletal muscle mitochondria, *J. Neurol. Sci.* **38**, 295 (1978).
- [5] M. Eguchi, Y. Iwama, F. Ochiai, K. Ishikawa, H. Sakakibara, H. Sakamaki, and T. Furukawa, Giant mitochondria in acute lymphocytic leukemia, *Exp. Mol. Pathol.* **47**, 69 (1987).
- [6] S. Suresh, Biomechanics and biophysics of cancer cells, *Acta Mater.* **55**, 3989 (2007).
- [7] A. A. Bhagat, H. Bow, S. W. Hou, S. J. Tan, J. Han, and C. T. Lim, Microfluidics for cell separation, *Med. Biol. Eng. Comput.* **48**, 999 (2010).
- [8] J. Xuan and M. L. Lee, Size separation of biomolecules and bioparticles using micro/nanofabricated structures, *Anal. Methods* **6**, 27 (2014).
- [9] P. Sajeesh and A. K. Sen, Particle separation and sorting in microfluidic devices: A review, *Microfluid. Nanofluid.* **17**, 1 (2014).
- [10] M. Sonker, D. Kim, A. Egatz-Gomez, and A. Ros, Separation phenomena in tailored micro- and nanofluidic environments, *Annu. Rev. Anal. Chem.* **12**, 475 (2019).
- [11] R. Eichhorn, P. Reimann, and P. Hänggi, Brownian Motion Exhibiting Absolute Negative Mobility, *Phys. Rev. Lett.* **88**, 190601 (2002).
- [12] Ł. Machura, M. Kostur, P. Talkner, J. Łuczka, and P. Hänggi, Absolute Negative Mobility Induced by Thermal Equilibrium Fluctuations, *Phys. Rev. Lett.* **98**, 040601 (2007).
- [13] J. Spiechowicz, P. Hänggi, and J. Łuczka, Brownian motors in the microscale domain: Enhancement of efficiency by noise, *Phys. Rev. E* **90**, 032104 (2014).
- [14] A. Slapik, J. Łuczka, P. Hänggi, and J. Spiechowicz, Tunable Mass Separation via Negative Mobility, *Phys. Rev. Lett.* **122**, 070602 (2019).
- [15] A. Ros, R. Eichhorn, J. Regtmeier, T. T. Duong, P. Reimann, and D. Anselmetti, Absolute negative mobility, *Nature* **436**, 928 (2005).
- [16] R. Eichhorn, J. Regtmeier, D. Anselmetti, and P. Reimann, Negative mobility and sorting of colloidal particles, *Soft Matter* **6**, 1858 (2010).
- [17] J. Luo, K. Muratore, E. Arriaga, and A. Ros, Deterministic absolute negative mobility for micro- and submicrometer particles induced in a microfluidic device, *Anal. Chem.* **88**, 5920 (2016).
- [18] P. Hänggi and F. Marchesoni, Artificial Brownian motors: Controlling transport on the nanoscale, *Rev. Mod. Phys.* **81**, 387 (2009).
- [19] J. Spiechowicz, J. Łuczka, and Ł. Machura, Efficiency of transport in periodic potentials: Dichotomous noise contra deterministic force, *J. Stat. Mech.* **2016**, 054038 (2016).
- [20] J. Spiechowicz and J. Łuczka, Subdiffusion via dynamical localization induced by thermal equilibrium fluctuations, *Sci. Rep.* **7**, 16451 (2017).
- [21] P. Reimann, C. Van den Broeck, H. Linke, P. Hänggi, J. M. Rubi, and A. Perez-Madrid, Giant Acceleration of Free Diffusion by use of Tilted Periodic Potentials, *Phys. Rev. Lett.* **87**, 010602 (2001).
- [22] J. Spiechowicz and J. Łuczka, Josephson phase diffusion in the superconducting quantum interference device ratchet, *Chaos* **25**, 053110 (2015).
- [23] B. Lindner and I. M. Sokolov, Giant diffusion of underdamped particles in a biased periodic potential, *Phys. Rev. E* **93**, 042106 (2016).
- [24] J. Spiechowicz, P. Talkner, P. Hänggi, and J. Łuczka, Non-monotonic temperature dependence of chaos-assisted diffusion in driven periodic systems, *New J. Phys.* **18**, 123029 (2016).

- [25] J. Spiechowicz, M. Kostur, and J. Łuczka, Brownian ratchets: How stronger thermal noise can reduce diffusion, *Chaos* **27**, 023111 (2017).
- [26] J. Spiechowicz, J. Łuczka, and P. Hänggi, Transient anomalous diffusion in periodic systems: Ergodicity, symmetry breaking and velocity relaxation, *Sci. Rep.* **6**, 30948 (2016).
- [27] J. Spiechowicz, M. Kostur, and Ł. Machura, GPU accelerated Monte Carlo simulation of Brownian motors dynamics with CUDA, *Comp. Phys. Commun.* **191**, 140 (2015).
- [28] E. Platen, and N. Bruti-Liberati, *Numerical Solution of Stochastic Differential equations with Jumps in Finance*, Stochastic Modelling and Applied Probability (Springer, Berlin, 2010).
- [29] D. Speer, R. Eichhorn, and P. Reimann, Transient chaos induces anomalous transport properties of an underdamped Brownian particle, *Phys. Rev. E* **76**, 051110 (2007).
- [30] J. Nagel, D. Speer, T. Gaber, A. Sterck, R. Eichhorn, P. Reimann, K. Ilin, M. Siegel, D. Koelle, and R. Kleiner, Observation of Negative Absolute Resistance in a Josephson Junction, *Phys. Rev. Lett.* **100**, 217001 (2008).
- [31] A. Slapik, J. Łuczka, and J. Spiechowicz, Negative mobility of a Brownian particle: Strong damping regime, *Commun. Nonlinear Sci. Numer. Simul.* **55**, 316 (2018).
- [32] J. Howard, *Mechanics of Motor Proteins and the Cytoskeleton* (Sinauer Associates, Massachusetts, USA, 2001).
- [33] J. Happel and H. Brenner, *Low Reynolds Number Hydrodynamics* (Prentice Hall, Englewood Cliffs, NJ, 1965).
- [34] X. Yang, C. Liu, Y. Li, F. Marchesoni, P. Hänggi, and H. P. Zhang, Hydrodynamic and entropic effects on colloidal diffusion in corrugated channels, *Proc. Natl. Acad. Sci.* **114**, 9564 (2017).
- [35] M. J. Beauchamp, G. P. Nordin, and A. T. Woolley, Moving from millifluidic to truly microfluidic sub-100- $\mu\text{m}$  cross-section 3D printed devices, *Anal. Bioanal. Chem.* **409**, 11 (2017).
- [36] D. T. Chiu, D. Di Carlo, P. S. Doyle, C. Hansen, R. M. Maceiczky, and R. C. Wootton, Small but perfectly formed? Successes, challenges and opportunities for microfluidics in the chemical and biological sciences, *Chemistry* **2**, 201 (2017).



# OPEN Tunable particle separation via deterministic absolute negative mobility

A. Słapik & J. Spiechowicz✉

Particle isolation techniques are in the spotlight of many areas of science and engineering. In food industry, a harmful bacterial activity can be prevented with the help of separation schemes. In health care, isolation techniques are used to distinguish cancer and healthy cells or in therapy for Alzheimer's and Parkinson's diseases. We consider a cloud of Brownian particles of different sizes moving in a periodic potential and subjected to an unbiased driving as well as a constant force. We reveal an efficient separation strategy via the counterintuitive effect of negative mobility when particles of a given size are transported in a direction opposite to the applied constant force. We demonstrate a tunable separation solution in which size of the particle undergoing separation may be controlled by variation of the parameters of the external force applied to the system. This approach is an important step towards the development of point-of-care lab-on-a-chip devices.

Separation of (sub)micro sized particles is of paramount importance due to its vast applications including in particular medical diagnostics<sup>1</sup>. Anomalies in a bioparticle size often indicate various illnesses. This is apparent, for instance, for Alzheimer's, Parkinson's<sup>2</sup> and Huntington's disease<sup>3</sup>, needless to say that often cancer cells noticeably deviates in size from healthy ones<sup>4</sup>. A reliable and effective approach to separating bioparticles is therefore much in demand. They span a large size range covering several orders of magnitude from nanometers to micrometers<sup>5,6</sup> what crucially complicates the development of such highly anticipated strategies. For instance, deadly viruses like HIV or COVID-19 are approximately 0.1 micrometer in diameter<sup>7</sup>. On the other hand, the soma of a neuron can vary from 4 to 100 micrometers in diameter<sup>8</sup>. For such a broad (sub)micrometer scale, efficient isolation techniques are required to allow tunability of the particle size intended for separation. Unluckily, the latter are rather scarce<sup>9,10</sup>, however, recently some progress has been made in this direction<sup>11–13</sup>.

In this work we aspire to partially fill this significant know-how gap by demonstrating a nonintuitive, yet efficient separation strategy taking advantage of a paradoxical mechanism of negative mobility<sup>14–17</sup>. We show that under the action of a static bias only particles of a given linear size move in the direction opposite to this net force whereas the others migrate concurrently towards it. This effect creates a possibility of steering different species of particles in opposite directions under identical experimental conditions thus facilitating their separation. A proof-of-principle experiment of a similar isolation scheme was performed with insulator dielectrophoresis in a nonlinear, symmetric microfluidic structure with electrokinetically activated transport<sup>18,19</sup>. Recently, such a setup allowed to induce the negative mobility not only for a colloidal particle but also for a biological compound in the form of mouse-liver mitochondria<sup>20</sup>.

Motivated by the large size range encountered in biochemical applications, a crucial result of this work is a demonstration of a tunable separation strategy, in which the size of the particle undergoing separation may be effectively controlled by variation of the parameters characterizing the external force applied to the particle, e.g. the magnitude of the static bias. The same setup can be applied to segregate particles with respect to their mass in a similar tunable manner<sup>21</sup>. This approach may provide selectivity required for individual isolation of nano and micro particles, proteins, organelles and cells and thus constitutes an important step towards the development of robust lab-on-a-chip devices exploited in both research and industrial applications, in particular point-of-care medical diagnostics.

The paper is organized as follows. In “Model” section we outline the model of a Brownian particle dwelling in a spatially periodic potential under the action of both an external harmonic driving as well as a constant bias. In the next section we exemplify the negative mobility phenomenon. “Negative mobility” section provides crucial results of the paper, namely, a tunable particle separation strategy. In “Tunable particle separation” section we

Institute of Physics, University of Silesia, 40-007 Katowice, Poland. ✉email: jakub.spiechowicz@us.edu.pl

discuss the possibility of tailoring particle isolation in the considered system. Finally, the last section is devoted to summary and conclusion.

### Model

The system considered in this study is a classical inertial Brownian particle of mass  $M$  which moves in a spatially periodic one-dimensional potential  $U(x) = U(x + L)$  of the period  $L$ , additionally subjected to an unbiased time-periodic force  $A \cos(\Omega t)$  of the amplitude  $A$  and the angular frequency  $\Omega$ , as well as an external static force  $F$ . Dynamics of such a particle is described by the Langevin equation<sup>22</sup>

$$M\ddot{x} + \Gamma\dot{x} = -U'(x) + A \cos(\Omega t) + F + \sqrt{2\Gamma k_B T} \xi(t), \tag{1}$$

where the dot and the prime denote differentiation with respect to time  $t$  and the particle coordinate  $x$ , respectively. Coupling of the particle with thermal bath of temperature  $T$  is modeled by Gaussian white noise of zero mean and unity intensity, namely

$$\langle \xi(t) \rangle = 0, \quad \langle \xi(t) \xi(s) \rangle = \delta(t - s). \tag{2}$$

The noise intensity factor  $2\Gamma k_B T$  (where  $k_B$  is the Boltzmann constant) follows from the fluctuation-dissipation theorem<sup>23</sup> and ensures that the system reaches the equilibrium state when  $A = 0$  and  $F = 0$ . The potential  $U(x)$  is spatially periodic with the period  $L$  and the barrier height  $2\Delta U$ ,

$$U(x) = \Delta U \sin\left(\frac{2\pi}{L}x\right). \tag{3}$$

At first glance the studied system looks simply, however, it exhibits peculiar transport behaviour including noise-enhanced transport efficiency<sup>16</sup>, anomalous diffusion<sup>24,25</sup>, amplification of normal diffusion<sup>26,27</sup> and a non-monotonic temperature dependence of normal diffusion<sup>28</sup>.

As the first step of the analysis we transform the Eq. (1) into its dimensionless form. This aim can be achieved in several ways. It often allows to simplify the setup description as after the rescaling procedure some parameters appearing in the corresponding dimensional version may be eliminated thus reducing the complexity of the problem. Moreover, recasting into the dimensionless variables ensures that the results obtained later are independent of the setup which is essential to facilitate the choice in realizing the best setup for testing theoretical predictions in experiments. Here, we propose the use of the following scales as the characteristic units of length and time

$$\hat{x} = \frac{x}{L}, \quad \hat{t} = \frac{t}{\tau_0}, \quad \tau_0 = L\sqrt{\frac{M}{\Delta U}}. \tag{4}$$

The Langevin Eq. (1) transformed according to the above variables reads

$$\ddot{\hat{x}} + \gamma\dot{\hat{x}} = -\hat{U}'(\hat{x}) + a \cos(\omega\hat{t}) + f + \sqrt{2\gamma D} \zeta(\hat{t}). \tag{5}$$

The rescaled *dimensionless friction coefficient*  $\gamma$  is the ratio of two characteristic time scales

$$\gamma = \frac{\tau_0}{\tau_1} = \frac{\Gamma L}{\sqrt{M\Delta U}}, \tag{6}$$

where  $\tau_1 = M/\Gamma$  is characteristic time for the velocity relaxation of the free Brownian particle. The dimensionless mass is set to unity,  $m = 1$ . Other rescaled parameters are as follows:  $a = (L/\Delta U)A$ ,  $\omega = \tau_0\Omega$ ,  $f = (L/\Delta U)F$ . The dimensionless potential  $\hat{U}(\hat{x}) = U(L\hat{x})/\Delta U = \sin(2\pi\hat{x})$  has the period  $\hat{L} = 1$ . The dimensionless thermal noise  $\zeta(\hat{t})$  assumes the same statistical properties as  $\xi(t)$ , i.e.  $\langle \zeta(\hat{t}) \rangle = 0$  and  $\langle \zeta(\hat{t})\zeta(\hat{s}) \rangle = \delta(\hat{t} - \hat{s})$ . The dimensionless noise intensity  $D = k_B T/\Delta U$  is the ratio of thermal energy and half of the non-rescaled potential barrier. From now on, only the dimensionless variables will be used in this study and therefore, in order to simplify the notation, the  $\wedge$ -symbol will be omitted in the Eq. (5).

The dimensionless friction coefficient  $\gamma$  is the most important parameter for later mentioned process of the particle separation with respect to its size. It is due to the fact that even for the simplest model of hydrodynamic interactions occurring in this setup it depends on the linear size  $R$  of the particle. For instance, the spherical particle diffusing in the surrounding medium is subjected to Stokes drag  $-\Gamma\dot{x}$  where  $\Gamma = 6\pi\eta R$  and  $\eta$  is the viscosity of the environment<sup>29</sup>. We stress that (sub)micro sized particles typically possess small mass and therefore for them the dimensionless friction coefficient  $\gamma$  given by Eq. (6) is expected to be either of the order or larger than the dimensionless mass  $m = 1$ .

**The directed velocity.** The particle mobility describes its ability to move through the medium as a response to the biased force acting on it. Hence, the observable of foremost interest in this study is a directed velocity  $\langle v \rangle$  of the particle which may be written as

$$\langle v \rangle = \lim_{t \rightarrow \infty} \frac{1}{t} \int_0^t ds \langle \dot{x}(s) \rangle, \tag{7}$$

where  $\langle \cdot \rangle$  indicates averaging over all realizations of thermal noise as well as over initial conditions for the particle position  $x(0)$  and its velocity  $\dot{x}(0)$ . The latter is obligatory for the deterministic limit  $D \propto T \rightarrow 0$  when the dynamics may be non-ergodic and results can be affected by the specific choice of initial conditions<sup>30</sup>.

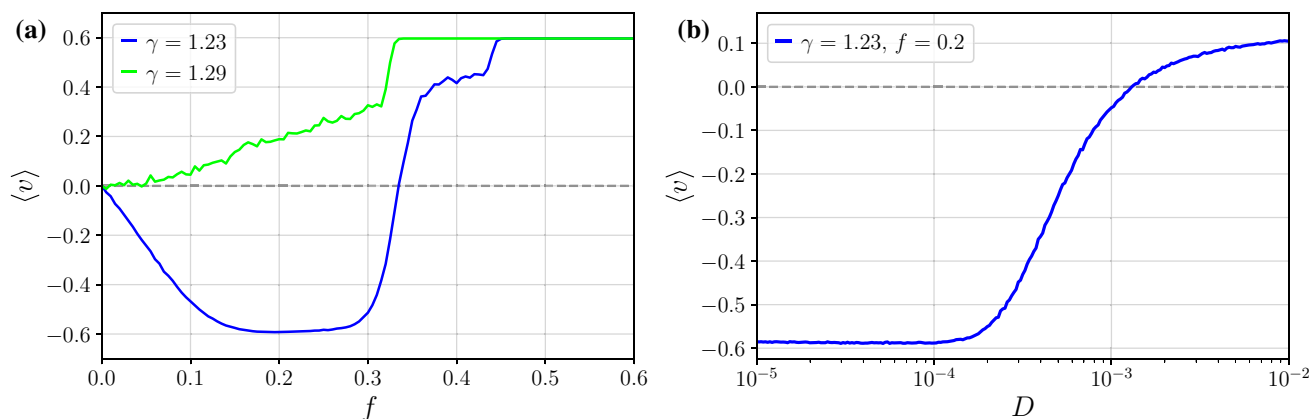


**Figure 1.** The average velocity  $\langle v \rangle$  depicted as a function of the static force  $f$  for two different values of the friction  $\gamma$ . Normal and anomalous transport behaviour in the form of negative mobility is observed for  $\gamma = 1.29$  and  $\gamma = 1.23$ , respectively. In the panel (b) we present the average velocity  $\langle v \rangle$  versus temperature  $D \propto T$  for  $\gamma = 1.23$ . Other parameters are:  $a = 4.5$ ,  $\omega = 3.75$ ,  $f = 0.2$ , and  $D = 0.0001$ .

The Fokker–Planck equation corresponding to the Langevin Eq. (5) cannot be solved analytically in a closed form. Therefore the system may be analyzed only by numerical simulations. Equation (5) is characterized by a 5-dimensional parameter space  $\{\gamma, a, \omega, f, D\}$  the detailed exploration of which is a very challenging task. All numerical calculations were performed using an innovative computational method which is based on employing graphics processing unit supercomputers. This procedure allowed us to speed up computations by about  $10^3$  times compared to traditional methods. For technical details we refer the reader to Ref.<sup>31</sup>.

### Negative mobility

In general, the directed velocity  $\langle v \rangle$  is an increasing function of the static force  $f$  and the resultant particle transport follows the direction of the bias, i.e.  $\langle v \rangle = \mu(f)f$  with a positive nonlinear mobility  $\mu(f) > 0$ . However, in the parameter space there are also regimes for which the particle moves on average in the opposite way, namely  $\langle v \rangle < 0$  for  $f > 0$ . Such anomalous transport behaviour is characterized by a negative mobility  $\mu(f) < 0$ <sup>15,32,33</sup>. The key ingredient for the occurrence of the latter effect is that the system is driven away from thermal equilibrium into a time-dependent nonequilibrium state<sup>15</sup>. This fact provides a negation of the Le Chatelier–Braun equilibrium principle<sup>34</sup> stating that the response of the system perturbed in equilibrium occurs into the direction of the applied bias towards a new equilibrium state. In our case this condition is guaranteed by the presence of the external harmonic driving  $a \cos(\omega t)$ .

It is known that there exist two fundamentally different mechanisms responsible for the emergence of negative mobility in the considered system. Firstly, it may be generated solely by the deterministic dynamics given by Eq. (5) with  $D \propto T = 0$ <sup>15,32</sup>. Secondly, it can be induced by an appropriate dose of thermal fluctuations<sup>15</sup>. Among the first mentioned class we distinguish two completely distinct scenarios. For the deterministic counterpart of the system the negative mobility may be induced either by chaos-assisted dynamics<sup>32</sup> or regular, non-chaotic attractors transporting the particle in the direction opposite to the applied bias<sup>35</sup>. Our numerical research reveals that the most common reason for the occurrence of the negative mobility is rooted in the complexity of the deterministic and chaotic dynamics<sup>35,36</sup>. This observation is of great importance for uncovering the parameter regimes allowing the particle separation.

In Fig. 1 we illustrate the negative mobility effect. For  $\gamma = 1.29$  the directed velocity  $\langle v \rangle > 0$  assumes the same sign as the force  $f > 0$  leading to the normal particle transport regime with  $\mu > 0$ . However, for  $\gamma = 1.23$ , the directed velocity  $\langle v \rangle < 0$  is opposite to the bias  $f > 0$  and in consequence the negative mobility effect emerges  $\mu < 0$ . If the value of  $f$  is positive and large enough then the sign of  $\langle v \rangle$  coincides with the force  $f$  again. Therefore this anomalous transport behaviour is observed only in the vicinity of the zero bias  $f = 0$  and often is termed as the *absolute* negative mobility<sup>37</sup>. As it is illustrated in the the panel (b) the presented parameter regime belongs to the class of deterministically induced negative mobility as for the limiting case of vanishing thermal noise intensity  $D \rightarrow 0$  the directed velocity is negative  $\langle v \rangle < 0$ . We want to stress that this limit should be considered with utmost care as in such a case attractors transporting the particle in opposite directions may coexist and the dynamics may be non-ergodic. It means that depending on the initial conditions, a particle would either move in the direction of the bias force or opposite to it<sup>32</sup>. Nevertheless, at any finite  $D > 0$ , possibly coexisting deterministic attractors turn metastable and due to thermally activated transitions between them the ergodicity of dynamics is restored. Consequently, the directed velocity  $\langle v \rangle$  is independent of the initial conditions. Moreover, as it is shown in the panel (b) the deterministically induced negative mobility effect is generally quite robust with temperature change and usually survives up to moderate thermal noise intensities.

### Tunable particle separation

We now want to harvest the negative mobility phenomenon to separate (sub)micrometer sized particles. This task may be achieved as follows. Imagine that there is a mixture of several species of spherical particles each differing by its linear size  $R$ . The friction coefficient  $\gamma$ , via e.g. Stokes formula, depends on the particle radius



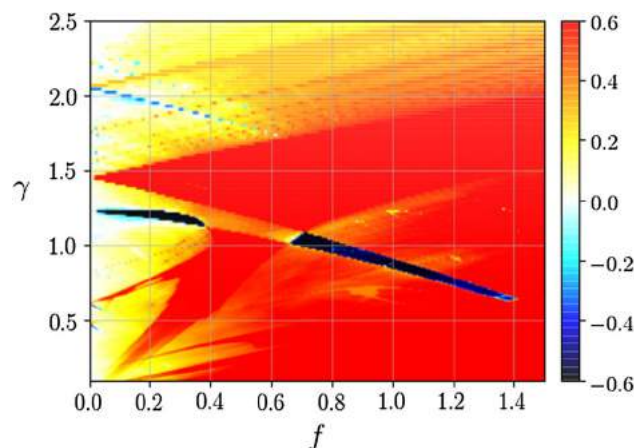


**Figure 2.** Two-dimensional map of the directed velocity  $\langle v \rangle$  as a function of the static force  $f$  and the friction coefficient  $\gamma$ . The magnitude of  $\langle v \rangle$  is indicated by the color bar. Blue areas represent the parameter regimes corresponding to the negative mobility. Parameter values:  $a = 4.5$ ,  $\omega = 3.75$  and  $D = 0$ .

$\gamma = \gamma(R)$ . We can extract the given species of particles  $R^*$  characterized by the friction coefficient  $\gamma^* \equiv \gamma(R^*)$  if only for this particular group of particles the negative mobility effect arises, i.e.  $\langle v \rangle < 0$  for  $\gamma^*$  and  $\langle v \rangle > 0$  for the rest. Therefore this task translates to discovery in the complex four-dimensional parameter subspace  $\{a, \omega, f, D\}$  regimes where in the characteristic  $\langle v \rangle(\gamma)$  there exists only one interval  $\delta\gamma$  of the friction coefficient around the desired particle size  $\gamma^*$  for which the negative mobility  $\langle v \rangle < 0$  emerges. In such a way only particles with the radius  $R^*$  would be extracted from the mixture.

Motivated by the large size range typically encountered in biochemical applications, we aim to develop a tunable scheme that allows to control the particle size targeted for isolation by changing only one parameter of the system. In Ref.<sup>21</sup> it has been shown that the negative mobility effect can be harvested to separate the (sub) micrometer sized particles with respect to their mass. The particle mass targeted for isolation might be effectively controlled over a regime of nearly two orders of magnitude upon changing solely the frequency  $\omega$  of the external harmonic driving. Moreover, in Ref.<sup>36</sup> an efficient separation mechanism based on thermal fluctuation induced negative mobility phenomenon has been proposed. By tuning solely temperature of the system  $D \propto T$ , one can extract from the mixture of particle species differing by size only those of a strictly defined radius. This scheme opens an opportunity to separate particles that carry no charge or dipole, however, it may be inconvenient since temperature variation typically takes too much time to offer a robust experimental implementation. Therefore, in contrast, in this work we harvest the negative mobility effect to develop the particle separation strategy in which the particle size intended for isolation will be controlled by changing only the parameters characterizing the externally applied force, namely, the static bias  $f$  or the amplitude  $a$  or the frequency  $\omega$  of the harmonic driving.

Unfortunately, there is no clear relationship between the presence of the negative mobility and the model parameter values. A tiny displacement in the parameter space may either cause a sudden emergence of the negative mobility or its rapid decay. Therefore, extensive numerical simulations of Eq. (5) were performed in order to systematically investigate the established parameter space. As the deterministically induced negative mobility is the most populated mechanism in the parameter space we set  $D = 0$ . Then Eq. (5) was simulated for several values of the bias  $f \in [0, 2]$  and a parameter domain in the area  $\gamma \times a \times \omega \in [0.1, 10] \times [0, 25] \times [0, 20]$  at a resolution of 400 points per dimension. Overall, we considered nearly  $10^9$  different parameter sets. This exceptional precision was possible only because of our innovative simulation method<sup>31</sup>.

The so collected data was transformed into two-dimensional maps presenting the directed velocity  $\langle v \rangle$  versus two chosen model parameters to facilitate the further analysis. The results of foremost interest are those with  $\gamma$  dependence since the friction coefficient may be used as an indicator to differentiate particles by their size. We explored the data to discover any correlations between the presence of the negative mobility, the friction coefficient  $\gamma$  as well as the magnitude of the parameters  $a$ ,  $\omega$  and  $f$ . We exemplify such a situation in Fig. 2 where we depict the directed velocity  $\langle v \rangle$  as a function of the static bias  $f$  and the friction coefficient  $\gamma$ . The color bar in the plot represents the magnitude of the directed velocity  $\langle v \rangle$ . The occurrence of the negative mobility is marked by blue areas for which  $\langle v \rangle < 0$ . The reader can observe a linear trend between the friction coefficient  $\gamma$ , the static bias  $f$  and the emergence of the anomalous transport. The negative mobility effect occurs for progressively smaller values of  $\gamma$  as the force  $f$  increases. Among many so discovered negative mobility regimes we distilled only those where the latter phenomenon is present solely for one indivisible interval  $\delta\gamma$  of the friction coefficient  $\gamma$  thus permitting the particle separation.

We exemplify this procedure in Fig. 3 where we depict the directed velocity  $\langle v \rangle$  versus the friction coefficient  $\gamma$  which can be identified with the particle size. As it is illustrated in the panel (a), among many particle sizes corresponding to the friction coefficient  $\gamma \in [0.2, 4]$  only those with the friction coefficient  $\gamma^* \approx 1.05$  will move in the direction opposite  $\langle v \rangle < 0$  to the applied bias  $f > 0$ . Other particles will travel concurrently towards it. As a result, only the particles with  $\gamma^* \approx 1.05$  will be extracted from the heterogeneous mixture. Panel (b) presents a magnification of the interval  $\delta\gamma$  where the effect of negative mobility emerges. It can be interpreted as a

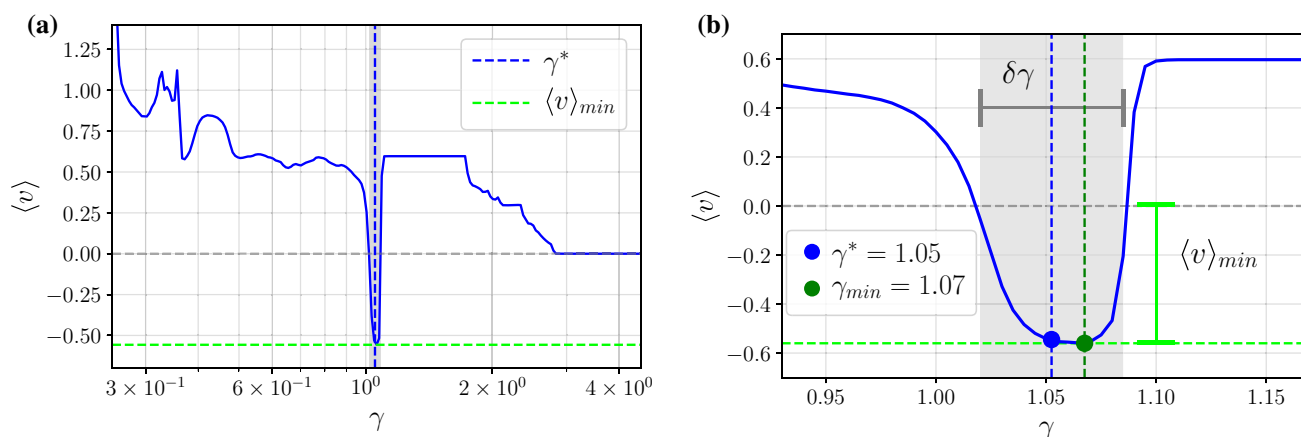


**Figure 3.** Panel (a): the directed velocity  $\langle v \rangle$  versus the friction coefficient  $\gamma$ . The negative mobility is observed solely for a narrow interval  $\delta\gamma$  marked by the grey region. The particle size intended for separation  $\gamma^*$  is chosen as the middle of this window. Panel (b) presents a blow up of the interval where the negative mobility emerges. Parameter values:  $a = 4.5$ ,  $\omega = 3.75$ ,  $f = 0.7$  and  $D = 0.0001$ . Note that  $a$  and  $\omega$  is the same as in Figs. 1 and 2.

resolution capacity of this method. In this case it reads  $\delta\gamma \approx 0.0678$ . The selectivity of the proposed separation scheme is impressive as  $\delta\gamma/\gamma^* \approx 0.06$ . Moreover, as it is illustrated, typically the velocity  $\langle v \rangle$  is noticeably peaked in the interval  $\delta\gamma$  where the negative mobility occurs. The mechanism of the latter anomalous transport effect is rooted in the deterministic dynamics and as such thermal fluctuations generally have destructive impact on it<sup>35,36</sup>. Therefore the above outlined particle separation strategy is viable in low to moderate temperature regimes in which the size targeted for isolation  $\gamma^*$ , i.e. the middle of the interval  $\delta\gamma$ , coincides well with the friction coefficient  $\gamma_{min}$  for which the directed velocity attains its minimal value  $\langle v \rangle_{min} \equiv \langle v \rangle(\gamma_{min})$ . It means that not only the selectivity of this method is impressive but also the particle separation process is quick.

Such approach allowed us to distill parameter regimes which reveal a specific functional dependence between the particle size tailored for separation  $\gamma^*$  and the parameters of the external force applied to the system thus allowing for tunable particle isolation. In Fig. 4 we present the friction coefficient  $\gamma^*$  versus the static bias  $f$ , the amplitude  $a$  and the frequency  $\omega$  all depicted for different temperature of the system  $D \propto T$ . The data were obtained from the characteristics  $\langle v \rangle(\gamma)$  computed for many values of the control parameter, c.f. Fig. 3. Each dot represents the friction coefficient  $\gamma^*$  undergoing the separation process at the fixed  $f$ ,  $a$  or  $\omega$ , see panels (a)-(d). The bars indicate the friction coefficient interval  $\delta\gamma$  where the negative mobility emerges. Here we note that the curves on the corresponding panels overlap with the one representing the deterministic solution  $D = 0$ . Therefore to visualize the impact of temperature on the separation process in the corresponding insets we schematically show the solutions depicting subsequent  $D$  values. The reader may observe that using those tailored parameters read off from Fig. 4 one is able to tune the negative mobility to the particle of a given size  $\gamma^*$  by changing solely the static bias  $f$  or the amplitude  $a$  or the frequency  $\omega$ . In this way it will be separated from the others possessing positive mobility and thus moving concurrently towards the applied bias  $f$ .

From the experimental point of view the most convenient way to manipulate the particle separation is presumably by altering the static bias  $f$ . It is because in many realistic setups it is implemented via the constant external field, e.g. in the microfluidic experiments in the form of a spatially uniform electric field which induces the particle electrophoresis<sup>10</sup>. In most cases its intensity can be changed relatively easily, as opposed to the frequency  $\omega$  of the external harmonic driving which often requires complete rebuilding of the experimental setup. We note that the parameter sets reported in Fig. 4 allow for the tunable separation of the particles in the regime of moderate-large friction coefficient which is characteristic for low Reynolds numbers, being typical for (sub) micro sized particles immersed in a solution<sup>38</sup>. For example in the panels (a) and (b) corresponding to the isolation driven by the constant force  $f$ , the friction coefficient  $\gamma^* \in [0.6, 2.5]$ , whereas in (d) when the separation is controlled by the frequency  $\omega$  the size  $\gamma^* \in [0.25, 1.75]$ . The reader can observe that the friction coefficient  $\gamma^*$  is a decreasing function of the force  $f$  and the frequency  $\omega$  (panels (a), (b) and (d)) while for the amplitude  $a$  it depicts an increasing dependence (panel (c)). Finally, we note that the dimensionless friction coefficient  $\gamma$  in Eq. (6) is influenced not only by the actual friction  $\Gamma$  but also by the parameters  $\Delta U$  and  $L$  of the potential. Therefore, experimentalists may exploit these characteristics of the periodic substrate to further adapt the particle size targeted for separation.

Last but not least, Fig. 4 reveals the impact of temperature  $D \propto T$  on the tunability of the separation process. As it was stated before, since the negative mobility effect derives from the deterministic dynamics of the system, thermal fluctuations have a destructive influence on it. When temperature increases the regions of negative mobility allowing for the controllable particle separation progressively shrink and eventually vanish completely. Therefore the reported tunability of the friction coefficient  $\gamma^*$  is optimized for low to moderate temperature regimes  $D \propto T$ . However, for instance, the panel (c) illustrates an interesting effect of thermal fluctuations. An increase of temperature leads not only to shrinking of the range of the friction coefficient  $\gamma^*$  for which the negative mobility is observed but also to significant decrease of the intervals where this phenomenon occurs, thereby optimizing the width  $\delta\gamma$ . It means that then the tunability of the method is limited but selectivity of the separation

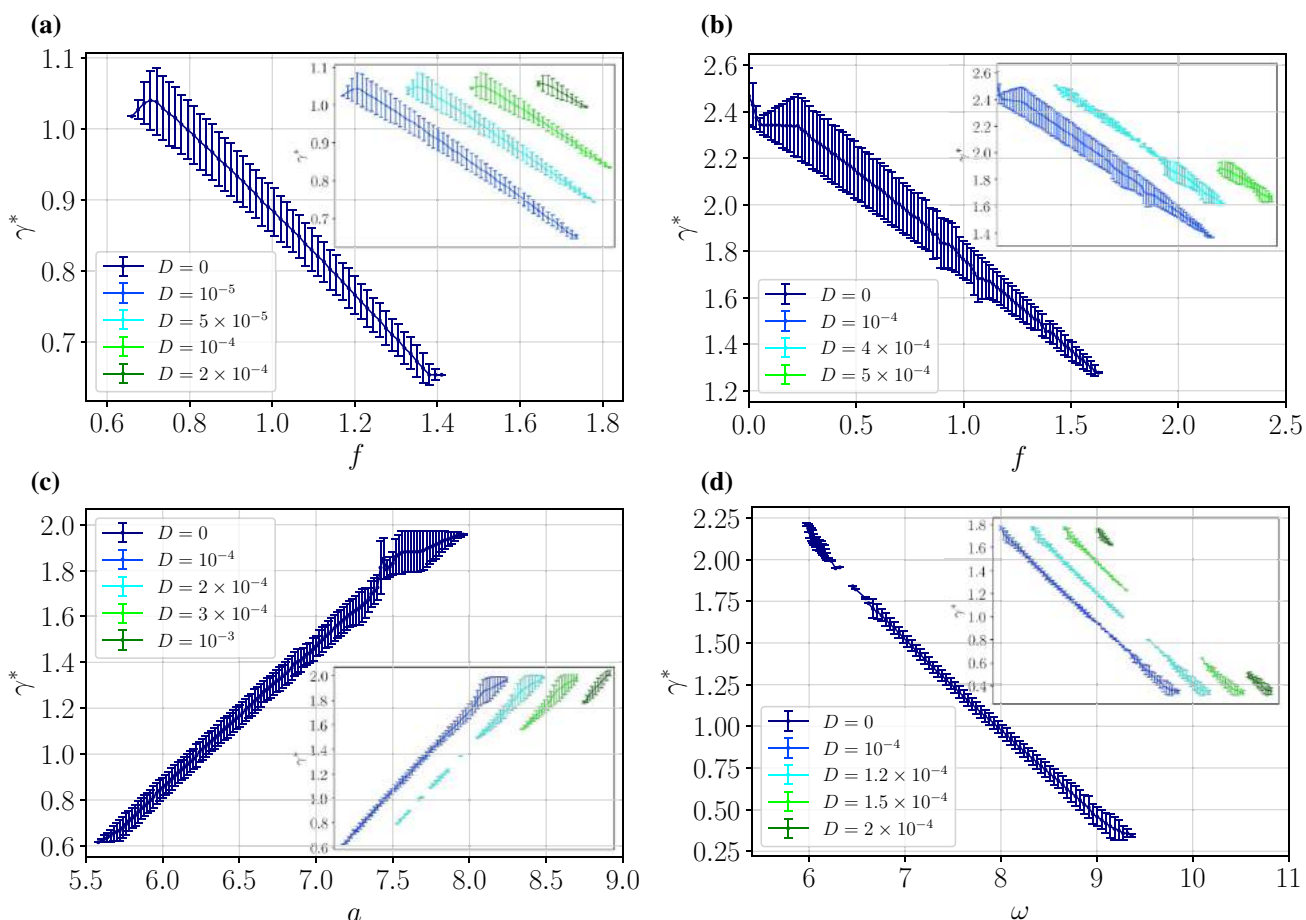


**Figure 4.** Tunable particle separation. The size targeted for separation  $\gamma^*$  is depicted as a function of the parameters of the external force applied to the particle. In panel (a) and (b) versus the static bias  $f$ , (c) vs the amplitude  $a$  and (d) vs the frequency  $\omega$ . All is depicted for different temperature  $D \propto T$  of the system. We stress that all curves for different temperatures shown on the corresponding panels overlap with each other. Therefore to visualize the impact of temperature on the separation process in the corresponding insets we schematically show the solutions depicting subsequent  $D > 0$  values. CAUTION: the insets do not have labels at  $x$ -axis to stress the fact that all curves presented there overlap with the deterministic  $D = 0$  solution and only  $\gamma^*$ -axis is relevant for the reader. Other parameters read (a):  $a = 4.5, \omega = 3.75$ , (b):  $a = 11.25, \omega = 6.8$ , (c):  $f = 1.5, \omega = 4.2$ , (d):  $f = 0.8, a = 9.375$ .

process increases. We remark that the particle isolation upon harvesting the negative mobility phenomenon is also present for different parameter regimes, however, the range of its tunability proves somewhat smaller.

### Tailoring particle separation

Now we consider another, complementary issue. Let us assume that we deal with particles of a given size  $\gamma^*$  which we want to extract from the heterogeneous mixture. We address the following question: for how many different sizes  $\gamma^*$  taken from the extended interval  $\gamma^* \in [0.1, 10]$  it is possible to find a parameter set  $\{a, \omega, f, D\}$  for which the negative mobility effect emerges in the small interval  $[\gamma^* - \delta\gamma/2, \gamma^* + \delta\gamma/2]$  around the targeted value  $\gamma^*$ , therefore allowing its separation in a unique manner, c.f. Fig. 3? We found that in most cases the magnitude  $\delta\gamma/\gamma^*$  is equal to a few percent but frequently is even smaller. We note that for a single  $\gamma^*$  there might be several parameter regimes fulfilling this condition thus facilitating the choice in realizing the best parameter set. We present the answer of this experimentally and practically relevant question in Fig. 5. The distribution of the size  $\gamma^*$  targeted for separation is shown there in the parameter plane of the amplitude  $a$  and the frequency  $\omega$  for different values of the static bias  $f$ . The color coded scale displays the friction coefficient  $\gamma^*$  value. We observe that small particles can be isolated when the static bias  $f$  is likewise small and moderate to large values of the frequency  $\omega$ . On the other hand, medium and large particles are separated for small frequencies  $\omega$ . We note that the distribution of the particle size targeted for isolation  $\gamma^*$  undergoes a stretching when the static bias  $f$  decreases. Moreover, in such a case the range of the particles which might be segregated by harvesting the negative mobility effect is extended as well. Finally, even though the considered panel depicts the deterministic  $D = 0$  dynamics, we found that the distribution of  $\gamma^*$  depicted there is quite robust with temperature change and survives up to moderate thermal noise intensity, see Fig. 1b.

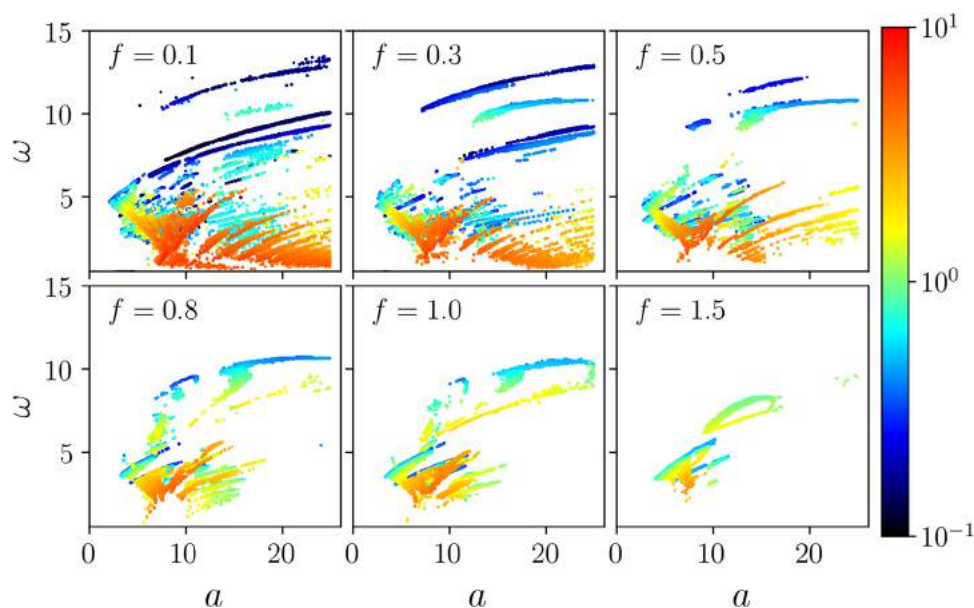


**Figure 5.** The particle size  $\gamma^*$  (color coded scale) targeted for separation via the negative mobility effect as a function of the amplitude  $a$  and the frequency  $\omega$  for different values of the bias  $f$ . Thermal noise intensity  $D$  is set to zero  $D = 0$ .

## Conclusion

In this work we provide an efficient method for tunable separation of (sub)micro sized particles via the negative mobility phenomenon. The approach presented here requires only a spatially periodic nonlinear structure in combination with an unbiased external time-periodic driving. In this scheme the particle size intended for isolation can be effectively controlled by changing solely the parameters of the external force applied to the system, namely, the static bias or the amplitude or the frequency of the external harmonic driving. The approach can be further adapted to the needs by proper fabrication of the nonlinear potential landscape determined by its barrier height and period. It allows the possibility to not deflect the separated particles along the different angles but to steer them in the opposite direction making the isolation process robust.

Our theoretical predictions should be used as a guide towards physical reality indicating the direction for future theoretical and experimental research. In particular, one needs to carefully consider higher dimensional systems as well as geometrical constraints together with hydrodynamic interaction which in real experiments may play essential role. We expect that such research would potentially lead to implementation of the proposed scheme in a lab-on-chip device, as it has been recently demonstrated for a similar system<sup>20</sup>. We envision that current lithographic techniques with advantageous fabrication costs may be used to develop high throughput separation applications concerning in particular biophysical and biochemical problems. Taking into account recent progress in 3D printing technologies allowing its scaling down to the nanometer range the proposed scheme may have even significant commercial potential in future<sup>39</sup>.

## Methods

We employed a weak 2nd order predictor-corrector method<sup>40</sup> to simulate stochastic dynamics given by Eq. (5). We integrated it with the time step scaled by the fundamental period  $T = 2\pi/\omega$  of the external harmonic driving, namely  $h = 10^{-2} \times T$ , with the exception of smallest  $\omega < 1$  values for which the step was chosen to be  $h = 10^{-3} \times T$ . The initial positions  $x(0)$  and velocities  $v(0)$  were uniformly distributed over the intervals  $[0, 1]$  and  $[-2, 2]$ , respectively. The directed velocity  $\langle v \rangle$  was averaged over the ensemble of  $2^{10} = 1024$  trajectories, each starting with a different initial condition according to the above distributions. The number of realisations of stochastic dynamics is not accidental and was chosen carefully to maximise the performance of the numerical simulation, see Ref.<sup>31</sup> for more details. The time span of the simulations was set to  $[0, 10^4 T]$  to guarantee that the directed velocity  $\langle v \rangle$  relaxed to its asymptotic long time stationary value.

Received: 10 May 2020; Accepted: 31 August 2020

Published online: 06 October 2020

## References

1. Yager, P., Edwards, T., Fu, E., Helton, K. & Nelson, K. Microfluidic diagnostic technologies for global public health. *Nature* **442**, 412 (2004).
2. Korecka, J. A., Verhaagen J. & Hol, E. M. Cell-replacement and gene-therapy strategies for Parkinson's and Alzheimer's disease. *Regen. Med.* **2**, 425 (2007).
3. Heffner, R. R. & Barron, S. A. The early effects of ischemia upon skeletal muscle mitochondria. *J. Neurol. Sci.* **38**, 295 (1978).
4. Suresh, S. Biomechanics and biophysics of cancer cells. *Acta Mater.* **55**, 3989 (2007).

5. Bhagat, A. A. *et al.* Microfluidics for cell separation. *Med. Biol. Eng. Comput.* **48**, 999 (2010).
6. Xuan, J. & Lee, M. L. Size separation of biomolecules and bioparticles using micro/nanofabricated structures. *Anal. Methods* **6**, 27 (2014).
7. Fehr A. R. & Perlman S. Coronaviruses: an overview of their replication and pathogenesis. In *Coronaviruses. Methods in Molecular Biology, vol 1282* (Humana Press, New York, 2015)
8. Kandel, E. R., Schwartz, J. H. & Jessell, T. M. *Principles of Neural Science* 4th edn. (McGraw-Hill, New York, 2000).
9. Sajeesh, P. & Sen, A. K. Particle separation and sorting in microfluidic devices: a review. *Microfluid. Nanofluid.* **17**, 1 (2014).
10. Sonker, M., Kim, D., Egatz-Gomez, A. & Ros, A. Separation phenomena in tailored micro- and nanofluidic environments. *Annu. Rev. Anal. Chem.* **12**, 475 (2019).
11. Bogunovic, L., Eichhorn, R., Regtmeier, J., Anselmetti, D. & Reimann, P. Particle sorting by a structured microfluidic ratchet device with tunable selectivity: theory and experiment. *Soft Matter* **8**, 3900 (2012).
12. Kim, D., Luo, J., Arriaga, E. A. & Ros, A. Deterministic ratchet for sub-micrometer (bio)particle separation. *Anal. Chem.* **90**, 4370 (2018).
13. Zhang, J. *et al.* Tunable particle separation in a hybrid dielectrophoresis (DEP)- inertial microfluidic device. *Sensors Actuat. B* **267**, 14 (2018).
14. Eichhorn, R., Reimann, P. & Hänggi, P. Brownian motion exhibiting absolute negative mobility. *Phys. Rev. Lett.* **88**, 190601 (2002).
15. Machura, Ł., Kostur, M., Talkner, P., Łuczka, J. & Hänggi, P. Absolute negative mobility induced by thermal equilibrium fluctuations. *Phys. Rev. Lett.* **98**, 040601 (2007).
16. Spiechowicz, J., Hänggi, P. & Łuczka, J. Brownian motors in the microscale domain: enhancement of efficiency by noise. *Phys. Rev. E* **90**, 032104 (2014).
17. Spiechowicz, J., Hänggi, P. & Łuczka, J. Coexistence of absolute negative mobility and anomalous diffusion. *New J. Phys.* **21**, 083029 (2019).
18. Ros, A. *et al.* Absolute negative mobility. *Nature* **436**, 928 (2005).
19. Eichhorn, R., Regtmeier, J., Anselmetti, D. & Reimann, P. Negative mobility and sorting of colloidal particles. *Soft Matter* **6**, 1858 (2010).
20. Luo, J., Muratore, K., Arriaga, E. & Ros, A. Deterministic absolute negative mobility for micro- and submicrometer particles induced in a microfluidic device. *Anal. Chem.* **88**, 5920 (2016).
21. Slapik, A., Łuczka, J., Hänggi, P. & Spiechowicz, J. Tunable mass separation via negative mobility. *Phys. Rev. Lett.* **122**, 070602 (2019).
22. Hänggi, P. & Marchesoni, F. Artificial Brownian motors: controlling transport on the nanoscale. *Rev. Mod. Phys.* **81**, 387 (2009).
23. Marconi, U. M. B., Puglisi, A., Rondoni, L. & Vulpiani, A. Fluctuation-dissipation: response theory in statistical physics. *Phys. Rep.* **461**, 111 (2008).
24. Spiechowicz, J. & Łuczka, J. Subdiffusion via dynamical localization induced by thermal equilibrium fluctuations. *Sci. Rep.* **7**, 16451 (2017).
25. Spiechowicz, J. & Łuczka, J. SQUID ratchet: statistics of transitions in dynamical localization. *Chaos* **29**, 013105 (2019).
26. Reimann, P. *et al.* Giant acceleration of free diffusion by use of tilted periodic potentials. *Phys. Rev. Lett.* **87**, 010602 (2001).
27. Spiechowicz, J. & Łuczka, J. Josephson phase diffusion in the superconducting quantum interference device ratchet. *Chaos* **25**, 053110 (2015).
28. Spiechowicz, J. & Łuczka, J. Diffusion in a biased washboard potential revisited. *Phys. Rev. E* **101**, 032123 (2020).
29. Landau, L. D. & Lifshitz, E. M. *Fluid Mechanics* 2nd edn. (Butterworth-Heinemann, Oxford, 1987).
30. Spiechowicz, J., Łuczka, J. & Hänggi, P. Transient anomalous diffusion in periodic systems: ergodicity, symmetry breaking and velocity relaxation. *Sci. Rep.* **6**, 30948 (2016).
31. Spiechowicz, J., Kostur, M. & Machura, Ł. GPU accelerated Monte Carlo simulation of Brownian motors dynamics with CUDA. *Comput. Phys. Commun.* **191**, 140 (2015).
32. Speer, D., Eichhorn, R. & Reimann, P. Transient chaos induces anomalous transport properties of an underdamped Brownian particle. *Phys. Rev. E* **76**, 051110 (2007).
33. Nagel, J. *et al.* Observation of negative absolute resistance in a Josephson junction. *Phys. Rev. Lett.* **100**, 217001 (2008).
34. Landau, L. D. & Lifshitz, E. M. *Statistical Physics, Part 1* 3rd edn. (Butterworth-Heinemann, Oxford, 1980).
35. Slapik, A., Łuczka, J. & Spiechowicz, J. Negative mobility of a Brownian particle: strong damping regime. *Commun. Nonlinear Sci. Numer. Simul.* **55**, 316 (2018).
36. Slapik, A., Łuczka, J. & Spiechowicz, J. Temperature-induced tunable particle separation. *Phys. Rev. Appl.* **12**, 054002 (2019).
37. Kostur, M., Machura, Ł., Talkner, P., Hänggi, P. & Łuczka, J. Anomalous transport in biased ac-driven Josephson junctions: negative conductances. *Phys. Rev. B* **77**, 104509 (2008).
38. Happel, J. & Brenner, H. *Low Reynolds Number Hydrodynamics* (Prentice Hall, Englewood Cliffs, 1965).
39. Chiu, D. T. *et al.* Small but perfectly formed? Successes, challenges and opportunities for microfluidics in the chemical and biological sciences. *Chemistry* **2**, 201 (2017).
40. Platen, E. & Bruti-Liberati, N. *Numerical Solution of Stochastic Differential Equations with Jumps in Finance in Stochastic Modelling and Applied Probability* (Springer, Berlin, 2010).

## Acknowledgements

This work has been supported by the Grant NCN No. 2017/26/D/ST2/00543 (J. S.).

## Author contributions

A.S. carried out numerical calculations. All authors contributed to the discussion and analysis of the results. J.S. wrote the manuscript.

## Competing interests

The authors declare no competing interests.

## Additional information

**Correspondence** and requests for materials should be addressed to J.S.

**Reprints and permissions information** is available at [www.nature.com/reprints](http://www.nature.com/reprints).

**Publisher's note** Springer Nature remains neutral with regard to jurisdictional claims in published maps and institutional affiliations.



**Open Access** This article is licensed under a Creative Commons Attribution 4.0 International License, which permits use, sharing, adaptation, distribution and reproduction in any medium or format, as long as you give appropriate credit to the original author(s) and the source, provide a link to the Creative Commons licence, and indicate if changes were made. The images or other third party material in this article are included in the article's Creative Commons licence, unless indicated otherwise in a credit line to the material. If material is not included in the article's Creative Commons licence and your intended use is not permitted by statutory regulation or exceeds the permitted use, you will need to obtain permission directly from the copyright holder. To view a copy of this licence, visit <http://creativecommons.org/licenses/by/4.0/>.

© The Author(s) 2020